Fall 12-12-2022

Regulation of the hyperpolarization-activated cyclic nucleotide gated ion channel 2, HCN2, by post-translational SUMOylation

Lori Forster

Regulation of the hyperpolarization-activated cyclic nucleotide gated ion channel 2, HCN2, by post-translational SUMOylation

by

Lori Forster

Under the Direction of Deborah Baro PhD

A Dissertation Submitted in Partial Fulfillment of the Requirements for the Degree of

Doctor of Philosophy

in the College of Arts and Sciences

Georgia State University

2022

ABSTRACT

The hyperpolarization activated cyclic nucleotide gated ion channels (HCN) are encoded by 4 isoforms (HCN1-4). These are nonspecific cation channels which mediate the slow inward current Ih. Dysregulation of HCN2 contributes to multiple disease states such as epilepsy, depression and anxiety, and chronic pain. The HCN2 channel is post-translationally modified by the small ubiquitin like modifier (SUMO), where SUMOylation of K669 is associated with an increase in Ih and surface expression. This dissertation work investigates how ion channel SUMOylation regulates hyperexcitability in inflammatory pain. Following complete Freund's adjuvant (CFA) induced inflammation, there is an increase in HCN2 protein level bilaterally, and a unilateral increase in pain behavior. Interestingly, we observe an increase in HCN2 SUMOylation unilaterally following inflammation suggesting that SUMOylation of HCN2 may play an important role in regulating Ih in inflammation. We examine the molecular mechanisms driving the increase in Ih and surface expression following SUMOylation of K669 in HCN2. Surface expression can be increased by promoting trafficking from the trans-Golgi to the plasma membrane, by reducing channel endocytosis and/or by increasing recycling of the endocytosed channel. Indeed, SUMOylation of HCN2 increases colocalization with the slow recycling marker, Rab11a, and a dominant negative form of Rab11a blocks the SUMO mediated increase in Ih. Together these results suggest a potential mechanism behind the increase in Ih in inflammatory pain. Additionally, investigating the mechanism behind SUMO regulation of another ion channel, Kv4.2, we observe a Rab11a mediated increase in IA. These findings suggest C-terminal SUMOylation of ion channels may represent a general mechanism for regulating the extent of ion channel recycling.

INDEX WORDS: Small ubiquitin-like modifier (SUMO), Ion channels, Pain, Inflammation, HCN2, Trafficking, Voltage gated ion channels

Regulation of the hyperpolarization-activated cyclic nucleotide gated ion channel 2, HCN2, by post-translational SUMOylation

by

Lori Forster

Committee Chair: Deborah Baro

Committee: Anne Murphy

Aaron Roseberry

Bingzhong Xue

Electronic Version Approved:

Office of Graduate Services

College of Arts and Sciences

Georgia State University

December 2022

DEDICATION

This work is dedicated to my family, my animals, and especially my husband Craig Forster. Without all of you I would not have been able to complete this work.

ACKNOWLEDGEMENTS

I would like to thank my Ph.D. advisor, Dr. Deborah Baro for her support and advice.

Second, I would like to thank my dissertation committee, Dr. Anne Murphy, Dr. Aaron Roseberry, and Dr. Bingzhong Xue, for their continued advice and support.

I would also like to thank the current and past members of the Baro lab - Leslie-Anne Jansen, Meghyn Welch, Anna Parker, X-zavyer Smith, Sarah Tasneem, Leah Middleton, Debasmita De, Prianca Griggs, and others throughout the years. Thank you all for your advice, support, and most of all your friendship.

I would like to thank the Roseberry, Xue and Shi labs for their technical help and

Finally, I would like to thank the Brains and Behavior Fellowship program for their support during my Ph.D.

TABLE OF CONTENTS

ACKNOWLEDGEMENTS ..... **V**

LIST OF TABLES ..... **X**

LIST OF FIGURES ..... **XI**

INTRODUCTION **1**

1.1 Pain and inflammation **1**

1.2 The role of Ih in pain **2**

1.3 The role of extranuclear SUMOylation **4**

1.4 Hypothesis **7**

2 ALTERATIONS IN SUMOYLATION OF THE HYPERPOLARIZATION-ACTIVATED CYCLIC NUCLEOTIDE GATED ION CHANNEL 2 DURING PERSISTENT INFLAMMATION **9**

2.1 Abstract **10**

2.2 Significance **11**

2.3 Introduction **11**

2.4 Materials and methods **14**

2.4.1 Animal Ethics ***14***

2.4.2 CFA model and tissue preparation ***14***

2.4.3 Antibodies and reagents ***15***

2.4.4 Immunohistochemistry ***15***

2.4.5 Immunohistochemistry analysis 16

2.4.6 Proximity ligation assay (PLA) 17

2.4.7 PLA analysis 18

2.4.8 Rat DRG membrane preparation and denaturing immunoprecipitation 18

2.4.9 Western Blot 19

2.4.10 Statistics 20

2.5 Results 20

2.5.1 Inflammation increases the level of HCN2 expression and the number of cells expressing HCN2 20

2.5.2 HCN2 is SUMOylated in the rat DRG 22

2.5.3 Significantly more HCN2 SUMO2/3 conjugation is observed in small diameter neurons from ipsilateral DRG on day 1 but not on day 3 post-CFA 24

2.5.4 Conjugation of SUMO1 to HCN2 channels was reduced in medium and large diameter DRG neurons on 1 day post-CFA, and increased in small neurons on day 3 post-CFA 26

2.6 Discussion 27

2.6.1 HCN2 protein expression and SUMOylation of HCN2 channel complexes are increased in small diameter neurons during CFA-induced inflammation 27

2.6.2 SUMOylation of HCN2 channel complexes is decreased in medium and large diameter neurons during CFA-induced inflammation 31

3 CHANGES IN PERIPHERAL HCN2 CHANNELS DURING PERSISTENT INFLAMMATION 49

3.1 Abstract 50

3.2 Introduction 51

3.3 Materials and methods 58

3.3.1 Animal Ethics 58

3.3.2 CFA model and tissue preparation 58

3.3.3 Antibodies and Reagents 59

3.3.4 Immunohistochemistry and analysis 59

3.3.5 Proximity ligation assays and analysis 59

3.3.6 Statistics 60

3.4 Results 61

3.4.1 HCN2 expression and SUMOylation in L4 DRG neurons on days 1 and day 3 post-CFA 61

3.4.2 HCN2 expression and SUMOylation in L6 DRG neurons on days 1 and day 3 post-CFA 62

3.5 Discussion 63

4 SUMOYLATION REGULATES RECYCLING OF THE HYPERPOLARIZATION ACTIVATED CYCLIC NUCLEOTIDE GATED CHANNEL 2 77

4.1 Introduction 78

4.2 Methods 80

4.2.1 Antibodies and plasmids 80

4.2.2 Cell Culture 80

4.2.3 Calcium Phosphate Transfection 80

4.2.4 Immunoprecipitation 81

4.2.5 Electrophysiology 81

4.2.6 Immunohistochemistry 82

4.2.7 Western blotting 83

4.2.8 Statistics 84

4.3 Results 85

4.4 Discussion 90

4.4.1 C-terminal SUMOylation of Ion Channels as a Common Mechanism to Regulate Surface Expression 90

4.4.2 Balance of SUMOylation and Ubiquitination to Regulate Surface Expression .. 91

5 CONCLUSION 104

5.1 C-terminal SUMOylation regulates slow recycling of ion channels 105

5.2 Ion channel SUMOylation increases hyperexcitability of DRG neurons 108

5.3 Limitations of animal models and heterologous expression systems 110

REFERENCES 113

LIST OF TABLES

Table 1: Fold Change in Mean HCN2 Expression in L4-L6 DRG..... 75

Table 2. Fold Change in Mean HCN2 SUMOylation in L4-L6 DRG..... 76

LIST OF FIGURES

Figure 0-1-1 The SUMO Pathway 8

Figure 2-1 Validation of anti-HCN2 and quantification of HCN2 positive cells. 32

Figure 2-3 CFA-induced inflammation alters HCN2 protein expression on 1 day post-CFA. 34

Figure 2-4 HCN2 protein expression is altered on day 3 post-CFA. 36

Figure 2-5 HCN2 is SUMOylated in rat DRG..... 38

Figure 2-6 Measuring HCN2 channel SUMOylation. 40

Figure 2-7 SUMO2/3 conjugation to HCN2 channels is increased in small diameter neurons from ipsilateral relative to contralateral DRG at 1 day post-CFA. 41

Figure 2-8 SUMOylation of HCN2 channels by SUMO2/3 does not change 3 days post-CFA.. 43

Figure 2-9 HCN2 channel SUMOylation by SUMO1 is diminished in medium and large diameter neurons from ipsilateral relative to contralateral DRG at 1 day post-CFA. 45

Figure 2-10 HCN2 channel SUMOylation by SUMO1 is increased in small neurons from ipsilateral relative to contralateral DRG at 3 days post-CFA. 47

Figure 3-1 HCN2 protein expression but not SUMOylation is altered in the L4 DRG 1 day post-CFA. 67

Figure 3-2 HCN2 protein expression and HCN2 SUMOylation are unaltered in the L4 DRG 3 days post CFA. 69

Figure 3-3 HCN2 protein expression and HCN2 SUMOylation are enhanced in the L6 DRG 1 day post-CFA. 71

Figure 3-4 HCN2 SUMOylation but not protein expression is altered in the L6 DRG 3 days post-CFA. 73

Figure 4-1 HCN2 SUMOylation prevents internalization of the channel 94

Figure 4-2 The endocytosis inhibitor, Pitstop2, mimics and occludes the effects of SUMOylation at K669 on HCN2 95

Figure 4-3 The effects of HCN2 SUMOylation are not due to clathrin mediated endocytosis.... 96

Figure 4-4 SUMOylation increases Ih through Rab11a dependent recycling 98

Figure 4-5 SUMOylation increases HCN2 protein expression through an increase in transcription of HCN2..... 100

Figure 4-6 Trip8b acts through the recycling pathway to regulate HCN2 101

Figure 4-7 SUMOylation regulates rab11a dependent recycling of Kv4.2 103

INTRODUCTION

1.1 Pain and inflammation

Chronic pain is a major challenge to our society, with serious impacts on life for those who are facing this debilitating condition, as well as significant impacts to the economy. It has an estimated cost burden of $635 billion a year to American society (Chapman & Vierck, 2017). Over the past two decades incidence of chronic pain in US adults has increased by ~10% (Zajacova, Grol-Prokopczyk, & Zimmer, 2021). The 2012 National Health Interview survey showed that 25.3 million US adults experienced chronic pain daily with even greater numbers, 40 million, experiencing severe pain (Blackwell, Lucas, & Clarke, 2014). Those with severe pain displayed worse health than those reporting less severe pain. The trend toward increasing pain is worrisome and drives urgency in increasing our understanding of the mechanisms behind chronic pain. Here, I describe and discuss pain as the summed experience of a real or perceived noxious sensory stimuli (painful, threatening stimuli), as well as the emotional and cognitive response (Dubin & Patapoutian, 2010); nociception is the detection of the stimuli. Chronic pain is defined as pain lasting beyond tissue damage and inflammatory processes associated with tissue healing (Chapman & Vierck, 2017). Chronic pain displays alterations to the normal pain pathway, showing hypersensitivity. These signs show that the pain has extended past its usefulness as a warning sign of impending tissue damage, and now becomes debilitating. Symptoms of chronic pain can be viewed during normal healing to some degree. For example, during normal healing, a person with sunburn will display allodynia, where a normal innocuous stimuli is perceived as painful, such as what would normally be a pleasant warm shower feeling painful and burning, from sensitization to both the temperature of the water and the touch from the water pressure on the skin (Basbaum, Bautista, Scherrer, & Julius, 2009). Additionally, someone could display

hyperalgesia, the exaggerated response to a normally noxious stimulus. These symptoms come about in response to reorganization of the pain circuitry, where ionic conductances are altered in a maladaptive manner to cause hyperalgesia or allodynia when they would not normally occur. This is normally in response to some insult – whether that is inflammation as in the case of arthritis (Muley, Krustev, & McDougall, 2016), or nerve damage as in the case of diabetic neuropathy (Calcutt, 2020), where the sensory neurons become hyperexcitable by the alterations in their ionic conductances (Berta, Qadri, Tan, & Ji, 2017; Gold & Gebhart, 2010; Pace et al., 2018; Reichling & Levine, 2009). Nociceptors are peripheral sensory neurons. They detect noxious temperature, pressure, and chemical stimuli and initiate pain signaling in response to this. They are pseudounipolar neurons with a single process from the soma which bifurcates forming the t-junction. One process projects to the periphery, such as the skin or viscera, and the other process to the spinal cord to innervate the central nervous system. The soma of these neurons resides in the dorsal root ganglia (DRG), and the trigeminal ganglia (Devor, 1999). The nociceptors of the DRG can be classified into three groups based on their conduction velocities and degree of myelination. C-fibers display the slowest conduction velocity, 0.6m/s, with small diameter and unmyelinated axons. Aδ fibers are small to medium diameter axons that are thinly myelinated with a conduction velocity of 3.3m/s, and Aβ nociceptors have large diameter axons that are thickly myelinated with a conduction velocity of 9.6m/s (Djouhri & Lawson, 2004).

1.2 The role of Ih in pain

The hyperpolarization activated cyclic nucleotide gated ion channels (HCN) are voltage gated ion channels that are activated by hyperpolarizing membrane potentials. They are nonspecific cation channels, and mediate a hyperpolarization activated current, Ih, which is a

slow inward current. This current has been termed a pacemaker current as it plays a role in initiation and regulation of the heartbeat and is involved in regulation of rhythmic currents in neural circuits (Baruscotti, Bucchi, & Difrancesco, 2005; Wahl-Schott & Biel, 2009). There are 4 isoforms, 1-4, which vary in their responsiveness to cAMP. Binding of cAMP to the cyclic nucleotide binding domain (CNBD) speeds up channel opening and shifts the voltage of activation to more positive voltages. Isoforms 2 and 4 are the most responsive to cAMP, with shifts of between +10 to +25mV observed upon cAMP binding, where 1 and 3 are only weakly affected by cAMP (Wahl-Schott & Biel, 2009). HCN channels can form homologous or heterologous tetramers(Tibbs, Posson, & Goldstein, 2016). I_h contributes to neuronal excitability by generating a depolarizing current that aids in restoring the membrane potential of a cell towards firing threshold. HCN channels play a role in homeostatic regulation of cells by either activating when needed to increase a cells activity or deactivating to decrease activity. There is some proportion of channels open at resting membrane potential; this causes there to be a slow tonic influx of Na+ ions into the cell, bringing the membrane potential to more depolarized values and is able to stabilize the membrane potential in subthreshold ranges. (Hutcheon & Yarom, 2000; Kase & Imoto, 2012; Shah, 2014; Wahl-Schott & Biel, 2009). Dysregulation of HCN channels can contribute to multiple neurological disease states (DiFrancesco & DiFrancesco, 2015). In epilepsy, genetic deletions of HCN2 leads to absence epilepsy phenotypes, loss of HCN expression occurs during the beginning of epileptogenesis in acquired epilepsy, and seizures promote changes in the pattern of HCN expression (Poolos, 2012). In major depression, rodent models of chronic social defeat display a decrease in HCN2 mediated currents in the ventral tegmental area which contribute to depressive and anxiety-like behaviors (Zhong et al., 2018). In Alzheimer's disease HCN2 mediated currents contribute to the

processing of Amyloid precursor protein (APP), as inhibition of the current with the Ih blocker ZD7288 showed decreased levels of Aβ and other APP cleavage products (Frykman et al., 2017). Additionally, HCN channels have been found to contribute to the development of pain.

Ih is increased in several models of chronic inflammatory and neuropathic pain in nociceptors (Djouhri et al., 2015; Emery, Young, Berrocoso, Chen, & McNaughton, 2011; Schnorr et al., 2014; Weng, Smith, Sathish, & Djouhri, 2012). Following CFA injection rats display inflammatory hypersensitivity, unilaterally, for at least 14 days as displayed by a decrease in the paw withdrawal threshold (Stein, Millan, & Herz, 1988). When a HCN channel blocker, ZD7288 is applied at 5 days post CFA there is a partial reverse of mechanical hypersensitivity (Weng et al., 2012). Additionally, when HCN2 channels specifically, are knocked out in NaV1.8-expressing neurons in mice failed to develop mechanical hypersensitivity, but still developed thermal hyperalgesia (Schnorr et al., 2014). The HCN2 isoform has been implicated in both inflammatory and neuropathic pain. For inflammatory pain, in the dorsal root ganglia increases in HCN2 immunoreactivity were observed at 1, 4 and 7 days post CFA induced inflammation in small and medium diameter DRG neurons, which corresponds to putative c-fiber nociceptors and Aδ nociceptors (Acosta et al., 2012; Weng et al., 2012).

1.3 The role of extranuclear SUMOylation

The small ubiquitin like modifier (SUMO) is a small ~100 amino acid protein that is a reversible, post-translational modification added to lysine residues in target proteins. SENPs, are SUMO proteases that remove SUMO from target residues. SENPs also aid in maturation of SUMOylation, they cleave the c-terminus to expose a di-glycine motif which is able to form a

thioester bond with the SUMO E1 enzyme. This step is ATP-dependent. Next activated SUMO is transferred to the sole E2 conjugating enzyme, Ubc9. Finally, SUMO is added to target proteins by the E2 enzyme alone, or with assistance from an E3 enzyme (Vertegaal, 2022) (Figure 1). The majority of SUMOylation, ~65% occurs within a SUMO consensus motif (Hendriks, D'Souza, Chang, Mann, & Vertegaal, 2015), ψKXE (where ψ represents a hydrophobic amino acid and X represents any amino acid), but SUMOylation also occurs at non-consensus K residues. Specificity for non-consensus SUMOylation can be guided through interaction with a SUMO interaction motif (SIM) in the target protein and recruiting the ubc9-SUMO thioester bond this way, or interaction of the target with an E3 ligase to position the SUMO in an orientation to aid in modification of the residue (Flotho & Melchior, 2013). There are 5 SUMO peptides, SUMO1-5, where SUMO2 and 3 are 97% identical and not readily distinguishable and often referred to as SUMO2/3, and SUMO1 is 47% similar to SUMO2/3. SUMO4 is likely not conjugated to substrates due to its specific amino acid sequence preventing SUMO maturation. SUMO 5 has been recently reported, but it's endogenous expression has not yet been confirmed suggesting it might be a SUMO pseudogene (Vertegaal, 2022).

SUMOylation was first discovered in the nucleus, and as such a large body of research focuses on its role there. Staining for SUMO with antibodies shows intense staining in the nucleus, and diffuse staining in the cytoplasm (See figure 2-1). In the nucleus one of the most well-defined roles of SUMOylation is its involvement in DNA damage repair where SUMOylation acts as a "glue", holding together the proteins involved in homologous recombination and nucleotide excision repair (Jentsch & Psakhye, 2013; Psakhye & Jentsch, 2016). Other roles of nuclear SUMOylation include SUMOylation of transcription factors to

enhance or repress transcription, formation of PML nuclear bodies, chromosome organization, and nuclear transport (Johnson, 2004). Proteins outside of the nucleus are also SUMOylated.

In neurons, extranuclear SUMOylation is involved in the development of the nervous systems, for proper differentiation, development of rods and cones in the retina, synapse formation, and regulation of excitability by regulating ion channels (Henley, Craig, & Wilkinson, 2014). In addition to HCN2, other ion channels are known to be SUMOylated. The potassium channels Kv4 (Meghyn A. Welch, Lori A. Forster, Selin I. Atlas, & Deborah J. Baro, 2019), Kv11 (Steffensen, Andersen, Mutsaers, Mujezinovic, & Schmitt, 2018), Kv7 (Qi et al., 2014; Xiong et al., 2017), Kv2 (Plant, Dowdell, Dementieva, Marks, & Goldstein, 2011), K2P1 (Plant et al., 2010; Rajan, Plant, Rabin, Butler, & Goldstein, 2005) and Kv1.5 (Benson et al., 2007) as well as SUMOylation of the sodium channels NaV1.2 (Plant, Marks, & Goldstein, 2016) and NaV1.5 (Plant, Xiong, Romero, Dai, & Goldstein, 2020), and the calcium channels CaV2.2 (Silveirinha et al., 2021) TRPV1 (Y. Wang et al., 2018b) and TRPM4 (Kruse et al., 2009), the Na+/Ca2+ exchanger (Cuomo et al., 2020) are SUMOylated.

The HCN2 ion channel is SUMOylated in rat nervous system tissue (Forster, Jansen, Rubaharan, Murphy, & Baro, 2020a; Parker et al., 2016). In HEK293 cells HCN2 channel SUMOylation can be enhanced by over expression of a plasmid containing the E2 conjugating enzyme, ubc9, and a plasmid encoding SUMO2. When SUMOylation of the channel is enhanced, the surface expression of the channel is increased as well as the maximal conductance. This is due to modification of K669, as mutation of the lysine to arginine prevented an increase in both surface expression and maximal conductance. Another high probability SUMOylation site, K534, did not influence either of these measures in this heterologous system (Parker et al., 2017). Additionally, HCN channel SUMOylation is dopamine and activity dependent. Tonic,

5nM levels of dopamine, permitted activity to regulate Ih in the lobster stomatogastric nervous system. These effects were occluded by perfusion of a cell-permeable tat-tagged active SUMO peptide (Parker, Forster, & Baro, 2019) suggesting that DA permitted activity dependent SUMOylation of the HCN channel, where SUMOylation increased Ih.

1.4 Hypothesis

How does ion channel SUMOylation regulate neuronal hyperexcitability in inflammation? This work uses a rat model of complete Freund's adjuvant induced inflammation to test the hypothesis that the HCN2 ion channel is differentially SUMOylated during inflammatory pain. It also uses a heterologous expression system to examine how post-translational SUMOylation regulates HCN2 surface expression and maximal conductance. In Chapter 2, SUMOylation of HCN2 in the DRG is shown, and in chapters 2 and 3 the pattern of HCN2 SUMOylation in lumbar levels 4-6 over 1-3 days following inflammation is characterized. In Chapter 4 the mechanism of regulation of surface expression of the HCN2 channel is examined after post-translational modification by SUMO, as well proposing a common mechanism in regulating other ion channels by SUMO.

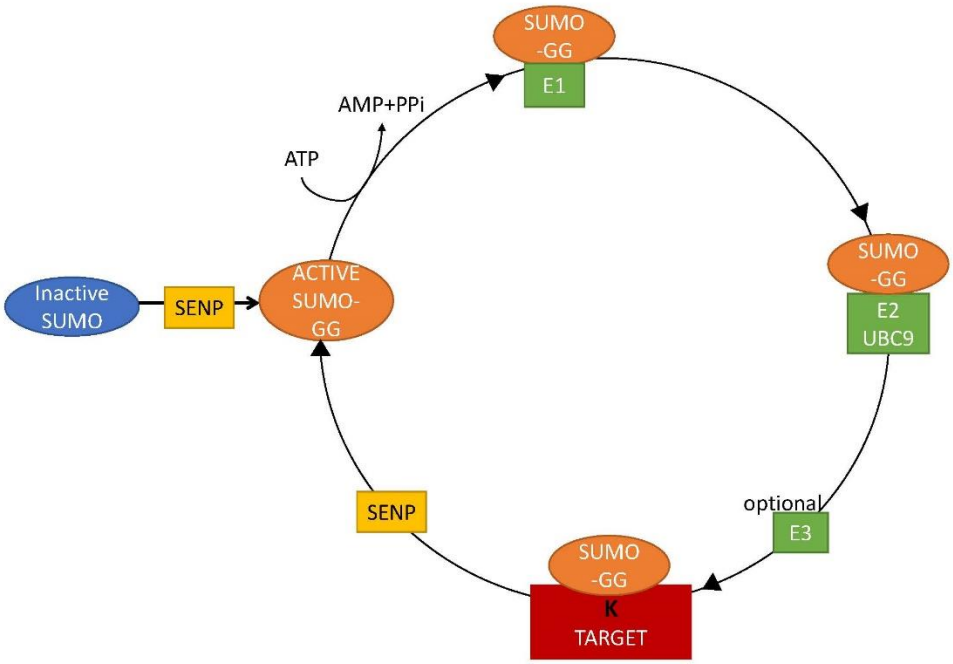

Figure 0-1-1 The SUMO Pathway

Inactive SUMO has c-terminal amino acids cleaved by SENP to expose a diglycine motif allowing it to be conjugated. Active SUMO is transferred to the E1 enzyme in an ATP dependent fashion. The sole E2 conjugating enzyme can conjugate SUMO to target lysine (K) residues on it's own, or can utilize an E3 enzyme to aid in target specificity. Figure modified from Flotho & Melchior, 2013 (Flotho & Melchior, 2013).

2 ALTERATIONS IN SUMOYLATION OF THE HYPERPOLARIZATION-ACTIVATED CYCLIC NUCLEOTIDE GATED ION CHANNEL 2 DURING PERSISTENT INFLAMMATION

Publication: **Forster LA**, Jansen LR, Rubaharan M, Murphy AZ, Baro DJ. 2020. Alterations in SUMOylation of the hyperpolarization-activated cyclic nucleotide-gated ion channel 2 during persistent inflammation. Eur J Pain. doi:10.1002/ejp.1606

Contribution Disclosure: Authors L. Forster, L-A. Jansen, AZ Murphy and D. Baro were responsible for the conception and design of the research presented. M. Rubaharan performed animal experiments. Authors L. Forster, L-A. Jansen contributed to the acquisition and analysis of the data. Authors L. Forster and L-A. Jansen contributed equally. Authors L. Forster, L-A

Jansen and D. Baro were responsible for drafting the manuscript, and all authors were involved in revising the manuscript.

2.1 Abstract

Unilateral injection of Complete Freund's Adjuvant (CFA) into the intra-plantar surface of the rodent hindpaw elicits chronic inflammation and hyperalgesia in the ipsilateral hindlimb. Mechanisms contributing to this hyperalgesia may act over multiple time courses and can include changes in ion channel expression and post-translational SUMOylation. Hyperpolarization-activated, cyclic nucleotide-gated (HCN) channels mediate the hyperpolarization-activated current, Ih. An HCN2-mediated increase in C-nociceptor Ih contributes to mechanical hyperalgesia in the CFA model of inflammatory pain. Changes in HCN2 post-translational SUMOylation and protein expression have not been systematically documented for a given DRG throughout the time course of inflammation.This study examined HCN2 protein expression and post-translational SUMOylation in a rat model of CFA-induced hindpaw inflammation. L5 DRG cryosections were used in immunohistochemistry experiments and proximity ligation assays to investigate HCN2 expression and SUMOylation, respectively, on days 1 and 3 post-CFA. Unilateral CFA injection elicited a significant bilateral increase in HCN2 staining intensity in small diameter DRG neurons on day 1 post-CFA, and a significant bilateral increase in the number of small neurons expressing HCN2 but not staining intensity on day 3 post-CFA. HCN2 channels were hyper-SUMOylated in small diameter neurons of ipsilateral relative to contralateral DRG on days 1 and 3 post-CFA. Unilateral CFA injection elicits unilateral mechanical hyperalgesia, a bilateral increase in HCN2 expression and a unilateral increase in post-translational SUMOylation. This suggests that enhanced HCN2

expression in L5 DRG is not sufficient for mechanical hyperalgesia in the early stages of inflammation and that hyper-SUMOylation of HCN2 channels may also be necessary.

2.2 Significance

Nociceptor HCN2 channels mediate an increase in Ih that is necessary for mechanical hyperalgesia in a CFA model of chronic pain, but the mechanisms producing the increase in nociceptor Ih have not been resolved. The data presented here suggest that the increase in Ih during the early stages of inflammation may be mediated by an increase in HCN2 protein expression and post-translational SUMOylation.

2.3 Introduction

Nociceptor signaling is increased in chronic pain states due, in part, to maladjustments in sensory neuron ionic conductances (Berta et al., 2017; Gold and Gebhart 2010; Pace et al., 2018; Reichling and Levine 2009). In most cases, the molecular and cellular processes leading to this peripheral sensitization are poorly understood. Mounting evidence suggests that widespread alterations in ion channel SUMOylation may contribute to conductance changes underpinning hyperalgesia associated with chronic pain.

Small ubiquitin like modifier (SUMO) is a ~12kDa peptide that is reversibly conjugated to lysine (K) residues of target proteins (Flotho and Melchior 2013). The majority of SUMOylation (~65%) occurs within identifiable consensus sequences (Hendriks et al., 2015). The phosphorylation status of a target protein often determines its ability to be SUMOylated (Dustrude et al., 2016). Additionally, the level of target protein SUMOylation depends upon the ratio of 2 opposing enzyme activities: conjugation by ubc9 and deconjugation by isopeptidases, the best studied being the SENP family (isoforms 1-7) (Kunz et al., 2018). A variety of E3 proteins can also stabilize ubc9-target protein interactions to promote SUMOylation (Flotho and

Werner 2012; Koidl et al., 2016; Werner et al., 2012). Of the 4 SUMO isoforms, SUMO1-3 are well-studied but the physiological relevance of SUMO4 is unclear (Watts 2013). SUMO2 and SUMO3 are 97% identical, and are referred to as SUMO2/3. SUMO1 shares 47% identity with SUMO2/3. Non-mutually exclusive consequences of target protein SUMOylation include: 1) prevention of other modifications that occur on the same K (Anderson et al., 2012); 2) binding to phosphoinositides (PIPs) concentrated in the trans-Golgi [PI(3)P] and plasma membrane [PI(3,4,5)P3] (Arendt et al., 2010; Hammond and Burke 2020; Kunadt et al., 2015); 3) prevention of protein-protein interactions through steric hindrance (Dustrude et al., 2016); and most commonly, 4) promotion of protein-protein interactions through binding domains in partner proteins that recognize SUMO (Psakhye and Jentsch 2012; Seifert et al., 2015).

Extracellular signaling and neuronal activity regulate the location and activity of the SUMOylation machinery and the SUMOylation status of target proteins (Craig et al., 2012; Hendriks et al., 2015; Loriol et al., 2013; Parker et al., 2019; Seifert et al., 2015). Both extracellular signals and nociceptor activity are altered during CFA-induced persistent inflammation, and a generalized increase in SUMOylation is observed in the DRG (Wang et al., 2018b). SUMOylation of TRPV1 channels is necessary for thermal hyperalgesia during CFA-induced persistent inflammation, and increasing SUMOylation by genetic knock-out of SENP1 in sensory neurons exacerbates thermal hyperalgesia during CFA-induced persistent inflammation (Wang et al., 2018b). SUMOylation of the NaV1.7 auxiliary subunit, CRMP2, prevents channel endocytosis (Dustrude et al., 2016). CRMP2 was hyper-SUMOylated in primary sensory afferents in a rat spared nerve injury model of chronic neuropathic pain, and blocking CRMP2 hyper-SUMOylation prevented mechanical and thermal hyperalgesia in this model (Dustrude et al., 2016; Dustrude et al., 2013; Francois-Moutal et al., 2018; Moutal et al.,

2017). These data suggest that nociceptor ion channel hyper-SUMOylation contributes to hyperalgesia during chronic inflammatory and neuropathic pain.

Several ion channel subunits can be SUMOylated. Existing data generally suggest that hyper-SUMOylation of ion channel subunits increases cell excitability. Enhancing K+ channel SUMOylation reduces outward currents mediated by Kv4 (Welch et al., 2019), Kv11 (Steffensen et al., 2018), Kv7 (Qi et al., 2014; Xiong et al., 2017), Kv2 (Plant et al., 2011), and K2P1 (Plant et al., 2010; Rajan et al., 2005). To our knowledge, only Kv1.5 does not fit this pattern and is increased by hyper-SUMOylation (Benson et al., 2007), however, Kv1.5 is not highly expressed in nociceptors (Zheng et al., 2019). Conversely, inward conductances are generally enhanced by hyper-SUMOylation, including conductances mediated by HCN2 (Parker et al., 2017), NaV1.2 (Plant et al., 2016), NaV1.7 (Dustrude et al., 2016) and TRPV1 (Wang et al., 2018a). While SUMO modulation of ion channels may be much more complex and vary according to which sites on the ion channel are SUMOylated (Welch et al., 2019), the data suggest a generalized increase in nociceptor ion channel SUMOylation could lead to increased excitability.

The nociceptor hyperpolarization-activated current (Ih) is increased in several models of chronic inflammatory and neuropathic pain (Djouhri et al., 2015; Emery et al., 2011; Schnorr et al., 2014; Weng et al., 2012). Ih plays a pivotal role in shaping neuronal excitability and synaptic integration by influencing several neuronal activity features including membrane potential, firing threshold, resonance frequency, temporal summation, and synaptic strength (Hutcheon and Yarom 2000; Shah 2014; Wahl-Schott and Biel 2009). Hyperpolarization-activated cyclic nucleotide gated ion channels (HCN) mediate Ih (Sartiani et al., 2017). There are four HCN isoforms. Genetic ablation of HCN2 in primary sensory afferents prevented mechanical and thermal hyperalgesia in a chronic constriction injury model of neuropathic pain (Emery et al.,

2011) and mechanical hyperalgesia in a CFA model of persistent inflammation (Schnorr et al., 2014). HCN2 protein expression increases in small DRG neurons during CFA-induced persistent inflammation (Acosta et al., 2012; Weng et al., 2012). HCN2 is SUMOylated by both SUMO1 and SUMO2/3 in the rodent brain (Parker et al., 2017). SUMOylation of HCN2 at K669 increases channel surface expression and Ih in a heterologous expression system (Parker et al., 2017). Here we investigate changes in HCN2 expression and SUMOylation in rat L5 DRG on days 1 and 3 of CFA-induced inflammation.

2.4 Materials and methods

2.4.1 Animal Ethics

Ethics approval was obtained from the Institutional Animal Care and Use Committee at Georgia State University, and all experiments were performed in compliance with Ethical Issues of the International Association for the Study of Pain and National Institutes of Health (NIH). Male Sprague-Dawley rats (Charles-River, MA) were pair-housed on a 12-hour light/dark cycle (lights on at 0700 hours) with ad libitum access to food and water.

2.4.2 CFA model and tissue preparation

60 day old male Sprague-Dawley rats were injected with 200 µl of CFA (Sigma, F5881, 1 ml contains 1 mg of heat-killed and dried *Mycobacterium tuberculosis* (strain H37Ra, ATCC 25177), 0.85 ml paraffin oil and 0.15 ml of mannide monooleate) into the mid-plantar surface of the right hindpaw. Control rats were handled, but did not receive CFA injections. Either 1 or 3 days later rats were anesthetized with 600 µl of sodium pentobarbital (390 mg/ml) in phenytoin sodium (50 mg/ml) followed by an intracardiac injection of heparin (NDC 25021-400-30, 1000 USP units/mL). Animals were perfused with ~200 ml of sodium nitrite saline followed by 350 ml of 4% paraformaldehyde. Hindpaws were measured. CFA-treated rats showed a significant

increase in ipsilateral hindpaw width relative to contralateral hindpaw width (p=0.0003). Control rats showed no change (p>0.9999). After fixation, bilateral L5 DRG were identified by counting down from T13 (located at the last rib) to L6. L5 DRG were dissected and placed into 18% sucrose at 4ºC overnight. The next day, the epineurium of each DRG was removed. DRG were embedded in 0.3% gelatin and sliced in 20 µm cryosections (Leica CM3050 S); slices were stored at 4ºC for short-term storage (<2 months), or at -80ºC for longer-term storage.

2.4.3 Antibodies and reagents

The HCN2 polyclonal rabbit antibody (Alomone, APC-030, Jerusalem) concentration used was 1:200 for Proximity Ligation Assays (PLA) and 1:250 for immunohistochemistry (IHC) experiments, 5 µg for immunoprecipitations (IP), and 1:1000 for Western Blots. A secondary Alexa 488 goat anti-rabbit was used at 1:400 (Jackson ImmunoResearch, PA) for IHC experiments. For PLA, a monoclonal mouse antibody against SUMO1 (Santa Cruz, Sc-5308) was used at 1:100, and a monoclonal mouse antibody against SUMO2/3 (Developmental Studies Hybridoma Bank, SUMO-2 8A2) was used at a concentration of 1:70 and developed by Matinus, M. at John Hopkins School of Medicine, created by the NICHD of the NIH and maintained at The University of Iowa, Department of Biology, Iowa City, IA 52242. All chemicals were obtained through Sigma-Aldrich unless otherwise stated.

2.4.4 Immunohistochemistry

A cryosection was encircled with a hydrophobic pen (Vector Laboratories), washed once with 0.1 M PBS, twice with HBSS, and incubated with 3.5 µg/mL of Wheat Germ Agglutinin CF® 594 (Biotium) to stain membranes. The cryosection was serially washed 2x times with HBSS, once with 0.1 M PBS, and permeabilized with 0.1 M PBS with 0.2% Triton X-100 (PBS-T). The cryosection was blocked for 30 minutes with 10% normal goat serum in PBS-T and

incubated with diluted anti-HCN2 in PBS-T overnight at room temperature. The cryosection was serially washed 3x times with 0.1 M PBS and incubated with Alexa 488 goat anti-rabbit diluted in 0.1 M PBS for 3 hours at room temperature. The cryosection was washed 3x in 0.1 M PBS and incubated with Dapi (300 nM) for 5 minutes. Serial washes with 0.1 M PBS were repeated 3x times, and the cryosection was mounted with ProLong Gold antifade reagent (Thermo-Fisher Scientific). All incubations were performed in a humidity chamber with a minimum volume of 17 μl per cryosection. IHC experiments were repeated on 7 experimental animals and 3 control animals for day 1, and 5 experimental animals and 4 control animals for day 3.

2.4.5 Immunohistochemistry analysis

Blind analyses were performed. DRG images were taken at 5x total magnification using an Olympus BX43 fluorescence microscope and cellSens software. Three images were taken per DRG. Images were analyzed with Photoshop. Each image was thresholded to remove the intensity of the sheath by successively increasing the tolerance of the magic wand tool. All remaining cells were considered HCN2 positive and were quantified if they showed a definitive nucleus and visible cell perimeter. Cells not meeting these criteria were ignored. All HCN2 positive cells were selected using the magnetic lasso tool and the diameter and gray mean values for each selection were obtained using the measurement feature. Cells were then classified by diameter: small ≤ 30 μm, medium 31- 40 μm, large > 40 μm. The gray mean values for all cells in each neuronal size class were averaged and taken to be the mean intensity for the size class. To measure frequency for each size class, the number of HCN2 positive cells in a class were divided by the total number of cells meeting the quantification requirements.

2.4.6 Proximity ligation assay (PLA)

Proximity ligation assays were performed using Duolink® in situ Red kit (Sigma-Aldrich) following manufacturer's instructions. Briefly, DRG cryosections were washed once in 0.1 M PBS, twice in HBSS then incubated with 5 µg/ml Wheat Germ Agglutinin-FITC (Sigma-Aldrich) to stain membranes. DRG sections were washed twice times with HBSS, once with 0.1 M PBS permeabilized with PBST. Each cryosection was blocked using 17 µl of Duolink® blocking solution for 30 minutes at 37ºC. Primary antibodies were diluted in Duolink® antibody diluent, 17 µl was applied to each cryosection and incubated overnight at room temperature. Slides were washed three times for 15 minutes in 0.1 M PBS, and incubated with Duolink® anti-mouse minus and Duolink® anti-rabbit plus secondaries for 1 hour at 37ºC. Slides were washed twice with Duolink® wash buffer A. The ligation reactions were performed at 37ºC for 30 minutes. Slides were washed twice for 2 minutes with wash buffer A. The amplification reaction time was extended by 10% to 110 minutes at 37ºC. Slides were washed twice for 10 minutes in wash buffer B then once in 0.1x wash buffer B before mounting with Vectashield non-hardening mounting medium (Vector laboratories, H-1000). Slides were sealed with clear nail varnish. All incubations were performed in a humidity chamber. All washes with PLA wash buffers A or B were performed in a minimum volume of 70 ml. PLA experiments using SUMO2/3 were repeated on 6 experimental animals and 3 control animals at 1 day, and on 7 experimental animals and 4 control animals at day 3. PLA experiments using SUMO1 were repeated on 6 experimental animals and 4 control animals at day 1, and 6 experimental animals and 3 control animals at day 3.

2.4.7 PLA analysis

Blind analyses were performed. Images were acquired with a Zeiss 700 confocal microscope using a 40x oil immersion objective within 5 days of the PLA experiment. Three sections were analyzed per DRG. For each section, a minimum of 3 z-stacks was acquired. Optical slices were 0.9 µm thick with an interval of 1 µm. Images were analyzed using the FIJI version of ImageJ. A maximum projection was created from 5 z-slices from the center of a cell. A projection contained a visible nucleus and clear cell boundaries and did not overlap with neighboring cells or fibers. Cells were outlined, and thresholded using the triangle method. The triangle method assumes that the intensity of the image is skewed in one direction and finds a value where the skew from background intensity is removed, leaving only signal above that value. Watershed analysis was performed to divide any coalesced signals. The analyze particle feature was used to obtain puncta number, mean pixel intensity and area for each punctum, as well as the area of the cell and Feret's diameter. Mean pixel intensity (MPI) of the puncta within 1 cell was obtained by a program developed by Alex Perez, to calculate the average mean puncta intensity within 1 cell and allow us to batch process large amounts of data.

2.4.8 Rat DRG membrane preparation and denaturing immunoprecipitation

Approximately 50 DRG were extracted from two rats and placed in autoclaved Dulbecco's phosphate buffer saline (DPBS) (2.7 mM KCl, 1.5 mM KH_2PO_4, 136.9 mM NaCl, 8.9 mM Na_2HPO_4) on ice. DPBS was removed and the DRG were mechanically homogenized in 250 µl of ice cold homogenization buffer [0.3 M sucrose, 10 µl of 0.1 M PBS pH 7.4, 1 mM EDTA, 1:100 protease inhibitor cocktail (Sigma, cat. P8340)] supplemented with 20 mM NEM to prevent SUMO deconjugation. The homogenate was collected and nuclei and cellular debris were pelleted by centrifugation at 14,000 RPM for 10 minutes at 4°C. The supernatant was

retained and membranes were separated by ultracentrifugation in a tabletop ultracentrifuge at 40,000g for 90 min at 4°C. The supernatant was removed, and membranes were resuspended in 20 µl of denaturing buffer [1% SDS, 50 mM Tris-HCl pH 7.4, 5 mM DTT, 1:100 protease inhibitor cocktail (Sigma, cat. P8340), 20 mM NEM]. The resuspended membrane pellet was shaken for 1 hour at 4°C to aid in the resuspension of membrane proteins. The membrane fraction was then brought to volume of 200 µl with dH_2O to dilute the SDS prior to IPs. To further denature proteins, the sample was heated at 95°C for 10 minutes. The boiled sample was cooled on ice before addition of the IP antibody. ~1000 µg of protein was used for each IP with 5 µg of rabbit anti-HCN2 or 5 µg of normal IgG for negative controls. IPs were performed using the Classic Magnetic IP/Co-IP Kit (Pierce, cat. 88804) according to the manufacturer's instructions. IP products were eluted in a volume of 50 µl.

2.4.9 Western Blot

An HCN2 IP and a negative IgG control from the same membrane preparation (see above) were run side by side in sets of 3 on the same 12% SDS-polyacrylamide gel. After electrophoresis, proteins were transferred from the gel for 2 h at 45 AMP to a PVDF membrane (Immobilon-P, cat. #IPVH00010) using a semi-dry electroblotting system (OWL). The membrane was cut into 3 pieces and each piece comprised one set of HCN2 and IgG IP products. Membranes were blocked in 5% non-fat dry milk in TBS (50 mM Tris-HCl pH 7.4, 150 mM NaCl) for 1 h at room temperature (RT). Blots were washed 1x for 10 minutes with TTBS (TBS+ 0.1% Tween20), and then primary antibodies, prepared in 1% non-fat dry milk in TTBS, were added and incubated overnight at 4°C. Each set was probed with a different antibody that recognized HCN2, SUMO1 (Cell Signaling, 4930S, 1:1500) or SUMO2/3 (Abcam, ab3742, 1:750). Blots were washed 3x for 5 minutes in TTBS and then incubated with goat anti-rabbit

alkaline phosphatase conjugated secondary antibody (Jackson ImmunoResearch, 1:4000), prepared in 1% non-fat dry milk in TTBS, for 2 h with agitation at RT. Blots were washed 3x for 10 min with TTBS. The membranes were incubated with alkaline phosphatase substrate (Biorad) for 5 minutes at RT, and then the membranes were exposed to X-ray film (MedSupply partners) and the chemiluminescent signals were visualized with a Kodak X-Omat 2000A imager.

2.4.10 Statistics

All statistical analyses were performed using GraphPad Prism. Data were tested for normality. Normal IHC data were analyzed with a one-way ANOVA followed by a Tukey's post-hoc test. Normal PLA data were analyzed with a paired t-test. Non-parametric data were analyzed with Kruskal-Wallis (KW) for IHC or Wilcoxon matched-pairs signed rank tests for PLA. All values are presented as the mean ± SEM. $p<0.05$ was considered statistically significant.

2.5 Results

2.5.1 Inflammation increases the level of HCN2 expression and the number of cells expressing HCN2

Previous studies examined the effects of cutaneous hindlimb inflammation in L5 DRG on day 7 post-CFA and in L4 DRG on days 1 and 4 post-CFA (Acosta et al., 2012; Weng et al., 2012). This study examined the results of CFA-induced inflammation in L5 DRG on days 1 and 3 post-CFA. In the experimental treatment group, CFA was injected into the right hindpaw of each adult male Sprague-Dawley rat. In the control treatment group, rats were handled but not injected. Animals were perfused on day 1 or 3 post-CFA injection/handling. L5 DRG were dissected, cryosectioned (20 µm) and used in immunohistochemistry (IHC) experiments. The specificity of the HCN2 antibody (anti-HCN2, Alomone Labs) was previously verified in a

rigorous series of experiments (Acosta et al., 2012) and was confirmed here in a series of preliminary IHC experiments using antibody that was pre-absorbed with the immunogen provided by the manufacturer. Pre-absorption greatly diminished staining intensity (Figure 1A). As described in Materials and Methods, raw images of IHC experiments (Figure 1B, left panel) were processed, and HCN2-positive neurons were identified and circled (Figure 1B, right panel). Cells were classified into three groups according to diameter: small (≤ 30 μm), medium (30 μm < x <40 μm), and large (> 40 μm). HCN2 immunoreactivity (IR) was measured as the mean pixel intensity for each cell and as the frequency of HCN2 expressing cells. The number of cells expressing HCN2 was quantified for each of the three cell sizes by dividing the number of HCN2 positive cells in each size category by the total number of cells in the DRG section (HCN2-positive and -negative) and multiplying by 100. This was termed frequency.

The mean pixel intensities measured on day 1 post-CFA were compared between control and experimental DRG (Figure 2B). The average mean pixel intensity for small diameter neurons in experimental animals significantly increased by ~50% in both contralateral (21.3 ± 1.4) and ipsilateral (22.8 ± 1.7) relative to control DRG (14.9 ± 0.8). The average mean pixel intensity for medium diameter neurons increased by ~40% in experimental (ipsilateral, 25.4 ± 2.6; contralateral, 23.2 ± 1.5) relative to control DRG (18.0 ± 1.3). The increase was statistically significant only for the ipsilateral DRG (Figure 2 legend). There were no significant differences in the average mean pixel intensity between large diameter neurons (contralateral, 25.1 ± 2.1; ipsilateral, 28.3 ± 3.8; control, 20.5 ± 2.2). A comparison of the mean frequency showed that there were no significant differences between control and experimental animals or between ipsilateral and contralateral DRG for any neuronal size class (Figure 2C). In general, ~55-65% of all DRG neurons examined here expressed HCN2, and small-diameter neurons had the greatest

number of HCN2-positive cells (contralateral: small, 37.3 ± 4.8%; medium, 12.4 ± 1.8% large, 13.1 ± 2.0%) (ipsilateral: small, 34.1 ± 5.6%; medium, 13.8 ± 2.3%; large, 15.9 ± 4.4%) (control: small, 22.3 ± 5.7%; medium, 14.2 ± 2.5%; large, 17.2 ± 1.9%).

The situation changed by day 3 post-CFA such that there was a significant increase in the number but not intensity of cells expressing HCN2 (Figure 3). The average mean pixel intensities were no longer significantly different for any size class (Figure 3B), although there was still a slight elevation in contralateral (small, 21 ± 3.1; medium, 23.6 ± 3.7; large, 26.1 ± 4.7) and ipsilateral DRG (small, 19.6 ± 2.5; medium, 22.4 ± 3.5; large, 24.8 ± 4.3) relative to control DRG (small, 15 ± 1.9; medium, 16.9 ± 2.1; large, 18.7 ± 2.1). On the other hand, the number of cells expressing HCN2 significantly increased in small and medium but not large diameter neurons in experimental relative to control animals (Figure 3C). Mean frequency in both contralateral (small, 35.8 ± 8.3%; medium, 17.2 ± 1.7%) and ipsilateral DRG (small, 30.6 ± 3.5%; medium, 15.8 ± 1.4%) were significantly increased relative to control DRG (small, 11.9 ± 2.4%; medium, 9.5 ± 0.7%), but were not significantly different from one another.

In sum, unilateral hindpaw inflammation initially produced a significant bilateral increase in HCN2 protein expression in small diameter neurons. CFA-induced inflammation also produced a significant ipsilateral increase in medium diameter neurons. As inflammation progressed, expression levels returned back toward normal, but the number of small and medium diameter cells expressing HCN2 increased bilaterally.

2.5.2 HCN2 is SUMOylated in the rat DRG

SUMOylation of HCN2 channels has never been examined in DRG neurons. To determine if HCN2 channels were SUMOylated in DRG neurons, denaturing immunoprecipitation (IP) experiments were performed using DRG membrane preparations and an antibody against HCN2

followed by western blot experiments with antibodies against HCN2, SUMO2/3 and SUMO1. The experiment was repeated 3 times (i.e. 6 rats, see Materials and Methods). A representative experiment shows that all 3 antibodies recognized the same appropriately sized ~100kD band (Figure 4). This band was not observed in IP experiments using a non-specific rabbit IgG on the same membrane preparation. In order to prevent non-covalent interactions between proteins, i.e. co-IP, the membrane preparations were denatured with a high concentration of SDS (1%) and high heat treatment (95°C for 10min) prior to the IPs (see Materials and Methods). These data indicate that SUMO1 and SUMO2/3 are covalently linked to HCN2 □-subunits in the rat DRG. Next, in situ proximity ligation assays (PLA) were used to examine HCN2 channel SUMOylation in individual DRG neurons. Preliminary pre-absorption experiments on cryosectioned DRG confirmed the specificities of the SUMO1 (anti-SUMO1) and SUMO2/3 (anti-SUMO2/3) antibodies (Figure 5A). HCN2 channel SUMOylation was examined using anti-HCN2 and anti-SUMO2/3 in PLA on cryosectioned DRG (experimental). Primary antibodies were omitted in control PLA. SUMOylated HCN2 channels appeared as fluorescent puncta in confocal optical sections (Figure 5B, upper panels). Punctum area and intensity varied, which may reflect differences in the number of HCN2 channels represented by a punctum, e.g. solitary vs. clustered channels, and/or the extent of their SUMOylation. Puncta number and punctum mean pixel intensity were used as measures of the number of SUMOylated channels and the extent of channel SUMOylation, respectively. To measure HCN2 channel SUMOylation in a single cell, a confocal projection representing 5, ~1 µm optical sections from the center of a cell was obtained. Note that this represents ~ 1/4 (small) to 1/8 (large) of the volume of a neuron and that surface sections will be excluded, i.e., all plasma membrane staining lies along the perimeter of the cell. A cell was outlined and automatically thresholded to eliminate background (Figure

5B, bottom panels). ImageJ was then used to measure the area of the cell as well as the number and intensity of puncta from within the circled region. Control and experimental PLA were performed on alternating sections of L5 DRG. DRG from 3 animals were analyzed. Results showed significantly more puncta/µm2 in experimental vs. control treatment groups (Figure 5C). These data indicated that HCN2 channels were decorated with SUMO2/3 in rat L5 DRG and that this method could be used to examine HCN2 channel SUMOylation in individual neurons.

2.5.3 Significantly more HCN2 SUMO2/3 conjugation is observed in small diameter neurons from ipsilateral DRG on day 1 but not on day 3 post-CFA

In order to test if HCN2 channels were hyper-SUMOylated during CFA-induced inflammation, CFA was injected into the right hindpaw of adult male rats. Animals were perfused 1 or 3 days post-CFA. Bi-lateral L5 DRG were dissected and cryosectioned. In situ PLA was performed on the cryosections using anti-HCN2 and anti-SUMO2/3. Control animals were handled but not injected. HCN2 channels were decorated with SUMO2/3 in small, medium and large neurons from ipsilateral and contralateral DRG 1 day post-CFA (Figure 6A). The number of puncta per µm2 was determined for the 3 size classes of neurons. Comparisons of control and experimental animals showed no significant differences and are not reported here. On the other hand, paired comparisons between contralateral and ipsilateral DRG from the same experimental animal revealed significant differences. Most likely, differences were revealed in the latter analyses because biological variability was reduced by intra-animal comparison.

A significant ~25% increase in puncta number was observed in small neurons from ipsilateral relative to contralateral DRG (Figure 6B). No significant differences were observed in medium or large diameter neurons in contralateral vs. ipsilateral DRG (Figure 6B). Paired t-tests on left vs. right DRG in the control treatment group indicated no significant differences (small,

0.24 ± 0.04 vs. 0.23 ± 0.03, p=0.5389; medium, 0.23 ± 0.04 vs. 0.21 ± 0.06, p=0.6006; large, 0.26 ± 0.03 vs. 0.23 ± 0.04, p=0.6340; n=3 animals). Punctum intensity was divided by punctum area to obtain the mean pixel intensity per punctum, here termed puncta intensity. The average puncta intensity was calculated for each cell. Average puncta intensity was not significantly different between contralateral vs. ipsilateral DRG neurons for any size class (Figure 6C). Control animals showed no differences between left vs. right DRG (small, 47.82 ± 2.74 vs. 41.80 ± 4.32, p=0.25; medium, 47.72 ± 2.79 vs. 42.68 ± 4.77, p=0.1694; large, 48.96 ± 2.19 vs. 42.98 ± 5.32, p=0.2730; n=3).

Analyses were performed for animals perfused at 3 days post-CFA (Figure 7A). There were no significant differences in HCN2-SUMO2/3 puncta number (Figure 7B) or intensity (Figure 7C) between contralateral vs. ipsilateral DRG neurons from experimental animals for any neuronal size class. There were also no significant differences between left vs. right DRG in the control treatment group for either puncta number (small, 0.38 ± 0.08 vs. 0.39 ± 0.11, p=0.8946; medium, 0.43 ± 0.11 vs. 0.36 ± 0.12, p=0.2152; large, 0.50 ± 0.10 vs. 0.41 ± 0.11, p=0.0708; n=4) or puncta intensity (small, 71.23 ± 17.97 vs. 61.01 ± 12.95, p=0.1466; medium, 69.65 ± 16.31 vs. 61.14 ± 12.65, p=0.1181; large, 69.74 ± 17.88 vs. 61.03 ± 12.82, p=0.1987; n=4).

In sum, the number of HCN2 channels decorated with SUMO2/3 was transiently increased by ~25% in small neurons from ipsilateral relative to contralateral DRG on day 1 but not 3 post-CFA. There were no significant changes in the extent of channel SUMOylation.

2.5.4 Conjugation of SUMO1 to HCN2 channels was reduced in medium and large diameter DRG neurons on 1 day post-CFA, and increased in small neurons on day 3 post-CFA

PLA experiments were repeated for experimental and control animals except that anti-SUMO1 was used. HCN2 channels decorated with SUMO1 were observed on day 1 post-CFA (Figure 8). Paired t-tests indicated that the mean number of HCN2-SUMO1 puncta was not significantly different in small neurons from contralateral vs. ipsilateral DRG, but puncta number was significantly reduced by ~30% in medium and large diameter neurons from ipsilateral relative to contralateral DRG (Figure 8B). There were no significant differences in mean puncta number between left vs. right DRG from control animals for any cell size (small, 0.35 ± 0.06 vs. 0.34 ± 0.09, p=0.7672; medium, 0.31 ± 0.05 vs. 0.27 ± 0.08, p=0.3750; large, 0.39 ± 0.12 vs. 0.31 ± 0.07, p=0.2184; n=4). There were no significant differences in puncta intensity between contralateral vs. ipsilateral DRG for any neuronal size (Figure 8C). There were no significant differences in puncta intensity for left vs. right DRG from control animals (small, 55.22 ± 10.11 vs. 51.25 ± 7.35, p=0.6250; medium, 55.83 ± 10.77 vs. 53.47 ± 6.94, p=0.8750; large, 58.5 ± 11.15 vs. 55.65 ± 5.70, p>0.9999; n=4).

SUMO1 conjugation to HCN2 channels was examined 3 days post-CFA (Figure 9). HCN2-SUMO1 puncta number was significantly increased by ~27% in small neurons from ipsilateral relative to contralateral DRG (Figure 9B). There were no significant differences in medium or large diameter neurons in ipsilateral relative to contralateral DRG (Figure 9B). There were no significant differences in puncta number for left vs. right DRG from control animals (small, 0.28 ± 0.02 vs. 0.28 ± 0.08, p=0.9861; medium, 0.23 ± 0.01 vs. 0.27 ± 0.10, p=0.7612; large, 0.31 ± 0.03 vs. 0.33 ± 0.10, p=0.8797; n=3). As in all other cases, there were no significant differences in puncta intensity for contralateral vs. ipsilateral DRG for any cell size (Figure 9C).

Control animals also showed no differences in left vs. right DRG puncta intensity (small, 65.55 ± 16.13 vs. 48.64 ± 4.701, p=0.3539; medium, 71.14 ± 23.03 vs. 48.51 ± 3.7, p=0.3559; large, 67.96 ± 18.46 vs. 50.43 ± 2.37, p=0.3077; n=3).

In sum, SUMO conjugation to HCN2 channels was increased in small diameter neurons from ipsilateral DRG on days 1 and 3 post-CFA. Dynamic changes varied with the SUMO isoform. Whereas conjugation to HCN2 channels with SUMO2/3 increased on day 1, conjugation with SUMO 1 increased on day 3. In medium and large diameter neurons, SUMO1 conjugation to HCN2 channels was transiently reduced on day 1 post-CFA.

2.6 Discussion

An HCN2-mediated increase in I_h is necessary for mechanical hyperalgesia experienced during persistent inflammation. The present study investigated how HCN2 channels in L5 DRG were altered during early stages of inflammation. The major finding of this study was that an increase in HCN2 protein expression was not sufficient for mechanical hyperalgesia. Moreover, HCN2 channel SUMOylation was significantly increased in small diameter neurons and decreased in medium and large diameter neurons in ipsilateral relative to contralateral DRG.

2.6.1 HCN2 protein expression and SUMOylation of HCN2 channel complexes are increased in small diameter neurons during CFA-induced inflammation

Persistent inflammation is thought to be a primary mechanism whereby an acute injury leads to a chronic pain state (Dubin and Patapoutian 2010; Emery et al., 2012; Pinho-Ribeiro et al., 2017; Tsantoulas et al., 2016; Xu and Yaksh 2011). CFA administration elicits persistent inflammation (Millan et al., 1988; Stein et al., 1988). In rats, a unilateral, intraplantar CFA injection significantly reduces the mechanical force necessary to produce ipsilateral paw withdrawal 1 to 14 days after inflammation. The observed mechanical hyperalgesia is not present in the

contralateral paw (Goff et al., 1998; Hurley and Hammond 2000; Millan et al., 1988; Schnorr et al., 2014; Stein et al., 1988; Weng et al., 2012). The cutaneous inflammatory response is resolved by 17-21 days (Li et al., 2005). Inflammation alters several ionic currents in sensory neurons, including Ih, and specifically increases the excitability of C-fiber nociceptors (Herrmann et al., 2017; Pace et al., 2018; Takeda et al., 2014; Weng et al., 2012; Zemel et al., 2018). Ih increases the excitability of DRG sensory neurons by limiting membrane hyperpolarization and facilitating depolarization (Yagi and Sumino 1998). CFA-induced inflammation triggers an increase in the activation kinetics and maximal conductance of nociceptor Ih (Djouhri et al., 2015). Injections of pharmacological agents to block Ih as early as 1 day after CFA-induced inflammation prevent hyperalgesia (Schnorr et al., 2014; Weng et al., 2012).

The mechanism(s) producing a CFA-induced increase in nociceptor Ih is unknown. In rat DRG sensory neurons, Ih is mediated largely by HCN isoforms 1 and 2, and to a lesser extent, HCN3 (Gao et al., 2012; Kouranova et al., 2008; Weng et al., 2012), which can form homo- and hetero-tetramers. Channel complexes can also contain auxiliary subunits (Piskorowski et al., 2011; Santoro et al., 2011; Santoro et al., 2009; Saponaro et al., 2014). Genetic ablation of HCN2 from DRG sensory neurons attenuated mechanical hyperalgesia measured on day 3 post-CFA (Schnorr et al., 2014). Hindlimb inflammation elicited a transient increase HCN2 IR in small diameter neurons in ipsilateral rat L4 DRG on day 1 but not day 4 post-CFA, relative to uninjected controls (Acosta et al., 2012). A significant decrease was also observed in large diameter neurons on day 4 post-CFA (Acosta et al., 2012). A second study examined the effects of hindlimb inflammation on ipsilateral L5 DRG neurons 7 days post-CFA; it showed a significant increase in HCN2 IR in small diameter neurons and a significant increase in the number of small and medium diameter neurons expressing HCN2, but no change in HCN1 or

HCN3 expression relative to uninjected controls (Weng et al., 2012). The current study shows a significant bilateral increase in HCN2 IR in small and medium diameter L5 DRG neurons on day 1 post-CFA relative to uninjected controls. In addition, there is a significant bilateral increase in the number of cells expressing HCN2 on day 3 post-CFA. The bilateral changes were unexpected since CFA injection was unilateral. Unilateral peripheral nerve damage can result in unilateral hyperalgesia but bilateral changes in DRG cytokine and cytokine receptor mRNA and protein expression (Brazda et al., 2009; Dubovy et al., 2013; Jancalek et al., 2010; Jancalek et al., 2011) and NaV1.8 mRNA (Oaklander and Belzberg 1997). Such changes are thought to be due to a generalized inflammatory response. Several mechanisms could underlie bilateral effects (Koltzenburg et al., 1999).

Our data suggest that an increase in HCN2 protein expression is not sufficient for mechanical hyperalgesia because, unilateral injection of CFA produces unilateral hyperalgesia (Hurley and Hammond 2000; Stein et al., 1988) but a bilateral increase in HCN2 protein expression (Figures 2 & 3). Altered expression of additional ion channels and/or other proteins may be necessary for hyperalgesia (Pace et al., 2018). Alternatively, additional post-translational modifications to HCN2 channels may be required. Recent studies demonstrated that enhanced ion channel SUMOylation can contribute to hyperalgesia in models of chronic pain (Francois-Moutal et al., 2018; Moutal et al., 2017; Wang et al., 2018a). Post-translational SUMOylation can regulate ion channel biophysical properties, trafficking and surface expression (Benson et al., 2007; Chamberlain et al., 2012; Dai et al., 2009; Dustrude et al., 2016; Martin et al., 2007; Parker et al., 2017; Plant et al., 2010; Plant et al., 2016; Plant et al., 2012; Qi et al., 2014; Rajan et al., 2005; Steffensen et al., 2018; Wang et al., 2018b; Welch et al., 2019; Xiong et al., 2017). Our data indicate that unilateral CFA injection produces unilateral hyper-SUMOylation of HCN2

in small diameter neurons from L5 DRG. HCN2 SUMOylation produces an increase in channel surface expression and Ih in a heterologous expression system (Parker et al., 2017), but the effect of the enhanced DRG HCN2 SUMOylation observed here is unknown.

Because HCN2 □-subunits are SUMOylated in the DRG (Figure 4), the most parsimonious interpretation of the PLA experiments is that SUMOylation of HCN2 □-subunits is enhanced during inflammation. However, in order to produce a fluorescent punctum in a PLA, the HCN2 and SUMO proteins need to be within 40nM of one another so that their antibodies can interact to generate a punctate fluorescent signal. HCN channels can exist as heterotetramers in multiprotein complexes with auxiliary proteins like TRIP8b (Santoro et al., 2009) and MINT (Kimura et al., 2004), which also have predicted SUMOylation sites. This means that the increase in PLA puncta number could also represent increased SUMOylation of other HCN isoforms and/or auxiliary subunits that make-up the HCN2 channel complex. Indeed, it is well documented that a cell stressor can evoke group SUMOylation, whereby several proteins in a physically linked group are non-specifically SUMOylated, as opposed to targeting one specific protein within the group (Jentsch and Psakhye 2013).

The increase in SUMOylated HCN2 channel complexes is a modest ~27%, but it is fairly common for low levels of SUMOylation to exert substantial regulatory effects (Benson et al., 2007; Flotho and Melchior 2013). Nevertheless, there are examples of much greater increases in SUMOylation, for example, CRMP2 SUMOylation in the sciatic nerve, spinal dorsal horn and glabrous skin appears to increase by as much as ~300% in a rat model of neuropathic pain (Moutal et al., 2017). Small diameter DRG neurons can be classified into at least six cell types (Li et al., 2016; Usoskin et al., 2015), and it is possible that a specific nociceptor cell type representing a small fraction of the population shows a much larger increase in HCN2

SUMOylation. Since the cell type(s) exhibiting the CFA-induced enhancement of HCN2 protein expression and HCN2 channel SUMOylation were not identified, we cannot conclude that increased expression and SUMOylation are coincident in the same cell or that the inflammation-induced increase in nociceptor Ih depends upon a 2-step process.

There are four SUMO isoforms and three were examined in this study. Conjugation of SUMO2/3 vs. SUMO1 to HCN2 channel complexes was differentially regulated as inflammation progressed: SUMO2/3 but not SUMO1 conjugation to HCN2 channels was significantly increased on day 1 post-CFA, and the opposite was true on day 3 post-CFA. The sole SUMO conjugating enzyme, ubc9, does not show a preference for SUMO isoforms and interacts with a similar affinity for all isoforms (Knipscheer et al., 2007), but the SENP family of SUMO isopeptidases that mediate SUMO deconjugation can exhibit SUMO isoform specificity and can be differentially localized by post-translational modification (Kunz et al., 2018). Likewise, diverse E3 proteins that stabilize interactions between ubc9 and its targets can also exhibit SUMO isoform specificity (Cappadocia et al., 2015; Koidl et al., 2016; Tatham et al., 2005). Together, these data support the emerging ideas that inflammatory mediators regulate the nociceptor SUMOylation machinery and that this regulation may effect alterations in multiple ionic conductances during nociceptor sensitization.

2.6.2 SUMOylation of HCN2 channel complexes is decreased in medium and large diameter neurons during CFA-induced inflammation

SUMO1 conjugation to HCN2 channel complexes was transiently decreased in medium and large diameter neurons from ipsilateral L5 DRG on day 1 of inflammation. This regulation could potentially contribute to hyperalgesia which peaks on day 1 (Millan et al., 1988; Stein et al., 1988). Medium and large neurons could contribute directly to hyperalgesia as nociceptors

(Dubin & Patapoutian, 2010; Nagi et al., 2019), or they could indirectly influence nociceptor activity through presynaptic mechanisms and/or other circuit effects (Braz, Solorzano, Wang, & Basbaum, 2014; Guo & Hu, 2014; Mendell, 2014). It will be important to identify these neurons and how HCN2 channel deSUMOylation regulates their activity.

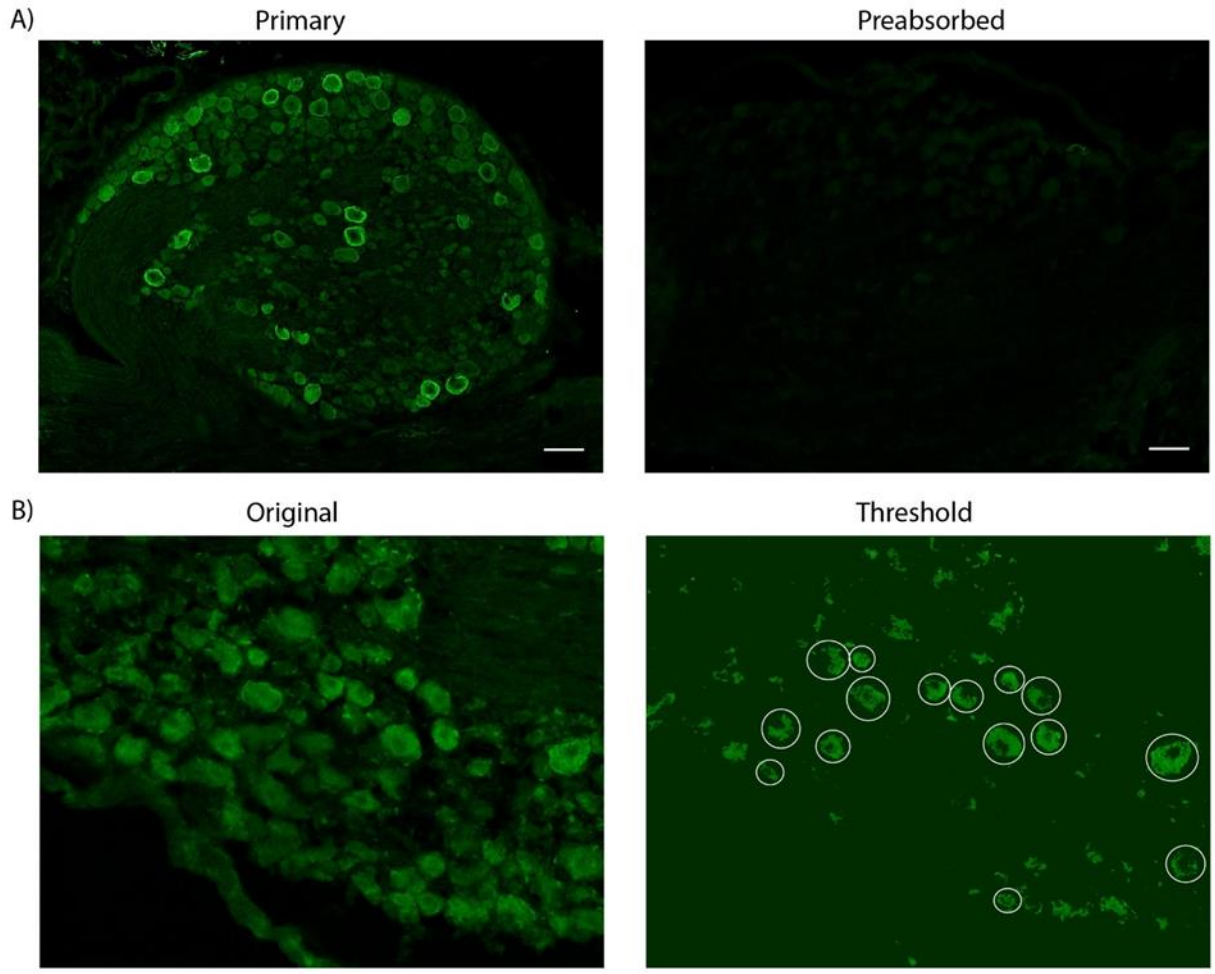

Figure 2-1 Validation of anti-HCN2 and quantification of HCN2 positive cells.

A) Representative IHC. Experiments using antibody and pre-absorbed antibody show anti-HCN2 specificity. Scale bars are 100 μm. **B) Representative analysis.** Sections show cells

before and after thresholding. Cells having an obvious nucleus and plasma membrane, and therefore meeting the criteria for analysis, are circled.

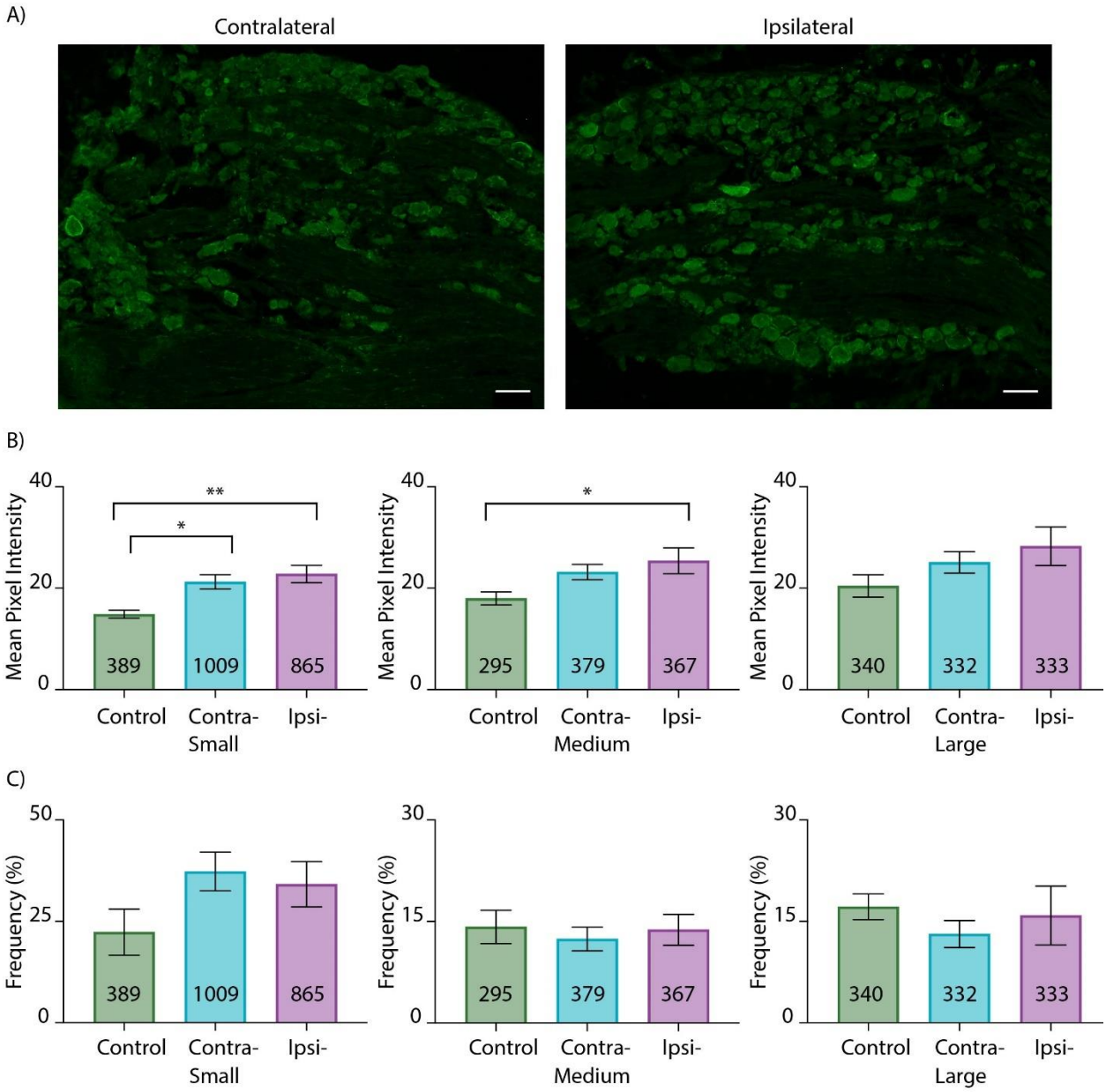

Figure 2-2 CFA-induced inflammation alters HCN2 protein expression on 1 day post-CFA.

A) Representative images of HCN2 IR in contralateral and ipsilateral L5 sections 1 day post-CFA injection. Scale bars are 100 μm. **B) HCN2 expression is elevated in experimental compared to control DRG.** Average mean pixel intensities ± SEMs are plotted for three size classes of DRG neurons. A one way ANOVA with a Tukey's post-hoc test that makes all possible comparisons shows HCN2 IR is significantly elevated in small cells for experimental vs. control treatment groups ($F(2,17)=8.468$; $p=0.0028$). Asterisks indicate which two-way comparisons were significant. A one way ANOVA with a Tukey's post-hoc shows HCN2 IR is significantly elevated in medium cells for ipsilateral vs. control treatment groups ($F(2,17)=3.748$; $p=0.0448$). Asterisks indicate which pairwise comparisons were significant: *, $p<0.05$; **,

$p<0.01$. A one way ANOVA shows that HCN2 IR was not significantly different between large cells from experimental and control DRG ($F(2,17)=1.794$; $p=0.1963$). **C) HCN2 frequency is unaltered 1 day post-CFA injection.** Bar plots of the frequency of HCN2 positive neurons in each size category ([HCN2-expressing cells per category ÷ total number of cells in all categories] x 100). Statistical tests show there were no significant differences between experimental and control animals for any cell type (small; $KW(2,17)=3.603$; $p=0.1682$; medium; $F(2,17)=0.1860$; $p=0.8317$; large; $KW(2,17)=1.999$; $p=0.3824$).

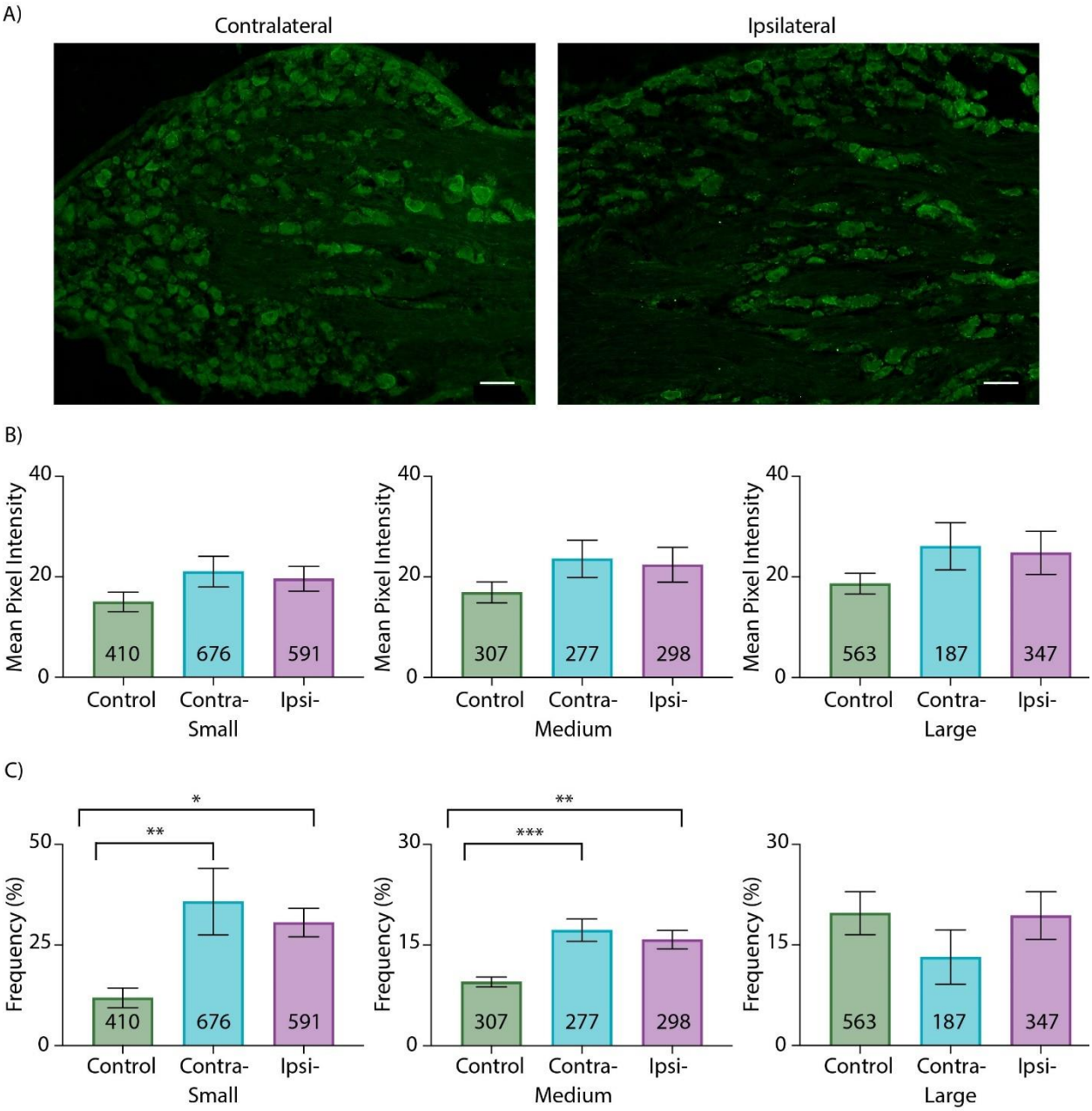

Figure 2-3 HCN2 protein expression is altered on day 3 post-CFA.
A) Representative images of HCN2 IR in contralateral and ipsilateral L5 sections 3 days post-CFA. Scale bars are 100 μm. **B) The intensity of HCN2 IR is unaltered 3 days post-CFA**. Bar plots of mean pixel intensity. One way ANOVAs show no significant differences between treatment groups for any size category (small; $F(2,15)=1.893$; $p=0.1849$; medium; $F(2,15)=1.667$; $p=0.2220$; large; $F(2,15)=1.499$; $p=0.2550$). **C) HCN2 frequency is significantly increased in small and medium diameter neurons in experimental compared to control animals.** Bar plots of the frequency of HCN2 IR in each size class ([HCN2-expressing cells per category ÷ total number of cells in all categories] x 100). A one way ANOVA with a Tukey's post-hoc test shows HCN2 frequency is significantly elevated in small

cells for experimental vs. control treatment groups ($F(2,15)=8.022$; $p=0.0043$). Asterisks indicate which two-way comparisons were significant. A one way ANOVA with a Tukey's post-hoc test shows HCN2 frequency is significantly elevated in medium cells for experimental vs. control treatment groups ($F(2,15)=13.51$; $p=0.0004$). Asterisks indicate significant differences in pairwise comparisons: *, $p<0.05$; **, $p<0.01$; ***, $p<0.001$. A Kruskal-Wallis test shows HCN2 frequency is not significantly different between large cells for experimental vs. control treatment groups ($KW(2,15)=3.058$; $p=0.2251$).

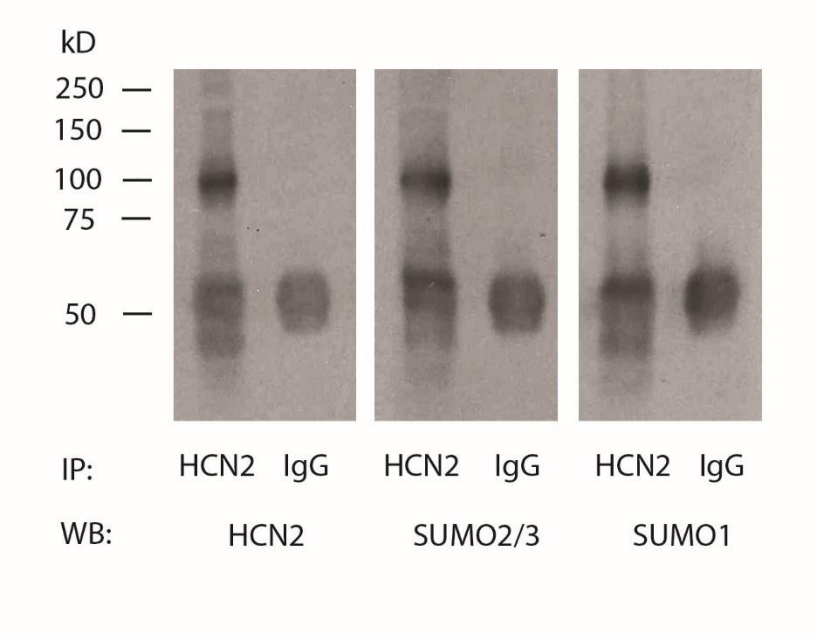

Figure 2-4 HCN2 is SUMOylated in rat DRG.
Denaturing immunoprecipitation (IP) experiments were performed on a DRG membrane preparation with an antibody against HCN2 or IgG (control). IP products from 1 membrane preparation were run in triplicate on an SDS-polyacrylamide gel followed by western blotting (WB). The blot was cut into 3, and probed for HCN2, SUMO2/3 and SUMO1. The experiment was repeated using 3 different DRG membrane preparations. A representative result from one experiment is shown. All 3 WB antibodies recognized the same ~100kD protein in the HCN2 IP product but not the IgG IP product. The data indicate that SUMO1 and SUMO2/3 are covalently linked to HCN2

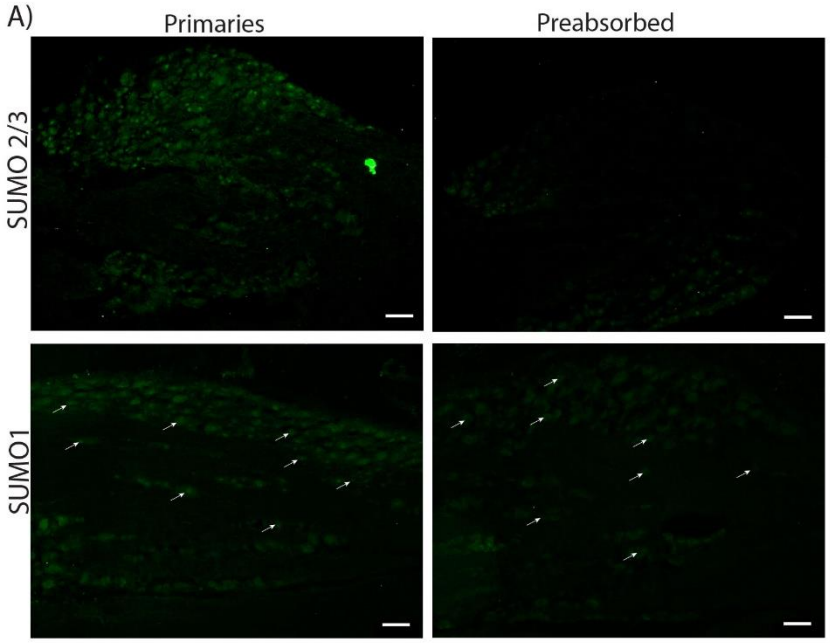
A)
Primaries
Preabsorbed
SUMO 2/3
SUMO1

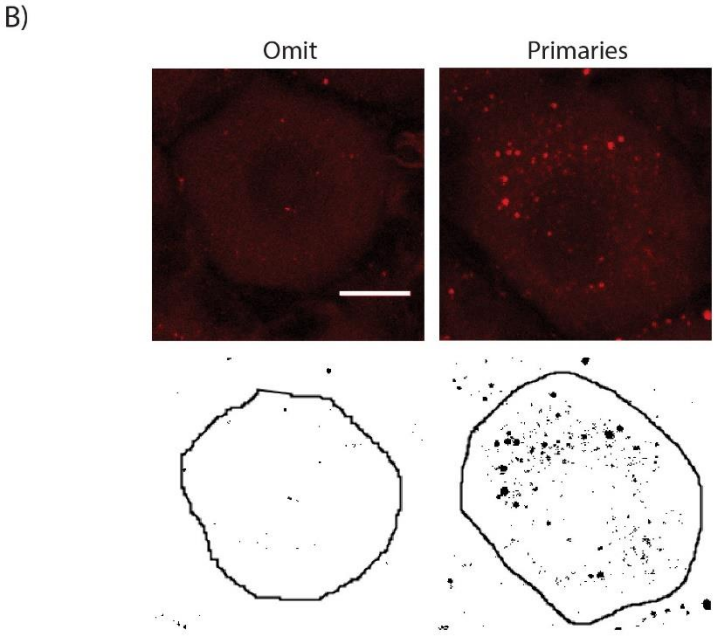
B)
Omit
Primaries

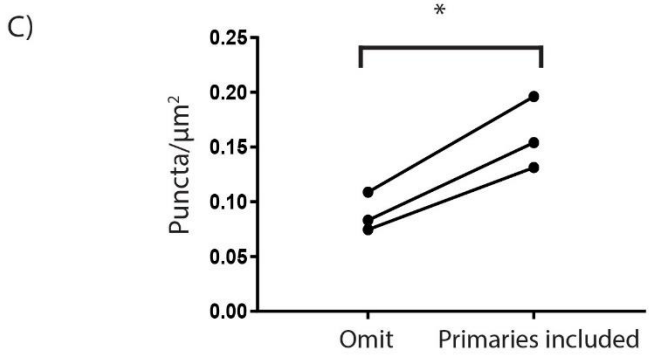
C)
*
Puncta/µm²
0.25
0.20
0.15
0.10
0.05
0.00
Omit
Primaries included

Figure 2-5 Measuring HCN2 channel SUMOylation.

A) Verification of SUMO antibodies. Antibodies were (right) or were not (left) preabsorbed with the corresponding peptide for SUMO2/3 (upper panel) or SUMO1 (lower panel). SUMO is predominately expressed in nuclei. Note the loss of nuclear staining following preabsorption, e.g. white arrows in bottom panel. Scale bars are 100 µm. **B) Method for quantifying HCN2 channel SUMOylation.** In situ PLA was performed on DRG cryosections with (experimental) or without (control) antibodies against SUMO2/3 and HCN2. Upper panel shows a 5µm projection of confocal optical slices through representative cells from control and experimental treatment groups. Each image represents a projection of 5 slices in continuous succession that together encompass the center of the cell. Each optical section is 0.9 µm with a z-stack interval of 1 µm. Note that the red puncta indicating SUMOylated HCN2 channels were largely absent when antibodies were omitted. Scale bar is 10 µm. The cells were circle and thresholded, and the resulting image is shown in the lower panel. Black puncta within the circled region were counted using the analyze particle tool on imageJ and normalized by the area (μm^2) of the circle. Note that all black puncta, regardless of size were counted. **C) HCN2 channels are SUMOylated in DRG neurons.** Plots of puncta per μm^2 show there are significantly more puncta when primary antibodies for HCN2 and SUMO2/3 were included (0.08 ± 0.01 vs. 0.16 ± 0.02, $p=0.0149$, paired t-test, n=3, 70 and 62 cells analyzed in total). The lines indicate that the cells were from the same experiment, i.e. alternate sections from a single DRG on the same slide receiving the same PLA reagents and treated in an identical fashion.

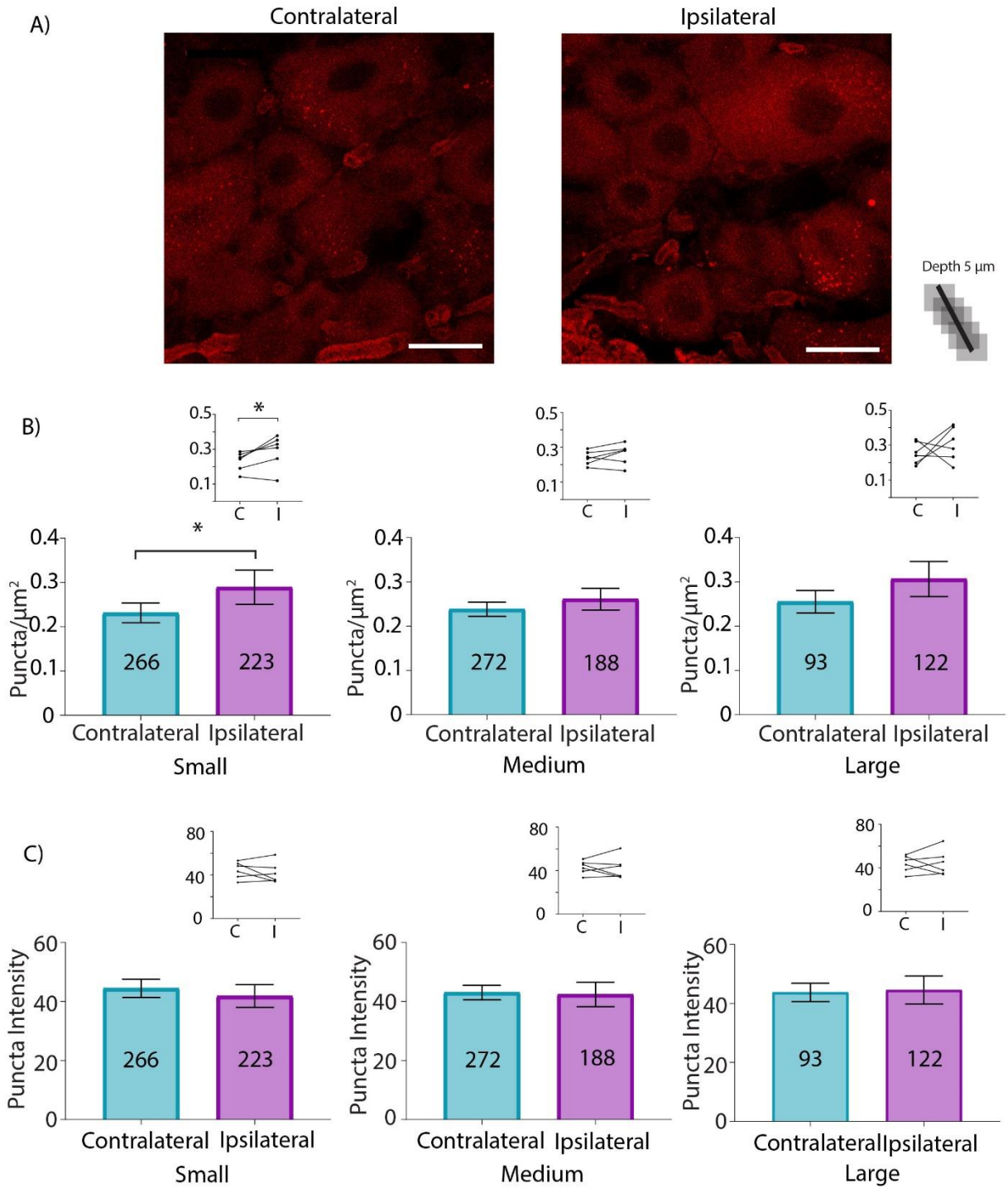

Figure 2-6 SUMO2/3 conjugation to HCN2 channels is increased in small diameter neurons from ipsilateral relative to contralateral DRG at 1 day post-CFA.
A) Representative PLA. Scale bars are 25 µm. Note that this image provides an overview, but for the purpose of quantification, individual projections were made for each cell, e.g. Figure 4B.
B) Plots of mean number of puncta/µm2 for all DRG from 6 CFA treated animals on day 1 post-CFA. The number inside the bar represents the total number of cells analyzed. Inset: Each

line compares the means for contralateral and ipsilateral DRG from one animal. Paired t-tests indicate the number of puncta significantly increased for small but not medium or large neurons in ipsilateral compared to contralateral DRG (small, 0.23 ± 0.02 vs. 0.29 ± 0.04, p=0.0499; medium, 0.24 ± 0.02 vs. 0.26 ± 0.02, p=0.2120; large, 0.26 ± 0.03 vs. 0.31 ± 0.04, p=0.4259. **C) Plots of mean puncta intensity on day 1 post-CFA.** Paired t-tests indicate mean puncta intensities were not significantly different between ipsilateral and contralateral DRG for any size category (small, 44.47 ± 3.1 vs. 41.86 ± 3.9, p=0.4495; medium, 43.06 ± 2.5 vs. 42.43 ± 4.1, p=0.8503; large, 43.74 ± 3.1 vs. 44.51 ± 4.8, p=0.8518).

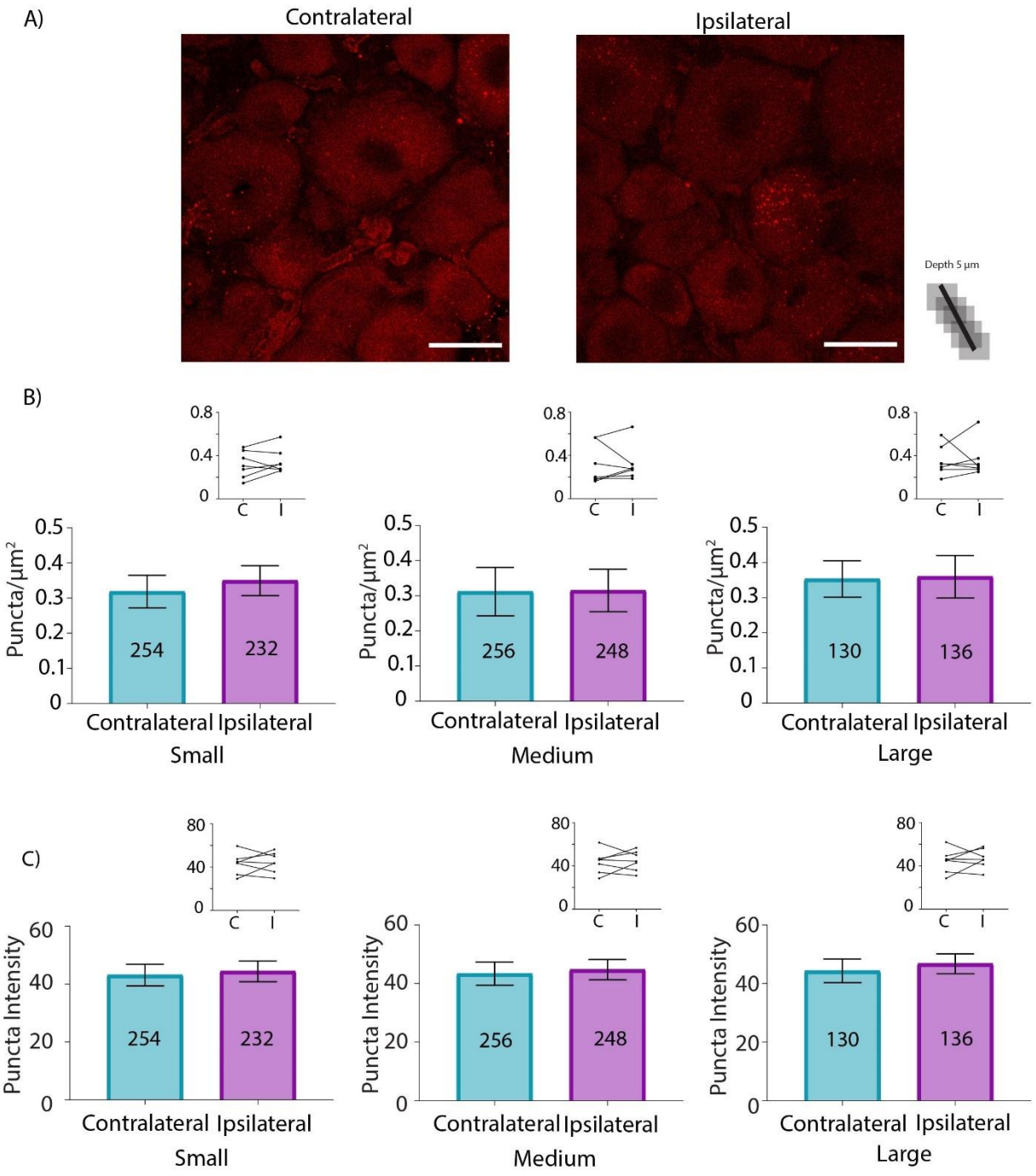

Figure 2-7 SUMOylation of HCN2 channels by SUMO2/3 does not change 3 days post-CFA.

A) Representative PLA. Scale bars are 25 µm. Note that this image provides an overview, but for the purpose of quantification, individual projections were made for each cell, e.g. Figure 4B.

B) Plots of mean number of puncta/µm2 for all DRG from 7 CFA treated animals on day 3 post-CFA. The number inside the bar represents the total number of cells analyzed. Inset: Each line compares means for contralateral and ipsilateral DRG from one animal. Wilcoxon matched-

pair tests indicate no significant difference in puncta number for small, medium or large diameter cells (small, 0.32 ± 0.05 vs. 0.35 ± 0.04, p=0.375; medium, 0.31 ± 0.07 vs. 0.32 ± 0.06, p=0.5781; large, 0.35 ± 0.05 vs. 0.36 ± 0.06, p=0.8125). **C) Plots of mean puncta intensity on day 3 post-CFA**. Paired t-tests indicate mean puncta intensities were not significantly different for any size category in ipsilateral compared to contralateral DRG (small, 43.13 ± 3.73 vs. 44.4 ± 3.56, p=0.731; medium, 43.4 ± 3.98 vs. 44.78 ± 3.45, p=0.7087; large; 44.35 ± 4.04 vs. 46.75 ± 3.36, p=0.5670).

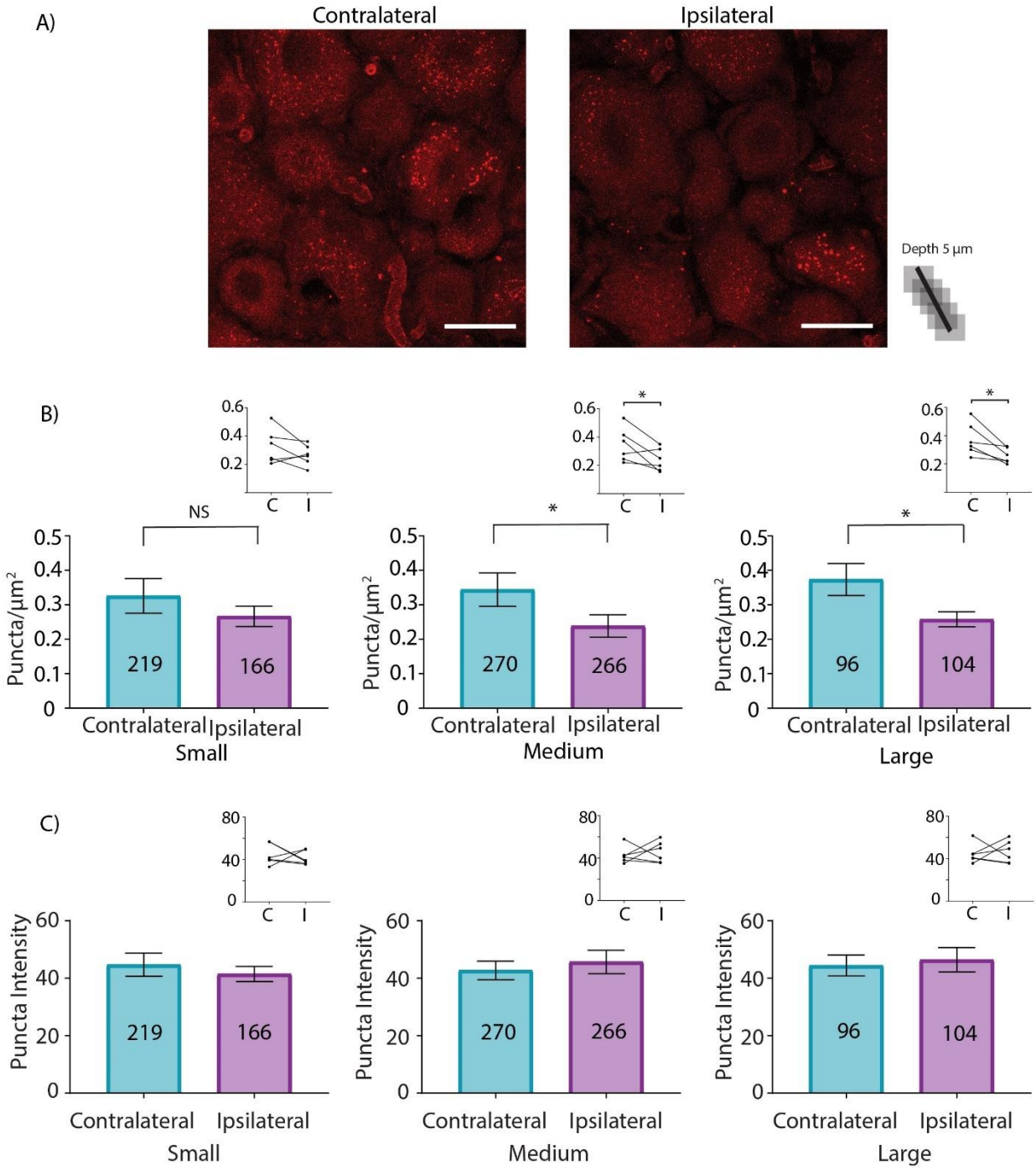

Figure 2-8 HCN2 channel SUMOylation by SUMO1 is diminished in medium and large diameter neurons from ipsilateral relative to contralateral DRG at 1 day post-CFA.
A) Representative PLA. Scale bars are 25 µm. Note that this image provides an overview, but for the purpose of quantification, individual projections were made for each cell, e.g. Figure 4B.
B) Plots of mean number of puncta/µm2 for all DRG from 6 CFA treated animals on day 1 post-CFA. The number inside the bar represents the total number of cells analyzed. Inset: Each line compares means for contralateral and ipsilateral DRG from one animal. Paired t-tests

indicate medium and large diameter cells contain significantly fewer puncta in the ipsilateral DRG relative to the contralateral DRG (small, 0.33 ± 0.05 vs. 0.27 ± 0.03, p=0.2058; medium, 0.34 ± 0.05 vs. 0.24 ± 0.03, p=0.0480; large, 0.37 ± 0.05 vs. 0.26 ± 0.02, p=0.0238**). C) Plots of mean puncta intensity on day 1 post-CFA.** Paired t-tests indicate mean puncta intensities were not significantly different for any size category in ipsilateral compared to contralateral DRG (small, 44.68 ± 4.03 vs. 41.48 ± 2.66, p=0.5986; medium, 42.7 ± 3.24 vs. 45.65 ± 4.06, p=0.6299; large, 44.44 ± 3.68 vs. 46.39 ± 4.27, p=0.7631).

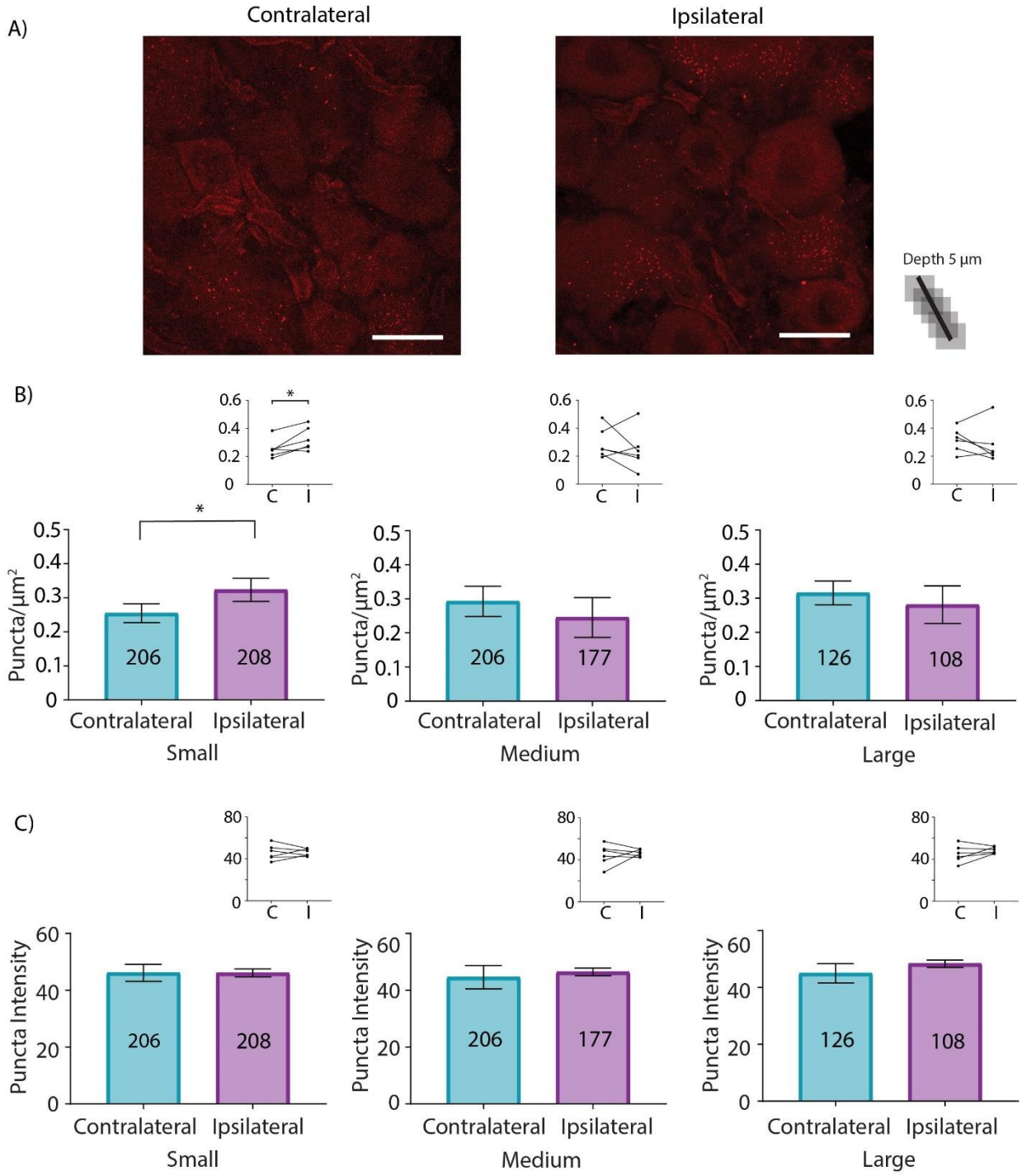

Figure 2-9 HCN2 channel SUMOylation by SUMO1 is increased in small neurons from ipsilateral relative to contralateral DRG at 3 days post-CFA.

A) Representative PLA. Scale bars are 25 µm. Note that this image provides an overview, but for the purpose of quantification, individual projections were made for each cell, e.g. Figure 4B.

B) Plots of mean puncta/µm² for all DRG from 6 CFA treated animals on day 3 post-CFA. The number inside the bar represents the total number of cells analyzed. Inset: Each line

compares means for contralateral and ipsilateral DRG from one animal. Significantly more puncta were observed in ipsilateral relative to contralateral DRG as indicated by paired t-tests or non-parametric alternative* (small, 0.25 ± 0.03 vs. 0.32 ± 0.03, p=0.0285; medium, 0.29 ± 0.05 vs. 0.25 ± 0.06, p=0.4310; large*, 0.32 ± 0.03 vs. 0.28 ± 0.06, p=0.5625). **C) Plots of mean puncta intensity on day 3 post-CFA.** Paired t-tests indicate mean puncta intensities were not significantly different for any size category in ipsilateral compared to contralateral DRG (small, 46.14 ± 3.0 vs. 46.08 ± 1.41, p=0.9826; medium, 44.58 ± 4.12 vs. 46.45 ± 1.32, p=0.6612; large, 44.99 ± 3.38 vs. 48.35 ± 1.27 p=0.2758).

3 CHANGES IN PERIPHERAL HCN2 CHANNELS DURING PERSISTENT INFLAMMATION

Publication: Jansen, L. R., **Forster, L. A**., Smith, X. L., Rubaharan, M., Murphy, A. Z., & Baro, D. J. (2021). Changes in peripheral HCN2 channels during persistent inflammation. Channels (Austin), 15(1), 165-179. doi:10.1080/19336950.2020.1870086

Contribution disclosure: Authors L. Forster, L-A. Jansen, AZ Murphy and D. Baro were responsible for the conception and design of the research presented. M. Rubaharan performed animal experiments. Authors L. Forster, L-A. Jansen, and X. Smith contributed to the acquisition and analysis of the data. Authors L. Forster and L-A. Jansen contributed equally. Authors L. Forster, L-A Jansen and D. Baro were responsible for drafting the manuscript, and all authors were involved in revising the manuscript.

3.1 Abstract

Nociceptor sensitization following nerve injury or inflammation leads to chronic pain. An increase in the nociceptor hyperpolarization-activated current, I_h, is observed in many models of pathological pain. Pharmacological blockade of I_h prevents the mechanical and thermal hypersensitivity that occurs during pathological pain. Alterations in the Hyperpolarization-activated Cyclic Nucleotide-gated ion channel 2 (HCN2) mediate I_h-dependent thermal and mechanical hyperalgesia. Limited knowledge exists regarding the nature of these changes during chronic inflammatory pain. Modifications in HCN2 expression and post-translational SUMOylation have been observed in the Complete Freund's Adjuvant (CFA) model of chronic inflammatory pain. Intra-plantar injection of CFA into the rat hindpaw induces unilateral hyperalgesia that is sustained for up to 14 days following injection. The hindpaw is innervated by primary afferents in lumbar DRG, L4-6. Adjustments in HCN2 expression and SUMOylation have been well-documented for L5 DRG during the first 7 days of CFA-induced inflammation. Here, we examine bilateral L4 and L6 DRG at day 1 and day 3 post-CFA. Using L4 and L6 DRG cryosections, HCN2 expression and SUMOylation were measured with immunohistochemistry and proximity ligation assays, respectively. Our findings indicate that intra-plantar injection of CFA elicited a bilateral increase in HCN2 expression in L4 and L6 DRG at day 1, but not day 3, and enhanced HCN2 SUMOylation in ipsilateral L6 DRG at day 1 and day 3. Changes in HCN2 expression and SUMOylation were transient over this time course. Our study suggests that HCN2 is regulated by multiple mechanisms during CFA-induced inflammation.

3.2 Introduction

Persistent inflammation and/or nerve injury can lead to chronic pain. This debilitating condition is characterized by allodynia (pain in response to non-noxious stimuli), hyperalgesia (increased sensitivity to noxious stimuli), and spontaneous painful and/or burning sensations in the absence of stimuli (Dubin & Patapoutian, 2010; Emery, Young, & McNaughton, 2012; Kuner & Flor, 2016; Pinho-Ribeiro, Verri, & Chiu, 2017; Tsantoulas, Mooney, & McNaughton, 2016; Xu & Yaksh, 2011). Chronic pain is underpinned by widespread reorganization of the pain circuitry, including changes to component neurons. While component neurons throughout the pain circuit can be altered (Boadas-Vaello, Homs, Reina, Carrera, & Verdu, 2017; Du, Wang, Cui, He, & Ruan, 2013a, 2013b), here we focus specifically upon nociceptors.

Nociceptors are peripheral sensory neurons that initiate pain signalling upon detecting noxious temperatures, pressures and chemicals (Dubin & Patapoutian, 2010). Nociceptor somata are located in the Dorsal Root Ganglia (DRG) and trigeminal ganglia. A single process projects from the soma; it bifurcates, and one process extends to the periphery and the other innervates the central nervous system. Nociceptors are functionally classified by their conduction velocities: C-fibers have small-diameter, unmyelinated axons; Aδ nociceptors have small to medium diameter, lightly myelinated axons; and, there is also a class of Aβ nociceptors that have larger diameter myelinated axons (Djouhri & Lawson, 2004; Nagi et al., 2019). The range of conduction velocities for each of these 3 classes varies with the species, but for the sake of comparison, the peak conduction velocities for C-, Aδ- and Aβ-fibers in a typical guinea pig compound action potential are approximately 0.6m/s, 3.3m/s and 9.6m/s, respectively (Djouhri & Lawson, 2004). Neurons within each class are functionally subdivided according to their threshold to noxious chemical, mechanical, and thermal stimuli. Recently, unbiased RNA

sequencing approaches have been included in classification schemes (C. L. Li et al., 2016; Usoskin et al., 2015), and several principal nociceptor cell types have been identified, each with a unique transcriptome, size and sensory function.

Nociceptors become hyper-excitable in chronic pain states elicited by nerve damage (neuropathic pain) and/or persistent, unresolved inflammation (inflammatory pain). This sensitization not only changes nociceptor responses to noxious and non-noxious stimuli, but also drives pathological changes to CNS components of the pain circuitry. Nociceptor sensitization is due, in part, to persistent alterations in a number of ionic currents that act to reduce threshold and increase cell excitability (Berta et al., 2017; Gold & Gebhart, 2010; Pace et al., 2018; Reichling & Levine, 2009; Tibbs et al., 2016; Zemel, Ritter, Covarrubias, & Muqeem, 2018). The hyperpolarization-activated, non-specific cation current, I_h, is a slowly depolarizing current that functions to enhance nociceptor excitability (Yagi & Sumino, 1998). Under normal conditions, I_h plays a limited role in pain transmission, and pain thresholds are largely unaffected by pharmacological inhibition or genetic ablation of I_h (Emery et al., 2011; Schnorr et al., 2014; Takasu, Ono, & Tanabe, 2010). However, during sensitization, I_h transitions into a pivotal role in pain signalling. In multiple models of chronic pain, nociceptor I_h amplitude is increased, and pharmacological agents that block I_h reduce nociceptor excitability and return pain thresholds to baseline (Chaplan et al., 2003; Dalle & Eisenach, 2005; Lee, Chang, Sorkin, & Chaplan, 2005; Luo et al., 2007; Richards & Dilley, 2015; Schnorr et al., 2014; Sun, Xing, Tu, Han, & Wan, 2005; Tibbs et al., 2016; Tsantoulas et al., 2017; Tsantoulas et al., 2016; X. Wang et al., 2016; Weng et al., 2012; Yao, Donnelly, Ma, & LaMotte, 2003). In addition, blocking I_h during chronic pain can also reduce the release of inflammatory mediators and glial activation (Huang, Zhang, & Huang, 2019).

The family of hyperpolarization activated, cyclic nucleotide gated ion channels, isoforms 1-4 (HCN 1-4), mediate I_h. These pore-forming α-subunits are assembled into homo- and hetero-tetrameric channels that are largely permeable to K^+ and Na^+, and may also display a small permeability for Ca^{2+} (Sartiani, Mannaioni, Masi, Novella Romanelli, & Cerbai, 2017; Wahl-Schott & Biel, 2009). Channels open upon hyperpolarization, but isoforms differ in their activation kinetics: HCN1 is the fastest and HCN4 is the slowest. All isoforms possess a cyclic nucleotide binding domain (CNBD), which when bound by cAMP shifts the voltage dependence of activation to more positive potentials. Isoforms show varying degrees of cAMP sensitivity, with HCN2 and HCN4 exhibiting the largest depolarizing shift in voltage dependence upon binding cAMP. Homo- and hetero-tetrameric channels composed largely of HCN1 and HCN2, and to a lesser extent, HCN3, conduct nociceptor I_h (Gao et al., 2012; Kouranova, Strassle, Ring, Bowlby, & Vasilyev, 2008; Weng et al., 2012).

Studies utilizing genetic ablation of specific HCN isoforms have begun to identify isoform-specific contributions to chronic pain. HCN1 contributes to cold allodynia during neuropathic pain (Momin, Cadiou, Mason, & McNaughton, 2008). HCN2 (Emery et al., 2011; Schnorr et al., 2014), but not HCN1 (Momin et al., 2008) or HCN3 (Lainez, Tsantoulas, Biel, & McNaughton, 2019) contributes to mechanical and thermal hyperalgesia; however, the role of HCN2 varies with the model under study. When Complete Freund's Adjuvant (CFA) was injected into the plantar surface of the hindpaw to elicit persistent inflammation, HCN2 knock out in sensory afferent neurons prevented mechanical but not thermal hyperalgesia on day 3 post-CFA (Schnorr et al., 2014). In contrast, ablation of HCN2 in sensory afferents prevented thermal but not mechanical hyperalgesia from 30min to 3hr after intra-plantar injection of the potent inflammatory mediator, PGE2 (Emery et al., 2011). Moreover, genetic ablation of HCN2 in

primary sensory afferents prevented both mechanical and thermal hyperalgesia from 2 to 21 days after the induction of neuropathic pain by chronic constriction of the sciatic nerve (Emery et al., 2011). Loss of HCN2 in primary sensory afferents also significantly reduced the pain behavior that is typically observed 1hr after intra-plantar injection of 4% formalin (licking, biting and paw lifting), and that is thought to be due to release of inflammatory mediators (Emery et al., 2011). These data suggest that there are likely to be numerous mechanisms that regulate HCN2 channels over multiple time courses, and that each mechanism may be differentially activated in a cell-type-specific manner and according to the catalyst(s) that triggers the pain state.

Current analgesic strategies to reduce I_h focus mainly on the development of isoform selective HCN channel blockers, e.g. small molecules that preferentially block channels containing HCN1 and/or HCN2 subunits (Dini et al., 2018; Resta et al., 2018). More generally, knowledge about the molecular mechanisms that alter ionic currents during pathological pain is being exploited to develop novel anti-nociceptive drugs tailored to a specific modulatory mechanisms (Francois-Moutal, Scott, et al., 2018; Moutal, Yang, et al., 2017). Several intracellular signalling pathways are known to drive nociceptor sensitization (Basbaum et al., 2009; Cheng & Ji, 2008; Djouhri, Dawbarn, Robertson, Newton, & Lawson, 2001; Hucho & Levine, 2007), but details on their modulation of HCN2 channels are limited.

A variety of molecular mechanisms may underpin the increase in nociceptor I_h during chronic pain states. Altered nociceptor HCN2 channel expression has been observed in multiple subcellular compartments during pathological pain, including the soma, peripheral terminals, central terminals, and along axons in nerves (Acosta et al., 2012; Papp, Hollo, & Antal, 2010; Schnorr et al., 2014; Smith, Al Otaibi, Sathish, & Djouhri, 2015; Weng et al., 2012). In some models of neuropathic pain, somatic nociceptor HCN2 protein expression appeared to decrease

despite an increased I_h (Chaplan et al., 2003; Jiang et al., 2008; Liu, Feng, & Zhang, 2015). In these cases, the decrease in expression may represent compensation for prolonged nociceptor hyperexcitability, or redistribution of the channels from soma to axon. In other models of inflammatory pain, both I_h and HCN2 protein expression increased (Acosta et al., 2012; Cho, Staikopoulos, Furness, & Jennings, 2009; Forster, Jansen, Rubaharan, Murphy, & Baro, 2020b; Papp et al., 2010; Richards & Dilley, 2015; Schnorr et al., 2014; Smith et al., 2015; Weng et al., 2012). In most instances, it was not clear if altered expression represented an adjustment to transcription, translation, and/or post-translational modifications that modify channel turnover. The rat model of CFA-induced chronic inflammatory pain highlights the idea that multiple mechanisms may be regulating HCN2 channels over different time courses. Unilateral, intra-plantar CFA injection elicits persistent inflammation and chronic pain in the ipsilateral hindlimb that is resolved by 14-21 days (W. M. Li et al., 2005; Millan et al., 1988). HCN2 expression is enhanced in multiple subcellular compartments leading to mechanical hyperalgesia (Acosta et al., 2012; Papp et al., 2010; Schnorr et al., 2014; Weng et al., 2012). A detailed immunohistochemical examination of somatic HCN2 protein expression in lumbar 5 (L5) DRG neurons that innervate the hindlimb showed that HCN2 immunoreactivity significantly increased on day 1 post-CFA in small and medium neurons relative to control animals that did not receive CFA injections (Forster et al., 2020b). HCN2 staining intensity then returned to baseline by day 3, but the number of neurons expressing HCN2 significantly increased (Forster et al., 2020b). By days 5-7 post-CFA, HCN2 staining intensity was once again significantly increased, and the number of neurons expressing HCN2 remained elevated relative to controls (Weng et al., 2012). In these studies, DRG neurons were only identified by soma size, and it is not known if all changes occurred in one cell type, or if HCN2 expression was altered in different cell types at

distinct time points. It is noteworthy that changes in somatic HCN2 protein expression on days 1 and 3 post-CFA were bilateral, while chronic pain only occurs in the ipsilateral hindlimb (Millan et al., 1988; Schnorr et al., 2014). This suggest that an increase in HCN2 protein expression may be necessary, but that the supplemental channels are not sufficient to produce pathological pain. One possibility is that a second ipsilateral mechanism acts on the supplemental HCN2 channels to alter their function and/or subcellular location.

It is well documented that HCN2 channel function is regulated by cAMP. Binding of cAMP to the channel's CNBD significantly shifts voltage dependence to more positive potentials, which will increase I_h under physiological conditions. DRG cAMP levels are elevated in models of chronic pain, and enhanced cAMP concentrations lower nociceptive thresholds and lead to hyperalgesia (Taiwo & Levine, 1991; Tsantoulas et al., 2017; Tsantoulas et al., 2016). Agonists of Gi/o-coupled receptors that reduce cAMP produce analgesia (Resta et al., 2016). In some models of neuropathic pain, genetic ablation of PKA had no effect on hyperalgesia, suggesting that direct binding of cAMP to the channel CNBD could increase I_h (Herrmann et al., 2017; Malmberg et al., 1997). In contrast, PKA is necessary for CFA-induced inflammatory pain (Herrmann et al., 2017). Knocking out either HCN2 or PKA prevented CFA-induced pathological pain, but deletion of the CNBD domain from the HCN2 channel had no effect on pain thresholds (Herrmann et al., 2017). Furthermore, on days 5-7 post-CFA, C-fiber but not Aδ nociceptors showed enhanced excitability due to a significant increase in I_h activation kinetics and amplitude, but there was no change in I_h voltage dependence of activation (Djouhri et al., 2015; Weng et al., 2012). PKA is known to phosphorylate HCN2 (Herrmann et al., 2017). Thus, the existing data suggest that CFA-induced persistent inflammation triggers cAMP activation of PKA, and perhaps, PKA phosphorylation of HCN2, which somehow leads to an increase in I_h.

HCN2 α-subunits interact with several auxiliary subunits that modify channel function, stability and surface expression (Brandt et al., 2009; Kimura, Kitano, Nakajima, & Nakanishi, 2004; Michels et al., 2008; Nawathe et al., 2013; Qu et al., 2004; Santoro, Wainger, & Siegelbaum, 2004). Protein-protein interactions can be regulated by post-translational SUMOylation (Flotho & Melchior, 2013). Small Ubiquitin-like MOdifier (SUMO) peptides are post-translationally conjugated to lysine residues on target proteins, e.g. HCN2. The SUMO moiety can then promote or prevent interactions between the target and its interacting partners. There are 4 SUMO isoforms (SUMO1-4): SUMO2 & SUMO3 (SUMO2/3) are ~97% identical; SUMO1 shares 47% identity with SUMO2/3; the physiological relevance of SUMO 4 is unclear. The majority of SUMOylation (~65%) occurs within identifiable consensus sequences (Hendriks et al., 2015), and HCN2 has several putative SUMOylation sites (Parker et al., 2017). HCN2 SUMOylation at K669 increased channel surface expression and I_h maximal conductance in a heterologous expression system (Parker et al., 2017). Inflammation causes a global increase in the SUMOylation of DRG proteins, and experimentally enhanced SUMOylation in sensory neurons produced pathological pain (Y. Wang et al., 2018a). In a rat model of CFA-induced inflammatory pain, HCN2 SUMOylation was increased in small DRG neurons on days 1 and 3 post-CFA (later times not examined) (Forster et al., 2020b). A target protein's phosphorylation status often determines its ability to be SUMOylated (Dustrude et al., 2016; Flotho & Melchior, 2013). Activation of the adenylyl cyclase-cAMP-PKA axis in an identified pattern generating neuron permitted the post-translational SUMOylation that led to an enhanced I_h (Parker et al., 2019). Thus, inflammatory mediators acting through PKA could alter the phosphorylation status of HCN2 channels to permit their SUMOylation, which could enhance surface expression. SUMOylation of HCN2 channels is dynamically regulated as inflammation progresses.

SUMO2/3 conjugation to HCN2 increased at day 1 post-CFA, and SUMO1 conjugation to HCN2 increased at day 3 post-CFA (Forster et al., 2020b). These data imply that inflammatory mediators regulate HCN2 interaction with components of the SUMOylation machinery that show target and SUMO-isoform specificity (Flotho & Melchior, 2013).

The rat hindpaw is innervated by sensory neurons in L4-L6 DRG. We previously reported the effects of CFA injection on HCN2 expression and SUMOylation in L5 DRG. Here, we complete the study and document changes in HCN2 expression and SUMOylation in L4 and L6.

3.3 Materials and methods

3.3.1 Animal Ethics

Ethics approval was obtained from the Institutional Animal Care and Use Committee at Georgia State University and all experiments were performed in compliance with the Ethical Issues of the International Association for the Study of Pain and the National Institutes of Health (NIH). 60-day old, male Sprague-Dawley rats were pair housed in a 12-hr light/dark cycle (lights on at 0700 hr) with ad libitum access to food and water.

3.3.2 CFA model and tissue preparation

A detailed description is found in Forster et al (Forster et al., 2020b). Briefly, 60-day old, male Sprague Dawley rats were injected with 200 µl of CFA into the mid-plantar surface of the right hindpaw. Control animals were handled, but not injected. 1 or 3 days later, animals were anesthetized, injected with heparin and perfused. Animals were fixed with 4% paraformaldehyde. Bilateral L4 and L6 DRG were extracted and placed into an 18% sucrose

solution at 4°C overnight. The following day, the epineurium was removed and DRG were embedded in 0.3% gelatin and sliced into 20 µm cryosections.

3.3.3 Antibodies and Reagents

The antibodies, dilution factors and applicable experiments are found in Forster et al (Forster et al., 2020b).

3.3.4 Immunohistochemistry and analysis

IHC was performed as previously described (Forster et al., 2020b). For each DRG, three 5x magnification images were taken. Blind analysis was performed on Photoshop. Images were thresholded to remove the intensity of the sheath. All cells above threshold with a definitive nucleus and visible cell perimeter were HCN2+ cells. Cells below threshold but meeting these quantification requirements were considered HCN2-. HCN2+ cells were sorted into classes by diameter: small ≤ 30 µm, medium 30- 40 µm and large > 40 µm. All gray mean values within a size class were averaged and is represented as the mean pixel intensity of that size class. The number of HCN2+ cells within a size class were divided by the sum of all HCN2+ and HCN2- cells and is represented as the frequency of that class. IHC experiments were repeated on 6 or 7 experimental animals and 4 or 5 control animals for L4 and L6 DRG at day 1 and day 3.

3.3.5 Proximity ligation assays and analysis

PLAs were performed using Duolink® In Situ Red Kit and manufacturer's guidelines as previously described (Forster et al., 2020b). Images were captured with a Zeiss 700 confocal microscope using a 40x oil immersion objective. Three cryosections were examined per DRG with a minimum of 3 z-stacks per cryosection. Blind analyses were performed using the FIJI

version of ImageJ. Cells with a visible nucleus, clear cell boundaries and no overlap with neighboring cells or fibers were selected for quantification. Maximum intensity projections of 5 z-slices from the middle of the cells were created. Cells were outlined and thresholded using the triangle method. Watershed analysis divided coalesced signals. For each cell, the average number of puncta was divided by the cell area to obtain puncta/μm^2. The mean pixel intensity (MPI) within 1 cell was processed by a program created by Alex Perez. PLA experiments were repeated on 6 experimental and 3 control DRG for L4 and L6 DRG at day 1 and day 3.

3.3.6 Statistics

All statistical analyses were preformed using GraphPad Prism. All data were tested for normality. The data for left and right DRG from each control animal were combined, because paired t-tests indicated left and right DRG showed no significant differences. IHC data were analyzed with a one-way ANOVA followed by Tukey's post hoc or Kruskal-Wallis followed by Dunn's post-hoc. Multiple comparison tests showed no significant differences in HCN2 SUMOylation between control and experimental DRG, therefore control data are not shown. Normal PLA data were measured using paired t-tests between ipsilateral and contralateral DRG. Non-parametric PLA data were analyzed with Wilcoxon-matched pairs. All values are presented as mean ± *SEM*. $p < 0.05$ was considered statistically significant.

3.4 Results

3.4.1 HCN2 expression and SUMOylation in L4 DRG neurons on days 1 and day 3 post-CFA

CFA was injected into the right hindpaw of experimental animals to elicit persistent inflammation, while control animals were handled, but not injected. Bilateral L4 and L6 DRG were dissected at day 1 or day 3 post-CFA and cryosectioned for immunohistochemistry (IHC) or proximity ligation assays (PLA), as previously described (Forster et al., 2020b). The IHC experiments were used to measure the level of HCN2 expression in a given cell (mean pixel intensity) and the percent of HCN2 expressing cells (frequency) in small (≤ 30 μm), medium (30- 40 μm) and large (> 40 μm) neurons. Values for left and right control DRG were not significantly different from each other; therefore, left and right values were combined and the datum for one control animal represents the average for left and right DRG. PLA experiments measured the number of SUMOylated HCN2 channels (puncta/μm^2) or the extent to which HCN2 channels were SUMOylated (puncta intensity) in ipsilateral relative to contralateral DRG.

Figure 1 shows representative cryostat sections and the results for L4 DRG 1 day post-CFA. A significant ~53% increase in HCN2 IR was observed in both ipsilateral and contralateral small cells relative to control (contralateral: 22.5 ± 1.5; ipsilateral: 23.4 ± 1.5; control: 15.0 ± 1.8) (Figure 1b). There were no significant differences in medium or large cell IR (Medium contralateral: 24.0 ± 2.0; ipsilateral: 25.8 ± 2.3; control: 18.4 ± 3.0) (Large contralateral: 27.2 ± 1.9; ipsilateral: 28.2 ± 2.8; control: 20.4 ± 3.6). In contrast, Figure 1c shows that CFA-injection produced a bi-lateral increase in the number of medium and large, but not small cells expressing HCN2 (Small contralateral: 37.3 ± 5.0; ipsilateral: 38.6 ± 5.6; control: 25.0 ± 5.5) (Medium contralateral: 19.1 ± 1.3; ipsilateral: 19.9 ± 2.1; control: 12.7 ± 1.0) (Large contralateral: 20.8 ±

1.7; ipsilateral: 20.6 ± 1.5; control: 13.1 ± 2.5). These experiments did not reveal any CFA-induced change in post-translational SUMOylation of HCN2 channels. There were no significant differences in the number or intensity of puncta between ipsilateral and contralateral L4 DRG 1 day post-CFA for any size class (Figure 1e,f).

These experiments did not reveal any CFA-induced change in HCN2 expression or post-translational SUMOylation in L4 DRG on day 3 post-CFA. There were no significant differences in HCN2 mean pixel intensity (Figure 2a) or frequency (Figure 2b) for any size class. The number (Figure 2c) and intensity (Figure 2d) of puncta were similar in ipsilateral and contralateral L4 DRG.

3.4.2 HCN2 expression and SUMOylation in L6 DRG neurons on days 1 and day 3 post-CFA

In the L6 DRG 1 day post-CFA, HCN2 expression bilaterally increased in experimental small cells relative to controls (Figure 3a). The mean pixel intensity was ~65% greater for experimental compared to control animals (contralateral: 25.5 ± 1.8; ipsilateral: 27.6 ± 2.2; control: 16.1 ± 1.1). Although mean pixel intensity increased in experimental vs. control for both medium and large cells, it was not statistically significant. There were no significant changes in HCN2 frequency for any size class (Small contralateral: 44.3 ± 4.2; ipsilateral: 54.1 ± 4.7; control: 42.1 ± 4.2) (Medium contralateral: 17.3 ± 1.9; ipsilateral: 17.6 ± 1.8; control: 16.0 ± 2.1) (Large contralateral: 13.3 ± 1.9; ipsilateral: 11.7 ± 1.3; control: 14.0 ± 2.8) (Figure 3b). There was a small but significant increase in the number of SUMOylated HCN2 channels in medium and large neurons (Figure 3c). The differences were isoform specific with SUMO 1 vs. SUMO 2/3 modification increasing in medium vs. large cells, respectively. There were no significant changes in puncta intensity (Figure 3d).

In the L6 DRG on day 3 post-CFA, there were no significant differences in HCN2 immunoreactivity (Figure 4a) or frequency (Figure 4b) for any L6 DRG neuronal size class. There were no significant changes in the number of SUMOylated HCN2 channels (Figure 4c). In contrast, HCN2 SUMO2/3 puncta intensity was significantly increased in ipsilateral small and medium cells, but not in large cells (Figure 4d).

3.5 Discussion

In this work, we investigated HCN2 expression and SUMOylation in L4 and L6 DRG at days 1 and 3 post-CFA injection. Using IHC, we found a bilateral increase in HCN2 mean pixel intensity in small neurons from L4 and L6 DRG at day 1, but expression levels returned to baseline by day 3. The number of medium and large neurons expressing HCN2 also transiently increased in L4 DRG on day 1 post-CFA. Using PLA, we found that HCN2 SUMOylation increased in L6 DRG at days 1 and 3. The number of SUMOylated HCN2 channels increased in medium and large cells at day 1, whereas the extent of HCN2 SUMOylation was enhanced in small and medium cells at day 3.

The patterns of change in HCN2 expression and SUMOylation are distinct for each of the lumbar DRG (Tables 1&2). This is not surprising given that for each DRG a different fraction of neurons project to the hindpaw. Whereas most neurons in the L5 DRG project to the hindpaw (Rigaud et al., 2008; Swett, Torigoe, Elie, Bourassa, & Miller, 1991), afferents in the L4 DRG project to the hindlimb, knee and hip joint (Nakajima et al., 2008; Rigaud et al., 2008; Salo & Theriault, 1997), and the neurons in L6 DRG mainly innervate visceral organs (Herrity, Rau, Petruska, Stirling, & Hubscher, 2014; Rigaud et al., 2008; Swett et al., 1991). Changes occurred

in all size classes of neurons, which is consistent with the fact that both C-fiber and Aβ fibers respond to CFA-induced inflammation (Belkouch et al., 2014).

Despite the fact that neurons in L4-L6 DRG differentially innervate the hindpaw, Table 1 shows that most changes in HCN2 expression occurred to the same extent in ipsi- and contra-lateral DRG for all 3 lumbar levels. This generalized change suggests that altered expression of HCN2 is likely to be a systemic response to CFA injection (Koltzenburg, Wall, & McMahon, 1999), which is not sufficient for the development of inflammatory pain at these time points. In contrast, Table 2 shows increased SUMOylation is observed exclusively in the ipsilateral side and may make a more direct contribution to the pain phenotype. In that respect, and given that SUMOylation of HCN2 is known to enhance surface expression of the channel (Parker et al., 2017), it may be that in DRGs where SUMOylation is increased, surface expression of HCN2 is also increased without necessarily altering total expression. Alternatively, SUMOylation of HCN2 may have a direct effect on the gating of the channel. There are several examples of SUMOylation altering ion channel biophysical properties (Benson et al., 2007; Dai, Kolic, Marchi, Sipione, & Macdonald, 2009; Plant et al., 2010; Plant et al., 2016; Steffensen et al., 2018; Y. Wang et al., 2018a; Meghyn A. Welch et al., 2019; Xiong et al., 2017). In our previous study, enhanced HCN2 SUMOylation in HEK cells did not alter I_h voltage dependence or kinetics (Parker et al., 2017). However, this result must be interpreted in the context of significant experimental caveats. First, since SUMO regulates protein-protein interactions, the effect of HCN2 SUMOylation will depend upon the available complement of interacting proteins, and the HCN2 interactome varies between cell types. Second, in our HEK cell experiments the level of HCN2 SUMOylation was altered in an uncontrolled fashion simply by increasing the cytosolic concentration of SUMO and the SUMO conjugating enzyme, ubc9.

HCN2 has multiple putative SUMOylation sites, but this manipulation increased SUMOylation at just a single site, so all potential effects of enhanced SUMOylation may not have been observed. Third, modulators play a permissive role in SUMOylation (Parker et al., 2019), and the phosphorylation state of a protein determines which sites can be SUMOylated (Dustrude et al., 2016; Flotho & Melchior, 2013). Thus, inflammatory mediators that alter phosphorylation states will likely produce a distinct pattern of HCN2 SUMOylation and associated effects that would not be replicated in the HEK cell experiments.

Emerging data suggest that altered SUMOylation may drive changes in several ion channels during nociceptor sensitization. The SUMOylation status of hundreds of proteins in a single cell is altered in response to a cellular stressor (Hendriks et al., 2015; Seifert, Schofield, Barton, & Hay, 2015). Chronic inflammation resulted in hyper-SUMOylation of the heat sensing TRPV1 channel, which lowered the temperature threshold of activation and led to thermal hyperalgesia (Y. Wang et al., 2018a). CRMP2, a subunit of the NaV1.7 channel, is hyper-SUMOylated in a rat model of chronic neuropathic pain, which enhances the sodium current; and, blocking CRMP2 hyper-SUMOylation in DRG neurons prevented mechanical and thermal hyperalgesia (Dustrude et al., 2016; Dustrude, Wilson, Ju, Xiao, & Khanna, 2013; Francois-Moutal, Dustrude, et al., 2018; Moutal, Dustrude, et al., 2017). A ~2-fold change in CRMP2 SUMOylation was observed in sciatic nerve, dorsal horn and glabrous skin during neuropathic pain (Moutal, Dustrude, et al., 2017) suggesting that larger changes in HCN2 SUMOylation may be observed in subcellular compartments such as axons and terminals relative to somata. Additional ion channels are known to be SUMOylated including Kv4 (Meghyn A. Welch et al., 2019), Kv11 (Steffensen et al., 2018), Kv7 (Qi et al., 2014; Xiong et al., 2017), Kv2 (Plant et al., 2011), K2P1 (Plant et al., 2010; Rajan et al., 2005), Kv1.5 (Benson et al., 2007), NaV1.2 (Plant

et al., 2016) and NaV1.5 (Plant et al., 2020). Their SUMOylation patterns have not yet been ascertained during chronic pain.

In sum, CFA-induced inflammation results in HCN2-dependent mechanical hyperalgesia. Inflammation-induced alterations in lumbar DRG sensory neurons include altered HCN2 expression and post-translational SUMOylation. Multiple mechanisms regulate HCN2 during the time course of CFA-induced inflammation. Identification of these mechanisms and the cell type in which they occur are worth further study.

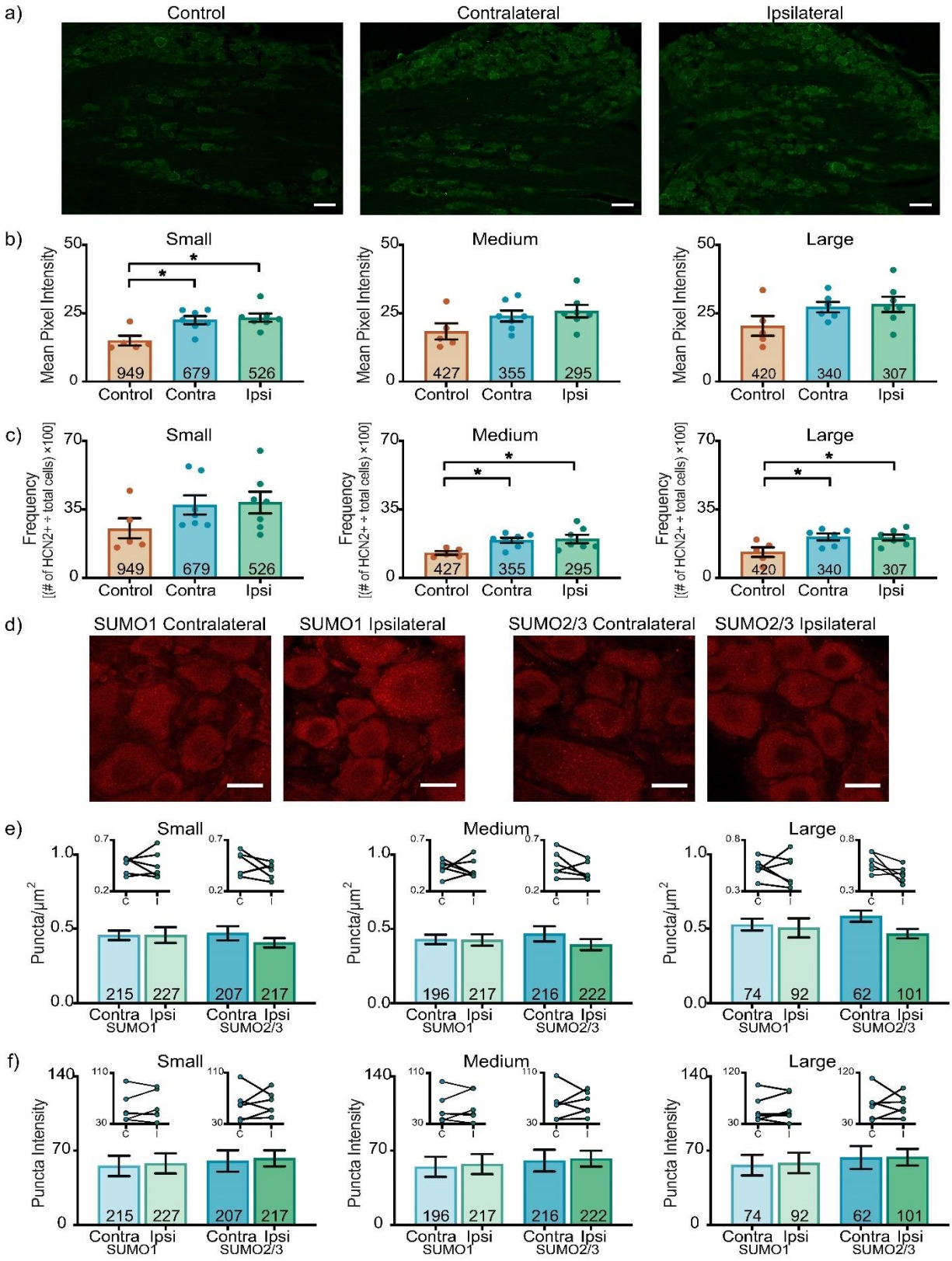

Figure 3-1 HCN2 protein expression but not SUMOylation is altered in the L4 DRG 1 day post-CFA.

A) Representative images of HCN2 IR. Scale bars are 100 μm. B) HCN2 mean pixel intensity is elevated in small diameter DRG neurons. Average mean pixel intensity ± SEM is shown for three size classes of DRG neurons (small: ≤ 30 μm; medium: 30- 40 μm; large: > 40 μm). Each dot represents the mean for one animal. Note that data for left and right DRG from each control were combined, because paired t-tests indicated left and right DRG showed no significant differences. The total number of cells examined for all animals within the treatment group is indicated in the bar. Asterisks indicate significance, *$p < 0.05$. Small cells: Kruskal-Wallis with Dunn's post-hoc test $(2,16)=7.750$; $p=0.014$; medium cells: one-way ANOVA $F(2,16)=2.378$; $p=0.125$; large cells: one-way ANOVA $F(2,15)=2.158$; $p=0.150$. C) The percent of medium and large diameter neurons expressing HCN2 increases 1 day post-CFA. Plot of percent HCN2 positive cells for each size class (frequency = # HCN2 positive cells for that size class ÷ total cell number for all classes). Bars indicate mean ± SEM. Asterisks indicate significance, *$p < 0.05$. Small cells: Kruskal-Wallis $(2,16)= 3.441$; $p=0.184$; medium cells: one-way ANOVA with Tukey's post hoc test $F(2,16)= 4.901$; $p=0.022$; large cells: one-way ANOVA with Tukey's post hoc test $F(2,15)= 5.188$; $p=0.019$. D) Representative confocal projections (5 μm) from PLA experiments. Scale bars are 25 μm. E) The number of SUMOylated HCN2 channels is unaltered 1 day post-CFA. The number of puncta/μm^2 for HCN2 SUMO1 (light bars) and SUMO2/3 (dark bars) conjugation is shown for three size classes of DRG neurons (small: ≤ 30 μm; medium: 30-40 μm; large: > 40 μm). SUMO1; small: 0.458 ± 0.054 vs 0.456 ± 0.032, $p=0.979$, paired t-test; medium: 0.424 ± 0.038 vs 0.429 ± 0.032, $p>0.999$, Wilcoxon-matched pairs; large: 0.505 ± 0.065 vs 0.528 ± 0.039, $p=0.740$, paired t-test; SUMO2/3; small: 0.405 ± 0.031 vs 0.469 ± 0.048, $p=0.271$, paired t-test; medium: 0.394 ± 0.037 vs 0.467 ± 0.050, $p=0.181$, paired t-test; large: 0.467 ± 0.032 vs 0.584 ± 0.038, $p=0.068$, paired t-test. Inset: compares the means for contralateral and ipsilateral DRG for each animal. F) SUMOylated HCN2 Puncta Intensities are unaltered 1 day post-CFA. Plot of average puncta intensity ± SEM for each size class. SUMO1; small: 57.86 ± 9.486 vs 55.55 ± 9.556, $p=0.615$, paired t-test; medium: 57.24 ± 9.442 vs 54.76 ± 9.484, $p=0.643$, paired t-test; large: 58.37 ± 9.707 vs 56.34 ± 9.626, $p=0.679$, paired t-test; SUMO2/3; small: 62.71 ± 7.576 vs 60.19 ± 10.08, $p=0.785$, paired t-test; medium: 62.44 ± 7.471 vs 60.60 ± 10.21, $p=0.824$, paired t-test; large: 63.80 ± 7.816 vs 63.46 ± 10.79, $p=0.975$, paired t-test.

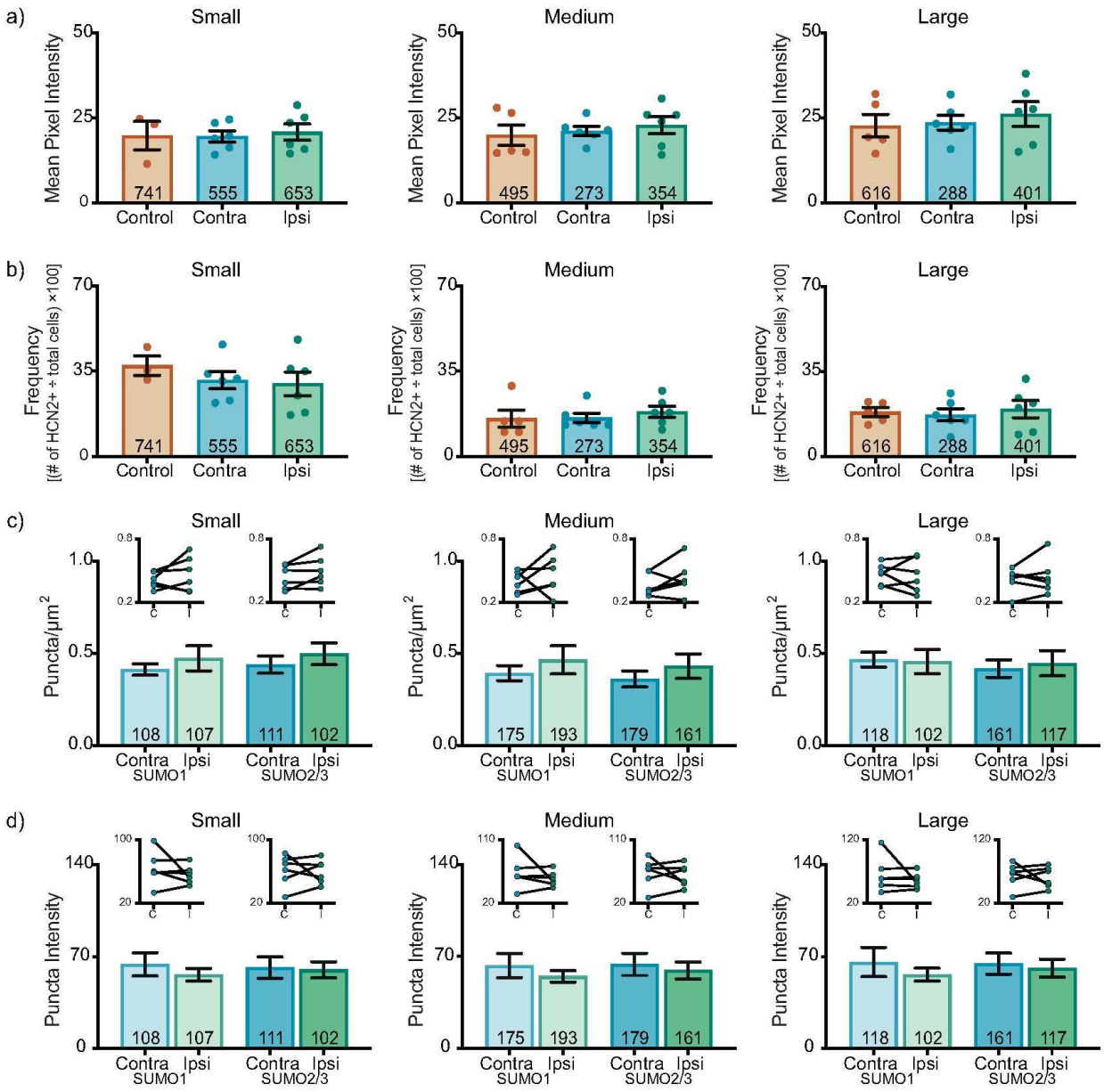

Figure 3-2 HCN2 protein expression and HCN2 SUMOylation are unaltered in the L4 DRG 3 days post CFA.

A) HCN2 mean pixel intensities do not change 3 days post-CFA. Average mean pixel intensity ± SEM is shown for three size classes of DRG neurons (small: ≤ 30 µm; medium: 30- 40 µm; large: > 40 µm). Each dot represents the mean for one animal. Note that data for left and right DRG from each control were combined, because paired t-tests indicated left and right DRG showed no significant differences. The total number of cells examined for all animals within the treatment group is indicated in the bar. Small cells: one-way ANOVA $F(2,12)=0.090$; $p=0.915$; medium cells: Kruskal-Wallis $(2,14)=0.438$; $p=0.819$; large cells: one-way ANOVA $F(2,14)=0.330$; $p=0.725$. B) The percent of HCN2 expressing cells does not change 3 days post-CFA. Plot of percent HCN2 positive cells for each size class (frequency = # HCN2 positive cells for that size class ÷ total cells number for all classes). Bars are mean ± SEM. Small cells: one-

way ANOVA F(2,12)=0.581; p=0.574; medium cells: Kruskal-Wallis (2,14)=1.358; p=0.531; large cells: one-way ANOVA F(2,14)=0.176; p=0.840. C) The number of SUMOylated HCN2 channels is unaltered in L4 DRG neurons. The number of puncta/μm^2 for HCN2 SUMO1 (light bars) and SUMO2/3 (dark bars) conjugation is shown for three size classes of DRG neurons (small: ≤ 30 μm; medium: 30- 40 μm; large: > 40 μm). SUMO1; small: 0.473 ± 0.068 vs 0.412 ± 0.031, p= 0.307, paired t-test; medium: 0.465 ± 0.076 vs 0.393 ± 0.041, p=0.418, paired t-test; large: 0.456 ± 0.066 vs 0.466 ± 0.040, p=0.847, paired t-test; SUMO2/3; small: 0.479 ± 0.059 vs 0.438 ± 0.047, p=0.121, paired t-test; medium: 0.431 ± 0.067 vs 0.361 ± 0.043, p=0.236, paired t-test; large: 0.446 ± 0.069 vs 0.417 ± 0.047, p=0.562, paired t-test. Inset: compares the means for contralateral and ipsilateral DRG for each animal. D) SUMOylated HCN2 Puncta Intensities are unaltered in L4 DRG neurons. Plot of average puncta intensity ± SEM for each size class. SUMO1; small: 56.16 ± 4.766 vs 64.04 ± 8.799, p= 0.382, paired t-test; medium: 54.92 ± 4.379 vs 63.08 ± 9.142, p=0.400, paired t-test; large: 56.32 ± 4.917 vs 65.79 ± 11.18, p=0.423, paired t-test; SUMO2/3; small: 59.62 ± 6.125 vs 61.62 ± 8.081, p=0.836, paired t-test; medium: 59.44 ± 6.444 vs 64.02 ± 8.447, p=0.609, paired t-test; large: 61.18 ± 6.817 vs 64.59 ± 7.984, p=0.691, paired t-test.

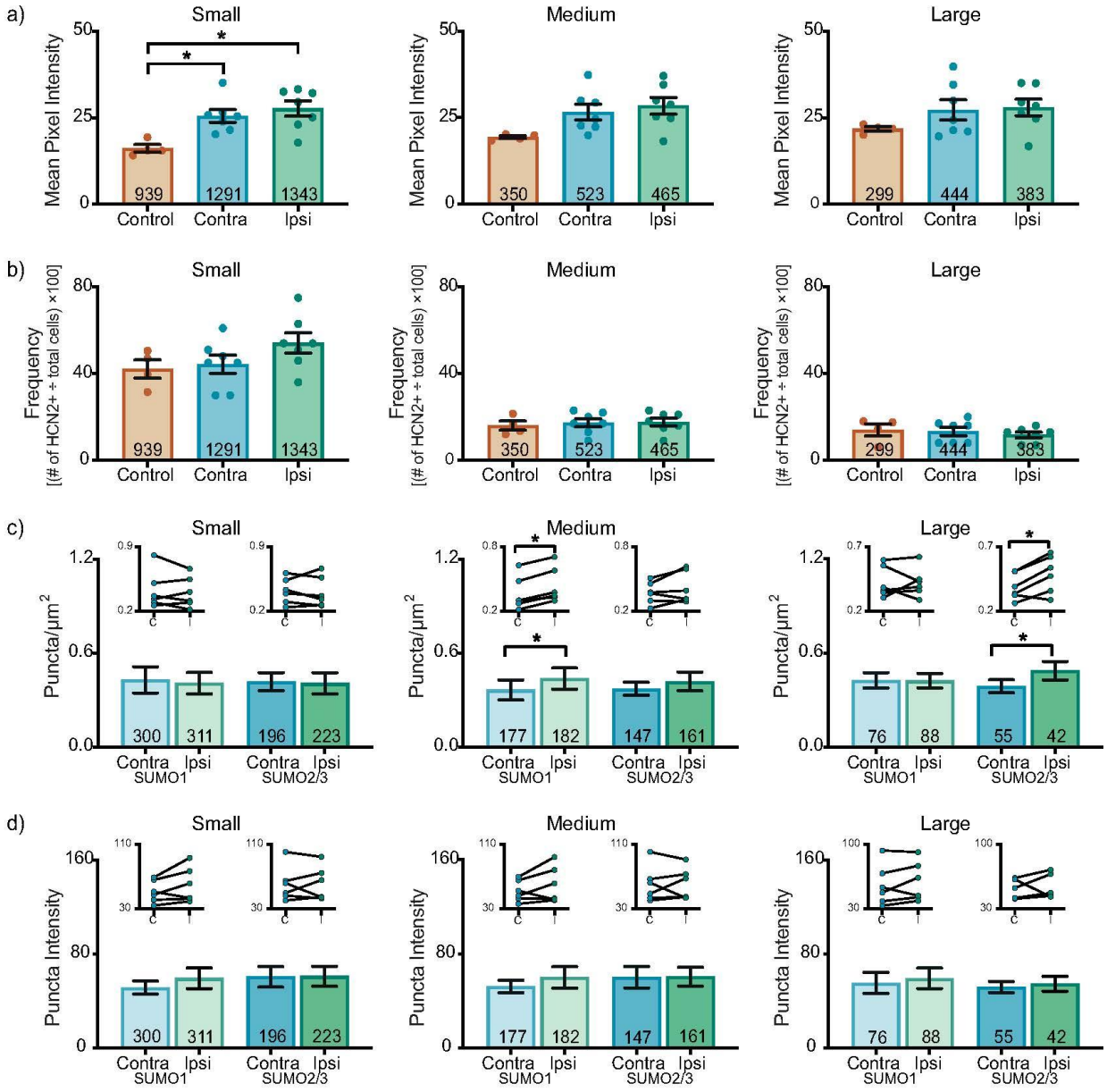

Figure 3-3 HCN2 protein expression and HCN2 SUMOylation are enhanced in the L6 DRG 1 day post-CFA.

A) HCN2 mean pixel intensity is elevated in small diameter neurons. Average mean pixel intensity ± SEM is shown for three size classes of DRG neurons (small: ≤ 30 μm; medium: 30-40 μm; large: > 40 μm). Each dot represents the mean for one animal. Note that data for left and right DRG from each control were combined, because paired t-tests indicated left and right DRG showed no significant differences. The total number of cells examined for all animals within the treatment group is indicated in the bar. Asterisks indicate significance, *$p < 0.05$. Small cells: one-way ANOVA with Tukey's post-hoc $F(2,15)=7.422$; $p=0.0060$; medium cells: one-way ANOVA $F(2,15)=3.542$; $p=0.055$; large cells: one-way ANOVA $F(2,15)=1.338$; $p=0.292$. B) The percent of HCN2 expressing cells is unaltered 1 day post-CFA. Plot of percent HCN2 positive cells for each size class (frequency = # HCN2 positive cells for that size class ÷ total

cells number for all classes). Bars indicate mean ± SEM. Small cells: one-way ANOVA $F(2,15)=1.980$; $p=0.173$; medium cells: one-way ANOVA $F(2,15)=0.147$; $p=0.865$; large cells: one-way ANOVA $F(2,15)=0.365$; $p=0.700$. C) The number of SUMOylated HCN2 channels increases in medium and large diameter neurons. The number of puncta/μm2 for HCN2 SUMO1 (light bars) and SUMO2/3 (dark bars) conjugation is shown for three size classes of DRG neurons (small: ≤ 30 μm; medium: 30- 40 μm; large: > 40 μm). Bars indicate the mean ± SEM. Asterisks indicate significance, *$p < 0.05$. SUMO1; small: 0.408 ± 0.068 vs 0.429 ± 0.083, $p=0.574$, paired t-test; medium: 0.438 ± 0.068 vs 0.365 ± 0.064, $p=0.031$, Wilcoxon matched-pairs; large: 0.424 ± 0.046 vs 0.426 ± 0.049, $p=0.961$, paired t-test; SUMO2/3; small: 0.407 ± 0.069 vs 0.418 ± 0.057, $p=0.752$, paired t-test; medium: 0.419 ± 0.060 vs 0.372 ± 0.042, $p=0.189$, paired t-test; large: 0.488 ± 0.059 vs 0.388 ± 0.042, $p=0.018$, paired-test. Inset: compares the means for contralateral and ipsilateral DRG for each animal. D) SUMOylated HCN2 Puncta Intensities are unaltered 1 day post-CFA. Plot of average puncta intensity ± SEM for each size class. SUMO1; small: 59.42 ± 8.867 vs 51.48 ± 5.557, $p=0.137$, paired t-test; medium: 59.92 ± 9.085 vs 52.20 ± 5.315, $p=0.189$, paired t-test; large: 59.39 ± 8.740 vs 55.49 ± 9.037, $p=0.316$, paired t-test; SUMO2/3; small: 61.16 ± 8.501 vs 60.61 ± 8.770, $p=0.916$, paired t-test; medium: 60.58 ± 8.002 vs 60.13 ± 9.115, $p=0.936$, paired t-test; large: 54.74 ± 6.259 vs 51.96 ± 4.790, $p=0.655$, paired t-test.

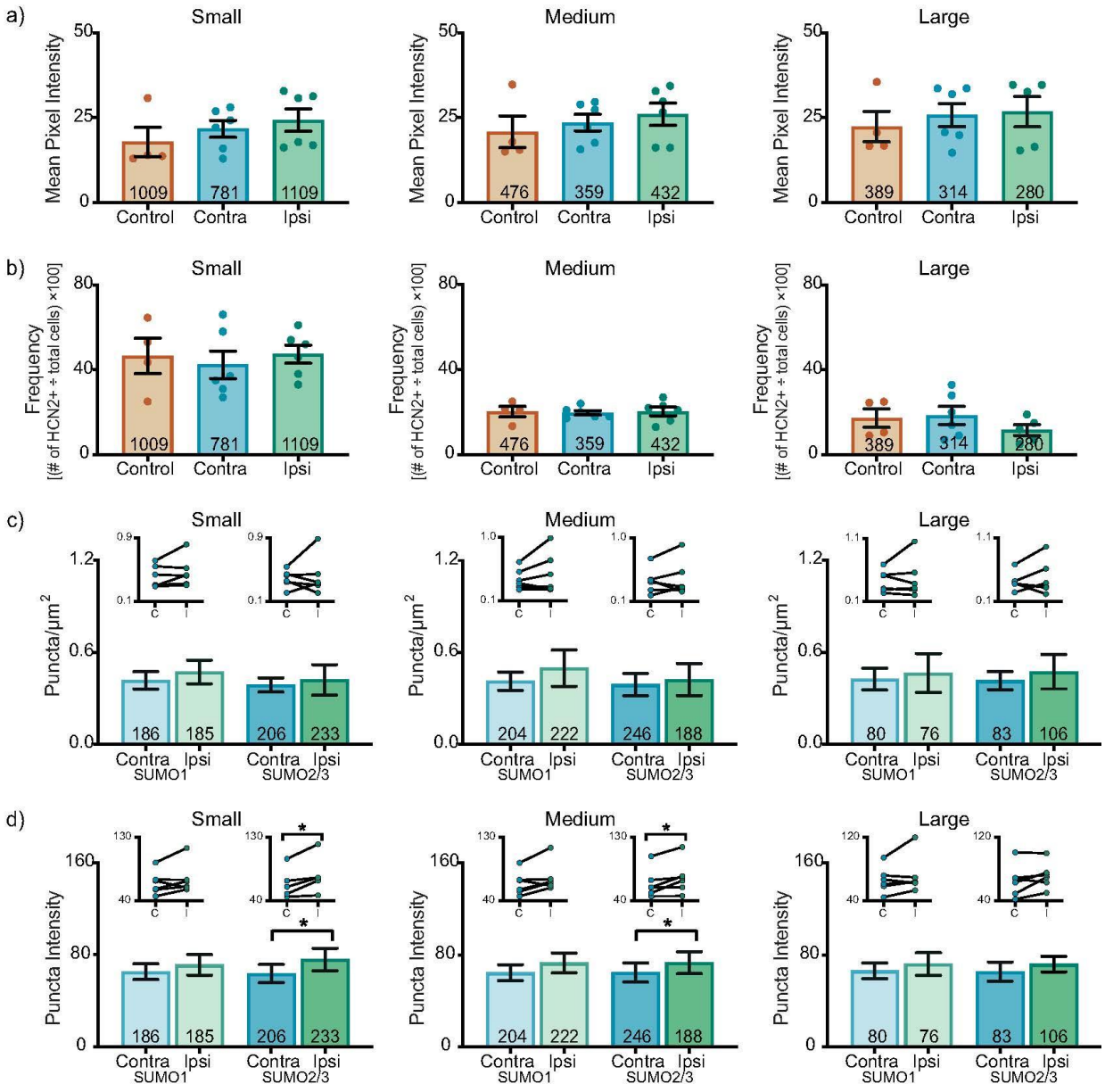

Figure 3-4 HCN2 SUMOylation but not protein expression is altered in the L6 DRG 3 days post-CFA.

A) HCN2 mean pixel intensities do not change 3 days post-CFA. Average mean pixel intensity ± SEM is shown for three size classes of DRG neurons (small: ≤ 30 µm; medium: 30-40 µm; large: > 40 µm). Each dot represents the mean for one animal. Note that data for left and right DRG from each control were combined, because paired t-tests indicated left and right DRG showed no significant differences. The total number of cells examined for all animals within the treatment group is indicated in the bar. Small cells: Kruskal-Wallis (2,13)=2.842; p=0.252; medium cells: Kruskal-Wallis (2,13)=1.309; p=0.543; large cells: Kruskal-Wallis (2,12)=0.061; p=0.977. B) The percent of HCN2 expressing cells does not change 3 days post-CFA. Plot of percent HCN2 positive cells for each size class (frequency = # HCN2 positive cells for that size class ÷ total cells number for all classes). Bars indicate mean ± SEM. Small cells: one-way

ANOVA F(2,13)=0.206; p=0.817; medium cells: one-way ANOVA (2,13)=0.043; p=0.958; large cells: one-way ANOVA F(2,12)=0.932; p=0.420. C) The number of HCN2 SUMOylated channels is unaltered 3 days post-CFA. The number of puncta/μm2 for HCN2 SUMO1 (light bars) and SUMO2/3 (dark bars) conjugation is shown for three size classes of DRG neurons (small: ≤ 30 μm; medium: 30- 40 μm; large: > 40 μm). SUMO1; small: 0.473 ± 0.077 vs 0.418 ± 0.057, p= 0.211, paired t-test; medium: 0.498 ± 0.118 vs 0.413± 0.06, p=0.219, paired t-test; large: 0.466 ± 0.127 vs 0.427 ± 0.071, p=0.593, paired t-test; SUMO2/3; small: 0.423 ± 0.099 vs 0.389 ± 0.046, p=0.678, paired t-test; medium: 0.424 ± 0.104 vs 0.392 ± 0.073, p=0.563, Wilcoxon matched-pairs, large: 0.475 ± 0.112 vs 0.417 ± 0.059, p=0.563, Wilcoxon matched-pairs. Inset: compares the means for contralateral and ipsilateral DRG for each animal. D) SUMOylated HCN2 Puncta Intensities are increased in small and medium cells. Plot of average puncta intensity ± SEM for each size class. SUMO1; small: 71.29 ± 8.984 vs 65.37 ± 6.805, p= 0.219, Wilcoxon matched-pairs; medium: 73.03 ± 8.633 vs 64.59 ± 6.927, p=0.094, Wilcoxon matched-pairs; large: 72.02 ± 9.835 vs 66.21 ± 6.770, p=0.313, Wilcoxon matched-pairs; SUMO2/3; small: 75.83 ± 9.743 vs 63.63 ± 7.899, p=0.031, Wilcoxon matched-pairs; medium: 73.25 ± 9.620 vs 64.71 ± 8.353, p=0.046, paired t-test; large cells: 71.93 ± 6.724 vs 65.46 ± 8.374, p=0.148, paired t-test.

Table 1: Fold Change in Mean HCN2 Expression in L4-L6 DRG

Fold Change in Mean HCN2 Expression in Experimental DRG relative to Control DRG						
HCN2 Expression	Small		Medium		Large	
	Contralateral DRG	Ipsilateral DRG	Contralateral DRG	Ipsilateral DRG	Contralateral DRG	Ipsilateral DRG
Mean Pixel Intensity Day 1						
L4	**1.5** (± 0.10)	**1.6** (± 0.10)	1.3 (± 0.11)	1.4 (± 0.12)	1.3 (± 0.09)	1.4 (± 0.14)
L5	**1.4** (± 0.10)	**1.5** (± 0.12)	1.3 (± 0.08)	**1.4** (± 0.14)	1.2 (± 0.10)	1.4 (± 0.19)
L6	**1.6** (± 0.11)	**1.7** (± 0.14)	1.4 (± 0.12)	1.5 (± 0.12)	1.3 (± 0.13)	1.3 (± 0.11)
Frequency Day 1						
L4	1.5 (± 0.20)	1.5 (± 0.22)	**1.5** (± 0.11)	**1.6** (± 0.17)	**1.6** (± 0.13)	**1.6** (± 0.11)
L5	1.7 (± 0.21)	1.5 (± 0.25)	1.0 (± 0.08)	1.1 (± 0.15)	0.8 (± 0.12)	0.9 (± 0.25)
L6	1.1 (± 0.10)	1.3 (± 0.11)	1.1 (± 0.12)	1.1 (± 0.11)	1.0 (± 0.14)	0.8 (± 0.10)
Mean Pixel Intensity Day 3						
L4	1.0 (± 0.08)	1.1 (± 0.12)	1.1 (± 0.07)	1.1 (± 0.13)	1.0 (± 0.10)	1.2 (± 0.16)
L5	1.4 (± 0.20)	1.3 (± 0.16)	1.4 (± 0.22)	1.3 (± 0.20)	1.4 (± 0.25)	1.3 (± 0.23)
L6	1.2 (± 0.14)	1.4 (± 0.18)	1.1 (± 0.12)	1.2 (± 0.16)	1.1 (± 0.15)	1.2 (± 0.20)
Frequency Day 3						
L4	0.8 (± 0.10)	0.8 (± 0.13)	1.0 (± 0.12)	1.2 (± 0.15)	0.9 (± 0.14)	1.1 (± 0.20)
L5	**3.0** (± 0.70)	**2.6** (± 0.30)	**1.8** (± 0.17)	**1.7** (± 0.15)	0.7 (± 0.21)	1.0 (± 0.18)
L6	0.9 (± 0.14)	1.0 (± 0.09)	1.0 (± 0.05)	1.0 (± 0.10)	1.1 (± 0.25)	0.7 (± 0.15)

Bold values = $p < 0.05$
± *SEM* are shown in parenthesis

Table 2. Fold Change in Mean HCN2 SUMOylation in L4-L6 DRG

Fold Change in Mean HCN2 SUMOylation in Ipsilateral DRG relative to Contralateral DRG						
HCN2 SUMOylation	Small		Medium		Large	
	SUMO1	SUMO2/3	SUMO1	SUMO2/3	SUMO1	SUMO2/3
Puncta/μm^2 Day 1						
L4	1.0 (± 0.12)	0.9 (± 0.07)	1.0 (± 0.09)	0.8 (± 0.08)	1.0 (± 0.12)	0.8 (± 0.05)
L5	0.8 (± 0.10)	**1.3** (± 0.17)	**0.7** (± 0.10)	1.1 (± 0.10)	**0.7** (± 0.06)	1.2 (± 0.16)
L6	1.0 (± 0.16)	1.0 (± 0.16)	**1.2** (± 0.18)	1.1 (± 0.16)	1.0 (± 0.11)	**1.3** (± 0.15)
Puncta Intensity Day 1						
L4	1.0 (± 0.17)	1.0 (± 0.13)	1.0 (± 0.17)	1.0 (± 0.13)	1.0 (± 0.17)	1.0 (± 0.12)
L5	0.9 (± 0.06)	0.9 (± 0.09)	1.1 (± 0.10)	1.0 (± 0.10)	1.0 (± 0.10)	1.0 (± 0.11)
L6	1.2 (± 0.17)	1.0 (± 0.14)	1.1 (± 0.17)	1.0 (± 0.13)	1.1 (± 0.16)	1.1 (± 0.12)
Puncta/μm^2 Day 3						
L4	1.1 (± 0.16)	1.1 (± 0.14)	1.2 (± 0.19)	1.2 (± 0.18)	1.0 (± 0.14)	1.1 (± 0.16)
L5	**1.3** (± 0.13)	1.1 (± 0.13)	0.8 (± 0.20)	1.0 (± 0.19)	0.9 (± 0.18)	1.0 (± 0.17)
L6	1.1 (± 0.18)	1.1 (± 0.25)	1.2 (± 0.29)	1.1 (± 0.27)	1.1 (± 0.30)	1.1 (± 0.27)
Puncta Intensity Day 3						
L4	0.9 (± 0.07)	1.0 (± 0.10)	0.9 (± 0.07)	0.9 (± 0.10)	0.9 (± 0.08)	0.9 (± 0.11)
L5	1.0 (± 0.03)	1.0 (± 0.08)	1.0 (± 0.03)	1.0 (± 0.08)	1.1 (± 0.03)	1.1 (± 0.08)
L6	1.1 (± 0.14)	**1.2** (± 0.15)	1.1 (± 0.13)	**1.1** (± 0.15)	1.1 (± 0.15)	1.1 (± 0.10)

Bold values = $p < 0.05$
± *SEM* are shown in parenthesis

4 SUMOYLATION REGULATES RECYCLING OF THE HYPERPOLARIZATION ACTIVATED CYCLIC NUCLEOTIDE GATED CHANNEL 2

4.1 Introduction

The hyperpolarization activated, cyclic nucleotide gated ion channel 2 (HCN2) mediates the slowly depolarizing, hyperpolarization-activated current (Ih) which is permeable to Na+/Ca+ ions. Ih is responsible for regulating the membrane potential of excitable cells, it has a reversal potential near -30mV which is generally higher than that of the threshold for firing an action potential (Kase & Imoto, 2012). It is active at hyperpolarized potentials, allowing the cell to repolarize following an action potential. It is present in the heart in the sinus node to act in pacemaker functioning and plays a role in the brain in synaptic integration (Wahl-Schott & Biel, 2009). Dysregulation of HCN channels contributes to multiple neurological disease states including epilepsy, chronic pain, and Parkinson's Disease (DiFrancesco & DiFrancesco, 2015). Understanding the regulation of HCN ion channels by mechanisms which can act through multiple time scales to contribute to these diseases is crucial. One such mechanism of regulation is post-translational modification (Forster et al., 2020a; Herrmann et al., 2017; Jansen et al., 2021).

The small ubiquitin like modifier (SUMO) is a ~100 amino acid peptide that is post-translationally added to lysine (K) resides of target proteins. The E1 activating enzyme utilizes ATP to conjugate SUMO to itself. Then SUMO is conjugated to the E2 conjugating enzyme UBC9. UBC9 can conjugate SUMO directly to target proteins or can work in conjunction with an E3 ligase for target specificity. SUMO can be added to target proteins in a SUMO consensus motif (ψKXD/E where ψ is a hydrophobic residue and X is any amino acid) (Flotho & Melchior, 2013) or in a non-consensus sequence with the assistance of an E3 ligase (Streich & Lima, 2016). Non-mutually exclusive effects of SUMOylation of proteins include 1) prevention of other post-translational modifications that occur at the same lysine residue 2) binding to

phosphoinositides in the trans-golgi and plasma membrane 3) prevention of protein-protein interactions through steric hindrance 4) promotion of protein interactions through SUMO interaction motif (SIM) domains. SUMOylation is involved in multiple disease states such as chronic pain, epilepsy, and brain ischemia where regulation of ion channels by SUMOylation is involved. For example in rodent models of pain there is an increase in SUMOylation of TRPV1 (Y. Wang et al., 2018b), the auxiliary subunit CRMP2 for NaV1.7 (Francois-Moutal, Dustrude, et al., 2018; Moutal, Dustrude, et al., 2017), and HCN2 (Forster et al., 2020a; Jansen et al., 2021); mouse models of epilepsy show a decrease in SUMOylation of KV7 and an subsequent reduction in M-current leading to hyperexcitability (Chen et al., 2021); and during ischemic conditions in the brain the sodium/calcium exchanger is SUMOylated and may provide a neuroprotective role (Cuomo et al., 2020). Other ion channels not already mentioned, have been shown to be SUMOylated including but not limited to Kv4.2 (M. A. Welch, L. A. Forster, S. I. Atlas, & D. J. Baro, 2019; Welch, Jansen, & Baro, 2021), KV2.1 (Dai et al., 2009; Plant et al., 2011), KV11 (Steffensen et al., 2018), CaV2.2 (Silveirinha et al., 2021) NaV1.5, and TRPM4 (Kruse et al., 2009).

In our previous studies we showed that SUMOylation of HCN2 K669 increased maximal conductance (Gmax) by increasing surface expression (Parker et al., 2017). However, we did not examine the mechanism by which SUMOylation acted to increase the surface expression of the channel. Here we pick up this story and examine the molecular mechanisms in SUMO regulation of HCN2 trafficking.

4.2 Methods

4.2.1 Antibodies and plasmids

A plasmid containing mCherry2-Cl was a gift from Michael Davidson (Addgene plasmid #54563). A plasmid containing SUMO-2 (Kamitani et al., 1998) was a gift from Edward Yeh (Addgene plasmid #17360). A plasmid containing Ubc9 (Yasugi and Howley, 1996) was a gift from Peter Howley (Addgene plasmid #14438). We obtained the trip8b plasmid from Bina Santoro (Santoro et al., 2004). (Santoro et al., 2009). Kv4.2g plasmid was provided by Dax Hoffman and is the same as we previously used (M. A. Welch et al., 2019; Welch et al., 2021). HA-KCHIP2a plasmid and HA-DPP10c plasmid were previously generated in or lab (Welch et al., 2021).

4.2.2 Cell Culture

Hek cells were obtained through ATCC and maintained in EMEM media (Corning, cat. #10009CV) supplemented with 10% fetal bovine serum (FBS; ATCC 30-2020) and 1% penicillin-streptomycin (Sigma, cat. #P4333) at 37°C / 5% CO_2. Hek-HCN2 stable lines were previously generated as described in Parker et al 2016. 250 µg/ml of geneticin (Gibco) was used to maintain selection of HCN2. Stable cell lines were not used past passage number 19. Hek cells were transiently transfected with Kv4.2g

4.2.3 Calcium Phosphate Transfection

Cells were plated at 1.8 x 10^6 cells per 60mm culture dish. The following day cells were transiently transfected with calcium phosphate. 10µg of plasmid DNA was used per transfection in 220µl total volume in TE buffer (10mM Tris-HCL pH 8, 1mM EDTA). When multiple plasmids were transfected equal amounts of plasmid DNA were co-transfected with the total amount of DNA remaining the same. 30µl of 2M $CaCl_2$ was added to the DNA, and then 250µl

of room temperature 2xHBS (275mM NaCL, 10mM KCl, 12mM dextrose, 1.4mM Na_2HPO_4, 40mM HEPES, pH 7.05-7.1) was added dropwise while flicking the microcentrifuge tube to mix. Immediately, the DNA mixture was added dropwise to the cells, and cells were returned to 37°C / 5 %CO_2 for 4 hours followed by a media change. Cells were allowed to grow and express the plasmid DNA for ~48 hours before use. Transfection efficiency was assessed by fluorescent microscopy and only plates with >80% transfection efficiency were used in experiments.

4.2.4 Immunoprecipitation

Cells were transfected with mCherry plasmid DNA, or mCherry + SUMO + UBC9 plasmid DNA 48-72 hours prior to lysing. If >80% transfection efficiency was observed, cells were lysed with IP lysis buffer (pierce magnetic co-ip kit, supplemented with 20mM NEM and 1:100 protease inhibitor cocktail (Sigma cat. # p8340). 500µg of protein was incubated with 1µl of anti-GFP (Abcam, ab290), overnight at 4°C, and immunoprecipitated following pierce magnetic co-IP kit protocol, eluting in 50µl of 2.2M glycine elution buffer before neutralizing in Tris-base pH 10.4.

4.2.5 Electrophysiology

35mm glass coverslips were covered with 100µg/ml of poly-L-lysine and then 70000-10000 cells were plated on them for use 1 day prior to recording. Coverslips were transferred to a recording chamber perfused with extracellular saline (in mM: 141 NaCl, 4.7 KCl, 1.2 MgCl2, 1.8 CaCl2, 10 glucose, 10 HEPES, pH 7.4, and osmolarity ~300-310 mOsm/L). Cells were visualized using a IX70 Olympus microscope, and transiently transfected cells were identified with fluorescent microscopy for mCherry or GFP expression. Borosilicate glass was pulled, and firepolished to generate patch pipettes with a resistance of 2-3MΩ when filled with intracellular

saline (in mM: 140 KCl, 1 MgCl2, 1 CaCl2, 10 EGTA, 2 MgATP, 10 HEPES, pH 7.2, and osmolarity ~290-295 mOsm/L). Pipettes were connected to a MultiClamp 700A amplifier (Axon Instruments). After forming a G Ω seal, negative pressure was used to break through the membrane, and only cells that maintained >700 MΩ seal following rupture and had less than 15 MΩ access resistance were examined. Whole cell capacitance was measured upon break-in. Fast and slow capacitance were compensated. Ih was elicited by holding at -50mV, and then a test pulse ranging from -50mV to -120mV for ____ in -10mV increments. The difference current was measured. IA was elicited with a series of 1 s pre-pulses to −90 mV each followed by a 250 ms test-pulse ranging from −50 to +50 mV in 10 mV increments. The leak current from a prepulse to -30 mV was subtracted offline. Current (I) was converted to conductance (G) using the equation G = I/Vm − Vr, with Vm being the membrane potential and Vr being the reversal potential. For Ih the reversal potential was set to 36 and for Ia the reversal potential was the reversal potential for potassium, -86mV. The maximal conductance (Gmax) was determined by plotting conductance against voltage and fitting the data with a first-order Boltzmann equation using Graphpad Prism. In some experiments, clathrin-mediated endocytosis was blocked with Pitstop2 (Abcam, ab120687). Cells were treated with 20 μM Pitstop2 for 20 min at 37◦C/5% CO2 before transferring to the recording chamber, in addition to being included in the extracellular saline at 20mM.

4.2.6 Immunohistochemistry

15mm coverslips were coated with 100μg/ml of Poly-L-Lysine. Cells were plated onto the coverslips and used the next day for experiments. Cells were washed 2x with PBS. Then incubated for 20 minutes at 4C in 4% paraformaldehyde. Cells were washed 1x with PBS briefly, and then washed 3x – 5 minutes each with PBST (PBS + 0.1% Triton-X-100) to permeabilize the

membrane. Cells were then incubated for 1 hour at room temperature in 10% normal goat serum in PBST to block. Block buffer was removed and primary antibodies (GFP 1:1000 sc-9996; Rab11a 1:100) were added in PBST overnight at 4°C. Primary antibodies were removed and coverslips were washed 3x with PBST for 5 minutes. Fluorescent labelled secondary antibodies (goat-anti-mouse-Alexa-488, goat-anti-rabbit-alexa-647) in 10% normal goat serum in PBST are added to coverslips and incubated for 3 hours at room temperature. Secondary antibodies are removed, the coverslips are washed 3x with PBS for 5 minutes and then mounted using Vectasheild non-hardening mounting media (Vector Labs, H-1000) and sealed with clear nail varnish. Coverslips were imaged using a Zeiss LSM-700 confocal microscope using a 63x oil immersion objective. Images were then analyzed using colocalization plugins available on FIJI.

4.2.7 Western blotting

After electrophoresis on 10% SDS-PAGE proteins were transferred to PVDF membranes (Immobilon-P, cat. #IPVH00010) using a wet transfer system at 100mA for 1 hour on ice in prechilled towbin's buffer (25 mM Tris, 192 mM glycine, 20% methanol, pH 8.1-8.5). Membranes were dipped in methanol and allowed to dry for 30 minutes before blocking for 1 hour at room temperature in 5% non fat dry milk in TBS (50 mM Tris-HCl pH7.4, 150 mM NaCl). Membranes were washed once in TTBS (TBS + 0.1% Tween 20) for 10 minutes. The membrane was then incubated overnight at 4°C in 1% non-fat dry milk with primary antibodies while shaking. Membranes were washed 3X 5 minutes in TTBS before incubating in 1% non-fat dry milk with alkaline phosphatase conjugated secondary antibodies for 2 hours at room temperature while shaking. Membranes were washed 3X 10 minutes in TTBS and alkaline phosphatase substrate was placed on the membrane for 5 minutes. Membranes were exposed to x-ray film (Research Products International) and the chemiluminescent signals were visualized

using a Kodak X-Omat 2000A imager. The optical density (OD) of the protein of interests was measured using ImageJ software as previously described (Parker et al., 2017). If a membrane was stripped and reprobed, the stronger signal was to be the second signal probed for (ie adaptin first, and GFP second). Membranes were washed 2x in mild stripping buffer for 10 minutes (20 mM glycine, 0.1% SDS, 1% Tween 20, 50 mM KCl, 20 mM Magnesium acetate, pH 2.2), 2x with PBS for 10 minutes, and 2x with TTBS for 5 minutes. Blots were then exposed to alkaline phosphatate substrate for 5 minutes, and a 10 minute exposure to xray film, to ensure that all chemiluminescent signal was gone prior to reprobing the blot. When blots were stripped, 0.1 and 0.2 µg BSA was included on the membrane to normalize the OD of the protein of interest of the pre-and post- stripped blot to account for any loss of protein during the stripping step. During stability assays, SYPRO RUBY total protein blot stain (Bio-Rad) was used. Whole cell lysates (10 µg) were resolved with PAGE and transferred to a PVDF membrane, as described above. Dried PVDF membranes were incubated protein side face-down in 7% acetic acid/10% methanol for 15 min and then washed 4X with dH2O for 5 minutes. Membranes floated protein side down in SYPRO Ruby Protein Blot Stain for 15 min and then washed 3X with dH2O for 1 minute. Stained protein was visualized using an Omega Ultra Lum imaging system using blue light transillumination and a 600nm filter. The optical density of the total protein signal in the entire lane was measured using ImageJ.

4.2.8 Statistics

All statistical analyses were performed using Graphpad prism software. Data were checked for normality and then performed a t-test or one-way ANOVA or appropriate non-parametric alternatives. Image analysis software for colocalization was performed with plug-ins

available on FIJI (Fiji Is Just ImageJ), and the mander's or pearson's coefficient (colocalization finder and Coloc 2) for each cell was input into Graphpad for statistical analysis between groups.

4.3 Results

We previously showed that SUMOylation at K669 is associated with an increase in Ih, and a corresponding increase in surface expression (Parker et al., 2017). To examine the mechanism responsible for this increase, we first asked if HCN2 internalization is regulated by SUMOylation of the channel. By using a modified cell surface biotinylation assay, surface proteins are biotinylated and then lysed and added to neutravidin beads to capture the surface expressed fraction of HCN2 channels. Internalized channels are measured by after biotinylating the surface fraction, cells are incubated at 18C for 2.5hr. Proteins remaining at the surface are stripped of biotin by incubating with a strong reducing agent, MESNA, leaving only proteins that have internalized during this time period to be labelled with biotin. The cells are lysed and added to neutravidin beads to capture the internalized HCN2 channels. A control plate where the cells were not allowed to internalize surface protein was stripped with MESNA prior to lysing (Figure 1A). HEK-HCN2 cells showed 22.87% of channels internalized after 2.5hr (Figure 1B). Transiently transfecting HEK-HCN2 cells with SUMO and UBC9 prevented internalization of the channel with only 6.38% internalized (Figure 1B). We next asked if SUMOylation at K669 is preventing internalization. The cell surface biotinylation experiment was repeated, but this time we used mutant HCN2-K669R cells where K has been mutated to R to prevent SUMOylation, as we previously showed (Parker et al., 2017). When HCN2-K669R cells were used only 8% of the channels internalized after 2.5 hours, and no further effect was observed when SUMO and UBC9 was transiently transfected (Figure 1B). These data suggest that SUMOylation of K669 increases surface expression and Ih by preventing internalization of the channel.

We next asked if the decrease in internalization with K669 SUMOylation is regulated by clathrin-mediated endocytosis. We performed whole cell patch clamp on HEK-HCN2 stable line that were or were not treated with the clathrin mediated endocytosis inhibitor Pitstop2. Application of Pitstop2 mediated an 80% increase in Ih Gmax compared to the stable line alone. When SUMO peptide is included in the patch pipette there is a 62% increase compared to stable line. However, when both pitstop and SUMO are applied, there is a 71% increase (Figure 2). The lack of an additive effect of SUMO and Pitstop, suggests that Pitstop both mimics and occludes the effect of SUMO on Ih. Additionally, we show that the addition of SUMO into the patch pipette increases Ih through K669, as no effect of SUMO is observed on HEK-HCN2-K669R cells. This is the same as long-term effects of transient transfections of SUMO and UBC9 plasmids (Parker 2017) (Figure 2B). These data suggest that the effect of acute SUMOylation is indeed acting on K669 rather than on endocytic machinery at the cell surface.

AP2 is the major adaptor protein during clathrin mediated endocytosis. HCN2 contains 5 AP2 consensus motifs YXXϕ, where X represents any amino acid and ϕ represents a hydrophobic amino acid, in its c-terminus. AP2 is a heterotetramer consisting of alpha, beta, mu and omega adaptin subunits. One possibility is that SUMOylation of HCN2 prevents the association of the channel and AP2 subunits, and this prevents internalization of the channel. To test this, we preformed co-immunoprecipitation experiments to see if SUMOylation regulated the amount of alpha-adaptin associated with HCN2. We saw no changes in adaptin protein co-IPed when HCN2 channel is SUMOylated (Student's t-test, p=0.6750; 0.3432 + 0.0413 vs 0.3696 + 0.425). These data suggest that SUMOylation is not altering clathrin-mediated endocytosis. Instead, we hypothesize that SUMOylation is acting downstream of internalization, and instead is acting to increase recycling of the channel to the plasma membrane. To test this hypothesis, we

used a dominant negative form of Rab11aS25N where this mutation keeps rab11a in its inactive GDP bound form. When Rab11aS25N was transiently transfected in HEK-HCN2 cells, we saw no difference in Ih from control. Additionally, when SUMO was added into the patch pipette, there was no change in Ih, suggesting that SUMO increases Ih through rab11-dependent recycling (Figure 4A,B). When pitstop was added into the superfusate, Ih increased, suggesting that Ih can still increase by preventing channel from being internalized without functional rab11a mediating recycling of the channel back to the membrane. To support these data, we used anti-rab11a to label endogenous rab11a in HEK293 cells and measured the amount of GFP-HCN2 and Rab11a colocalization with or without co-transfection with SUMO and UBC9. When SUMO and UBC9 are transiently transfected we see an increase in colocalization by Pearson's colocalization coefficient (student's t-test, 0.1391 v. 0.1829, p=0.0407), as well as an increase in Mander's overlap coefficient (student's t-test, 0.7618 v. 0.8050, p=0.0003) (Figure 4C,D). Together these data suggest that SUMOylation of HCN2 increases Ih through increased rab11a mediated slow-recycling.

Next, we asked if SUMOylation is stabilizing HCN2 protein expression. We ran lysates from HEK-HCN2 cells either transfected or not with SUMO and UBC9, and normalized GFP signal to SYPRO RUBY total protein stain. We saw an increase in HCN2 protein when SUMO and UBC9 were co-expressed (t-test, p=0.0027) (Fig 5A,B). To ask if this was due to SUMOylation of the channel, we repeated this experiment with HCN2-K669R stable line, and we also observed an increase in HCN2 protein (Figure 5 A,B). We next asked if SUMOylation was altering ubiquitination status of the protein and degradation of the channel in the proteasome. Ubiquitin Anti-FK1 recognizes ubiquitin chains but not free ubiquitin (Fujimuro, Sawada, & Yokosawa, 1994), we observed no change in ubiquitin chain modification of HCN2

with or without SUMO (figure 5C). Therefore, the increase in SUMOylation of the channel is not increasing protein by preventing proteasomal degradation of HCN2. These data suggest that increasing SUMOylation in HEK cells may be acting at the level of the transcriptome. To test this hypothesis, we preformed qPCR to measure transcript level of our HEK-HCN2 stable line with and without SUMO and UBC9 over expressed. We observed a non-significant 33% increase in copy number, (Figure 5D) that is in line with the 30% increase in protein level we observed (Figure 5 A,B). Together these data suggest that transiently transfecting SUMO and UBC9 increases HCN2 protein level, but that this does not account for the SUMO mediated increase in Ih Gmax (Parker et al 2017).

HCN2 interacts with a known auxiliary subunit TRIP8b. Association with the 1a-4 isoform of TRIP8b, the most abundantly expressed isoform in the brain, increases Ih Gmax in HEK cells. In the brain, this is associated with dendritic enrichment of HCN2 channels and proper surface expression and localization of the channel in the dendrite. Previously Lewis et al showed that TRIP8b prevented HCN2 from being targeted to the lysosomes, and in the hippocampus knocking out trip8b showed an increase in HCN2 protein in multivesicular bodies. The authors hypothesized that TRIP8b could be acting to direct HCN2 trafficking and localization, and by preventing targeting to the lysosome could instead be redirecting HCN2 to the recycling endosomes(Lewis et al., 2009). Additionally, Hardel showed that HCN2 is found in recycling vesicle pools in the heart and the pool of HCN2 in the endocytic recycling compartment regulated surface expression of HCN2 (Hardel, Harmel, Zolles, Fakler, & Klocker, 2008). Since we showed that post-translational SUMOylation regulates surface expression through a rab11a dependent recycling mechanism – we asked if TRIP8b might be acting in the same pathway as SUMOylation to produce these effects. First, we repeated internalization assays

and saw as expected that TRIP8b prevented internalization of HCN2 and this was to the same degree as SUMOylation (Figure 6A,B). Next, we transiently transfected TRIP8b in our HEK-HCN2 stable line and saw that TRIP8b did indeed increase Ih Gmax as expected, but no additive effect of SUMO was observed when SUMO was transiently transfected with SUMO and UBC9 plasmids (Figure 6 C,D) and this was also true with SUMO in the patch pipette (data not shown). These data suggest that Trip8b and SUMO are acting through the same pathway to increase Ih Gmax. Next, we transiently transfected HEK-HCN2 with Trip8b and Rab11S25N and observed that Ih no longer increased as it does when Trip8b is transfected alone. These data suggest that TRIP8b is acting to shuttle HCN2 through the endocytic pathway to Rab11a positive endocytic recycling compartments and increases Ih through rab11a dependent recycling in the same manner as SUMOylation of HCN2 (Figure 6C,D).

We previously examined the mechanism behind the increase in Ia Gmax upon SUMOylation of Kv4 when expressed in the ternary complex with DPP10c and KChIP2a (Welch 2021). Here Welch et al showed that SUMOylation prevented internalization of the channel and that it acted in a clathrin-mediated endocytosis independent manner. Here, I ask if Kv4.2 TC SUMOylation may be acting to increase Ia Gmax through rab11a dependent recycling in the same fashion as it does for HCN2. When Rab11aS25N is transiently transfected with Kv4.2g, KChIP2a and DPP10 and SUMO is or is not included in the patch pipette, we no longer see an increase in Ia Gmax through SUMOylation (Figure 7A,B). Suggesting that SUMOylation of the ternary complex is mediating the increase in Ia Gmax through recycling of the channel back to the surface. Additionally, when pitstop2 was added Ia Gmax increased. This is important since recycling is downstream of inhibiting endocytosis (Figure 7A,B).

4.4 Discussion

We found that HCN2 SUMOylation at K669 prevented internalization of the channel and did so in a clathrin-mediated endocytosis independent manner. SUMOylation of the channel increased the amount of total HCN2 protein, but this was not due to SUMOylation at K669, and was associated with a non-significant increase in transcript level. Additionally, SUMOylation increased colocalization of HCN2 with Rab11a, and using a dominant negative form of Rab11aS25N the effect of SUMOylation of HCN2 was blocked. Together this showed that SUMOylation of K669 in HCN2 increases surface expression through an increase in recycling of the channel to the membrane. Additionally, we show that HCN2 association with TRIP8b also increases surface expression through the rab11a-dependent slow recycling pathway. Finally, we show that the Kv4.2 ternary complex also acts to increase IA through this same pathway, suggesting that c-terminal SUMOylation of ion channels may be a common mechanism to regulate surface expression.

4.4.1 C-terminal SUMOylation of Ion Channels as a Common Mechanism to Regulate Surface Expression

Both HCN2 and Kv4.2 are SUMOylated in their c-terminus which in turn regulates their surface expression, Gmax and internalization (Parker et al., 2017; M. A. Welch et al., 2019; Welch et al., 2021). This may be a common mechanism that is utilized to regulate their surface expression, perhaps with c-terminal SUMOylation acting as a signal which is recognized by transport proteins in endocytic compartments to route them to the endocytic recycling compartment and will require rab11a to recycle the channels back to the plasma membrane as it did for both HCN2 and Kv4.2 ternary complex in HEK293 cells (Figure 4, 7). In fact, other membrane proteins have c-terminal SUMOylation such as Connexin 43 (Cx43). Cx43 is SUMOylated in its c-terminal tail

during endocytic transport (Kjenseth et al., 2012). Nephrin also shows c-terminal SUMOylation and shows increased surface expression compared with cells that were treated with the E1 inhibitor ginkgolic acid. The authors suggest that SUMOylation may be acting to regulate surface expression of the channel through regulation of recycling of the channel (Tossidou, Himmelseher, Teng, Haller, & Schiffer, 2014).

4.4.2 Balance of SUMOylation and Ubiquitination to Regulate Surface Expression

Isoform 1a-4 of Trip8b increases surface expression and Ih when transiently expressed with HCN2 (Lewis et al., 2009) and here we show that Trip8b increases Ih, and when dominant negative Rab11 is co-transfected with TRIP8b this increase is prevented – suggesting that theTRIP8b mediated increase in Ih requires the channel to exit the endocytic recycling compartment. Lewis et al showed that TRIP8b co-expression prevented HCN channel from trafficking to the lysosome and hypothesized that instead it must be recycled instead (Lewis et al., 2009) and our data support this original hypothesis. SUMOylation could be acting as a mediator for cross-talk between the SUMOylation system and the ubiquitination pathways – possibilities include 1) SUMOylation is preventing ubiquitination of a through SUMOylation of a K residue that is also a ubiquitination site (Ulman et al., 2021) 2) SUMO moiety causing steric hindrance preventing the association of ubiquitination machinery 3) SUMOylation increasing the association of deubiquitinases (DUBs) 4) SUMOylation decreasing the association of ubiquitin ligases and ubiquitin interacting proteins (Rott et al., 2017). For these scenarios this suggests that SUMOylation would act to recruit deubiquitinating enzymes or/prevent the addition of a ubiquitin moiety to the target protein and prevent the protein from being shuttled through the ESCRT system to be degraded by the lysosome. As such, the protein is left to be able to be recycled – however this assumes that recycling is a passive/default process – and instead it is

possible that SUMOylation could be acting to increase sorting to the endocytic recycling compartment. Our data suggest that SUMOylation of HCN2 increases the association of the channel with Rab11a (Figure 4) and that functional rab11 is required to mediate the SUMO effect on Ih (Figure 4). Often, recycling has been viewed as a default and passive process, where if transmembrane proteins were not actively sorted for degradation, they passively moved on for recycling (MacDonald, Savage, & Zech, 2020). Instead, there is a highly complex system of sorting proteins for both degradation by the lysosome and recycling pathways – with ubiquitin signaling for trafficking being more complex than a single mono-ubiquitin triggering internalization of a protein and poly-ubiquitination being a signal for proteasomal degradation (Ronai, 2016) and if ubiquitin moieties remain after the protein is internalized to the early endosome the protein will be sorted by the ESCRT system to multi-vesicular bodies and the lysosome for degradation (Weeratunga, Paul, & Collins, 2020).

Proteins such as SUMO targeting ubiquitin ligases (STUbLs) interact with SUMO modified proteins to ubiquitinate the target, which can then modify the function of the protein or lead to degradation of the protein by the proteasome(Kumar, Gonzalez-Prieto, Xiao, Verlaan-de Vries, & Vertegaal, 2017). The StUBl RNF4 can catalyze K48 (proteasome) or K63 (recruitment of ubiquitin binding motif containing proteins) linked UB chains (Keiten-Schmitz et al., 2020). Additionally, there are SUMO targeting ubiquitin proteases (STUPs) which can recognize SUMO modified proteins to modify ubiquitin chains on SUMOylated targets by removing ubiquitin moieties (Salas-Lloret & Gonzalez-Prieto, 2022). In addition to specialized ubiquitin ligases/proteases which bind to SUMOylated substrates, SUMOylation may be increasing these interactions through SUMO-interaction Motifs (SIMs) within ubiquitin ligases or deubiquitin ligases. Identified first in the nucleus during DNA damage and repair If SUMOylation is acting

in a similar manner here, we could predict that a decrease in association with a ubiquitin ligase and/or an increase in association with a deubiquitinase would result in an increase in the amount of channels recycled to the membrane.

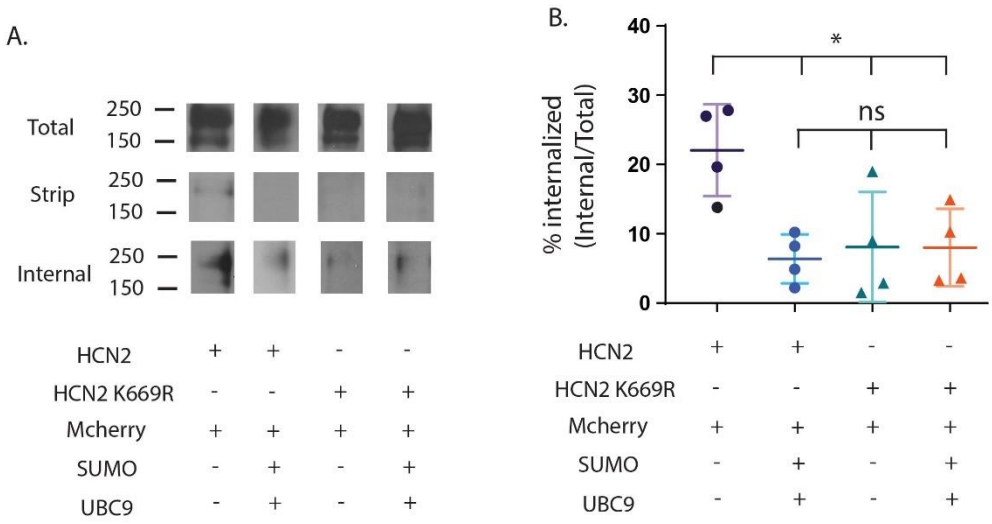

Figure 4-1 HCN2 SUMOylation prevents internalization of the channel

A) Western blots showing GFP signal of total, stripped, and internal HCN2 for wildtype HEK-HCN2 and mutant HEK-HCN2-K669R. **B)** Graph of the optical density of the internalized HCN2 doublet divided by the optical density of the total surface fraction of HCN2, (ANOVA with Tukey's multiple comparisons, $F(4, 15) = 4.886$, $p=0.01$; HEK-HCN2, mCherry 22 ± 6.6 % v. mCherry + SUMO + UBC9 6.4 ± 3.5 %; HEK-HCN2-K669R, mCherry 8.1 ± 7.9 % v. mCherry + SUMO + UBC9 8.0 ± 5.6 %). Circles = wildtype, Triangles = K669R, Data presented as mean ± SEM, * represents $p<0.05$.

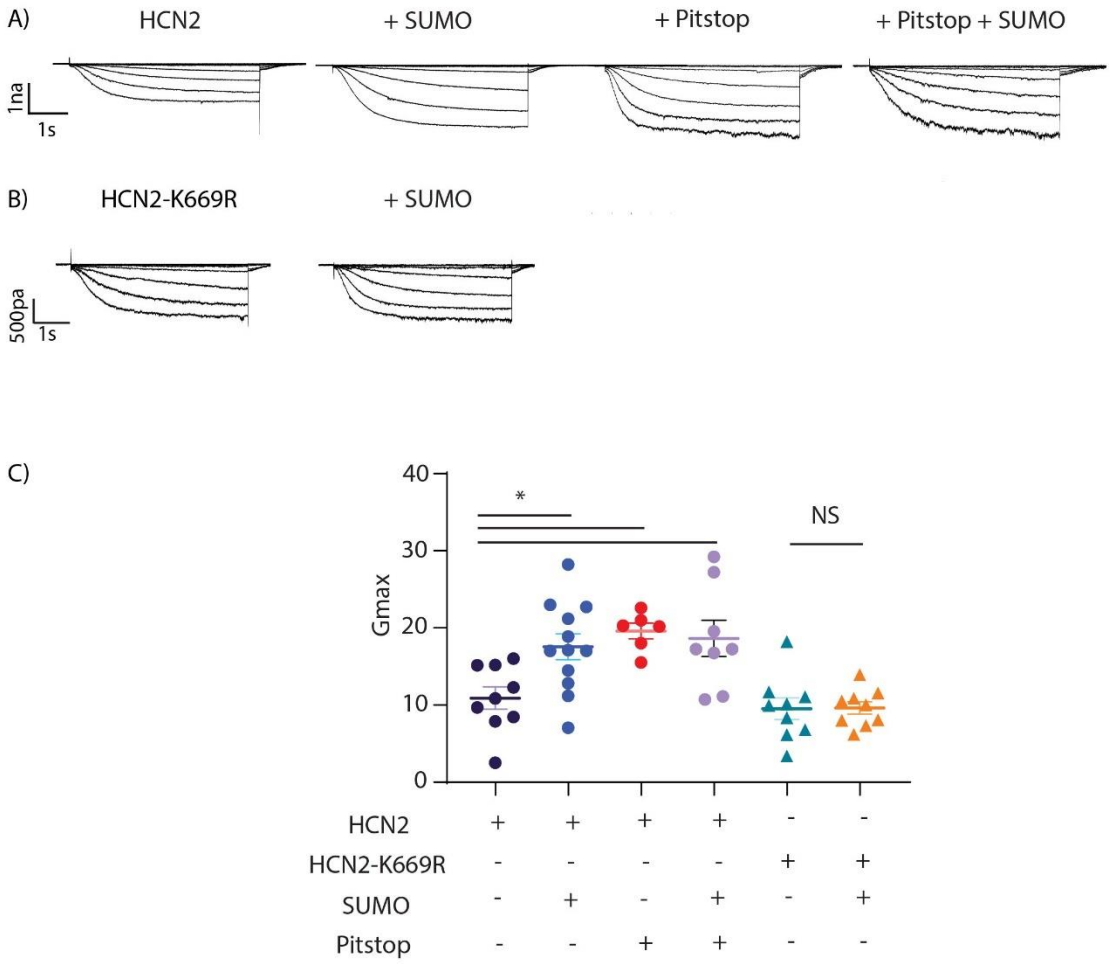

Figure 4-2 The endocytosis inhibitor, Pitstop2, mimics and occludes the effects of SUMOylation at K669 on HCN2

A) Representative traces of HEK-HCN2. **B)** Representative traces of HEK-HCN2-K669R. **C)** Graph of Gmax. Ih Gmax significantly increases with SUMO in the pipette or Pitstop2 applied, but there is no further effect of SUMO when added after pitstop (ANOVA with Tukey's multiple comparisons, $F(3,31)=4.672$, $p=0.0083$). SUMO has no effect on HEK-HCN2-K669R (t-test, $p=0.9587$). Circles = wildtype, Triangles = K669R, data presented as mean ± SEM, * represents $p<0.05$.

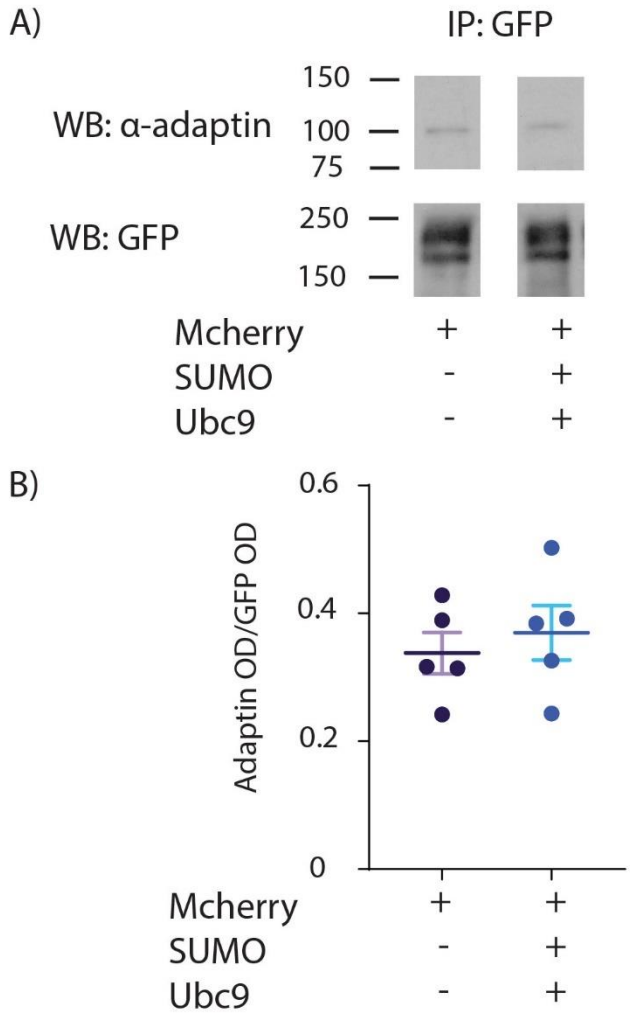

Figure 4-3 The effects of HCN2 SUMOylation are not due to clathrin mediated endocytosis

A) Western blot of α-adaptin (top) from co-ip with GFP (bottom) from HEK-HCN2 cells transfected with mCherry (left) or mCherry and SUMO and UBC9 (right). **B)** Graph of optical density of α-adaptin divided by optical density of GFP. (0.3379 ± 0.03243 v. 0.3696 ± 0.04257, t-test, p=0.6110). Data presented as mean ± SEM.

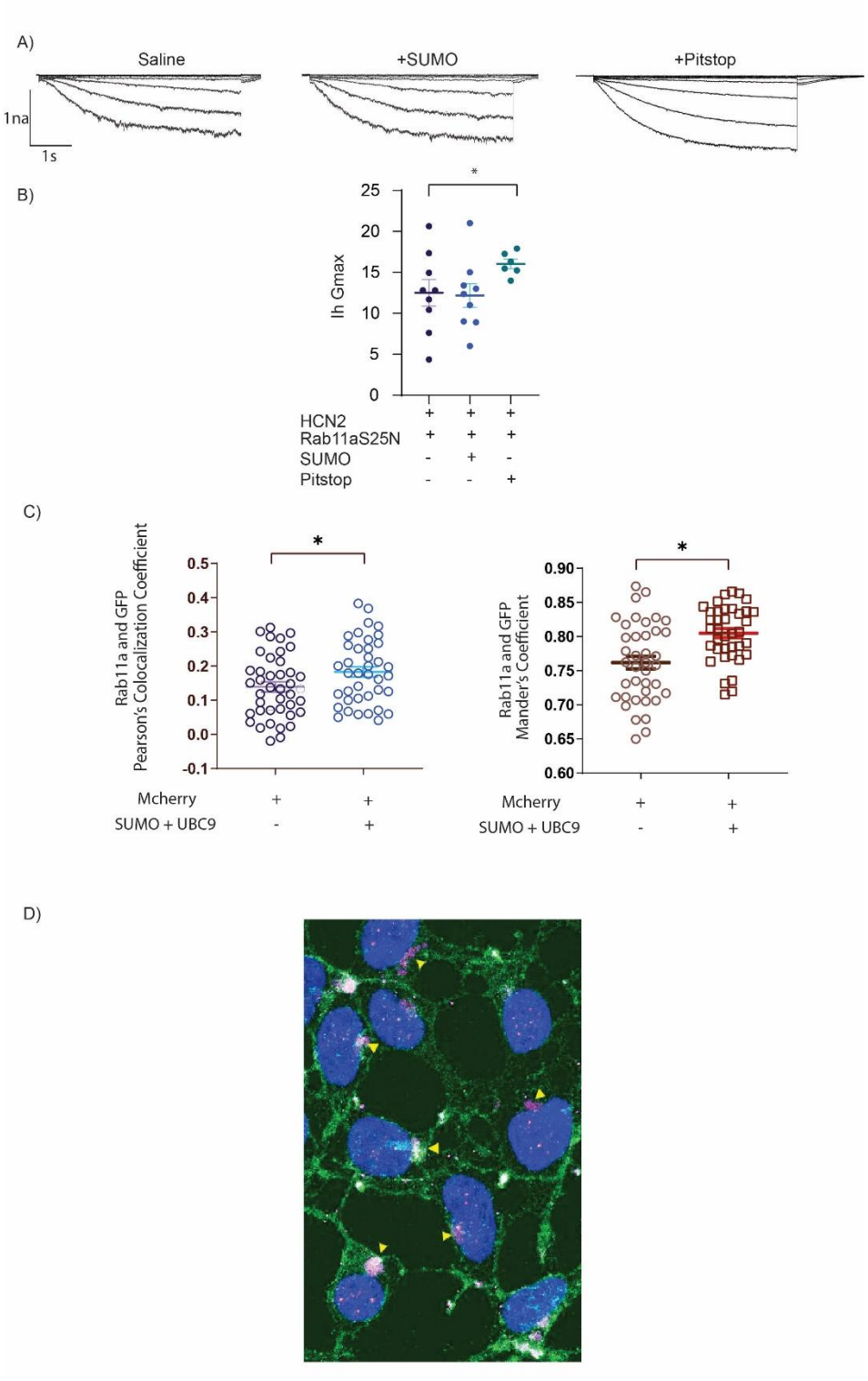
A)
Saline
+SUMO
+Pitstop
1na
1s
B)
*
25
20
15
10
5
0
Ih Gmax
HCN2 + + +
Rab11aS25N + + +
SUMO - + -
Pitstop - - +
C)
*
0.5
0.4
0.3
0.2
0.1
0.0
-0.1
Rab11a and GFP
Pearson's Colocalization Coefficient
Mcherry + +
SUMO + UBC9 - +
*
0.90
0.85
0.80
0.75
0.70
0.65
0.60
Rab11a and GFP
Mander's Coefficient
Mcherry + +
SUMO + UBC9 - +
D)

Figure 4-4 SUMOylation increases Ih through Rab11a dependent recycling
A) Representative traces of HEK-HCN2 cells transiently transfected with Rab11aS25N and either treated or not with SUMO in the pipette or Pitstop bath applied. **B)** Graph of Ih Gmax. SUMO in the pipette does not increase Gmax (t-test, p=0.4404; 12.52 ± 1.629 v. 12.18 ± 1.436), but pitstop can still increase Ih (t-test, p=0.0349; 12.52 ± 1.629 v. 16.03 ± 0.5833) **C)** Graphs of pearson's colocalization coefficient (0.1391 ± 0.09240 v. 0.1829 ± 0.09441, t-test, p=0.0407) and mander's overlap coefficient (0.7618 ± 0.05799 v. 0.8050 ± 0.04024, mann-whitney, p=0.0004). **D)** confocal microscopy image showing rab11a in magenta, HCN2-GFP in green and DAPI nuclear stain in blue. Yellow arrows point to perinuclear recycling endosomes. Data presented as mean ± SEM, * represents $p<0.05$.

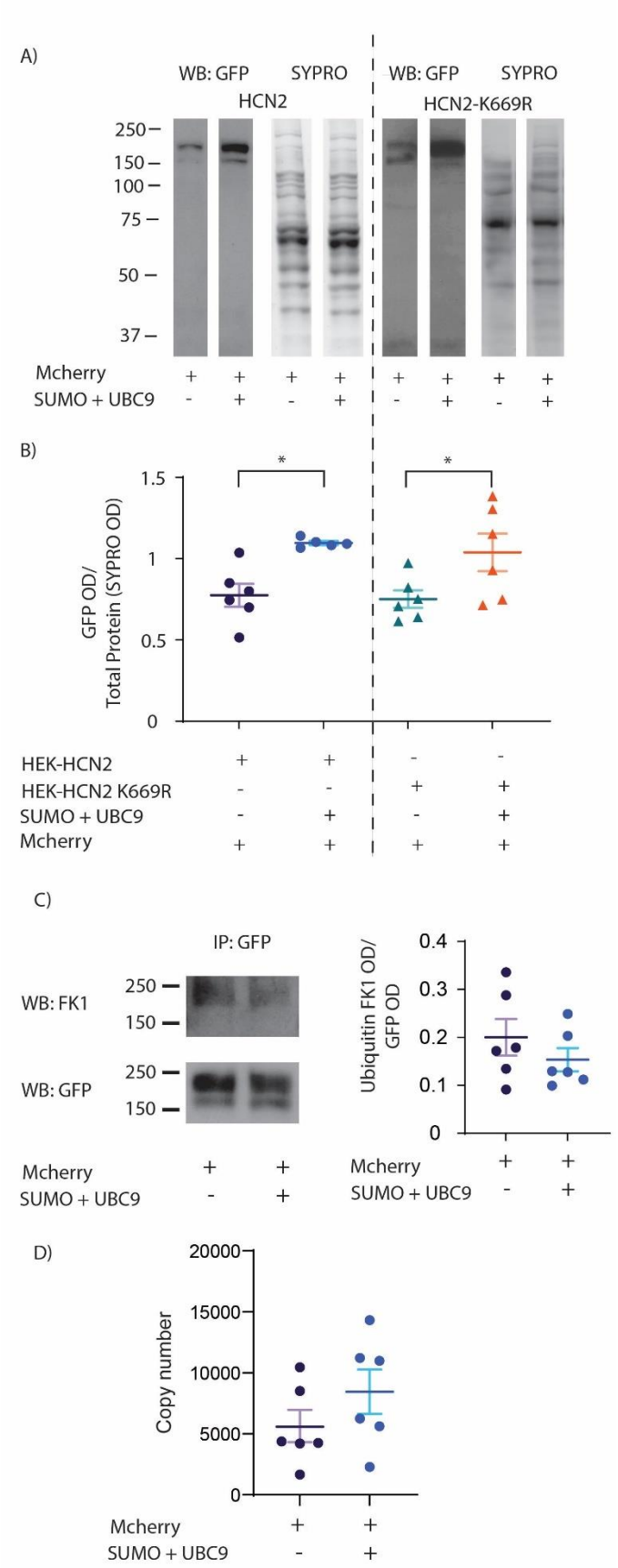
A)
WB: GFP
SYPRO
HCN2
WB: GFP
SYPRO
HCN2-K669R
250
150
100
75
50
37
Mcherry
SUMO + UBC9
B)
GFP OD/
Total Protein (SYPRO OD)
1.5
1
0.5
0
*
*
HEK-HCN2
HEK-HCN2 K669R
SUMO + UBC9
Mcherry
C)
IP: GFP
WB: FK1
WB: GFP
250
150
Ubiquitin FK1 OD/
GFP OD
0.4
0.3
0.2
0.1
0
Mcherry
SUMO + UBC9
D)
Copy number
20000
15000
10000
5000
0
Mcherry
SUMO + UBC9

Figure 4-5 SUMOylation increases HCN2 protein expression through an increase in transcription of HCN2

A) Western blot of lysates probed for GFP. Doublet between 250 and 150kD represents HCN2 protein. Total SYPRO protein stain of the full lane is shown to the right of the western. The dashed line separates wildtype and K669R mutant HCN2. **B)** Graph of the optical density of the GFP doublet divided by the optical density of the SYPRO stain for the whole lane. Transfecting with SUMO+UBC9 increases total HCN2 protein in both HEK-HCN2 (0.7750 ± 0.1724 v. 1.097 ± 0.0274; t-test, p=0.0027) and HEK-HCN2-k669R (0.7521 ± 0.1322 v. 1.039 ± 0.2839; t-test, p=0.0487). **C)** western blot of poly-ubiquitin (anti-FK1) above, and western blot of anti-GFP below from IP with GFP. Graph to the right shows optical density of anti-FK1 divided by the optical density of anti-GFP. No significant difference was observed when SUMO+UBC9 was transfected (0.2001 ± 0.09335 v. 0.1535 ± 0.05912; t-test, p=0.1035). D) Graph of HCN2 copy number following transfection with and without SUMO + UBC9 (5654 ± 1321 vs. 8455 ± 1822; t-test, p=0.2414). Data presented as mean ± SEM, * represents $p<0.05$.

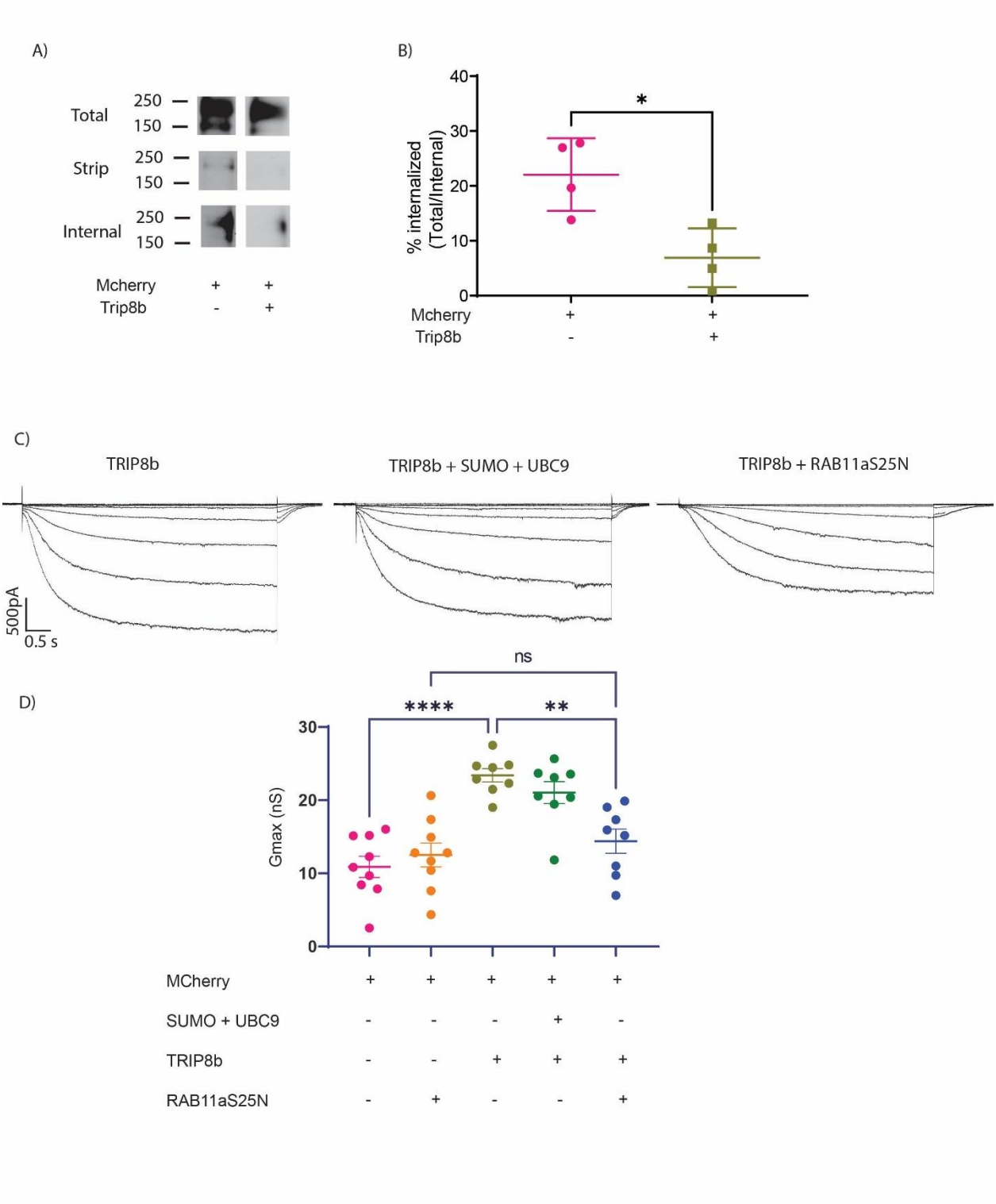

Figure 4-6 Trip8b acts through the recycling pathway to regulate HCN2

A) Western blots showing GFP signal of total, stripped, and internal HCN2 for wildtype HEK-HCN2 and HEK-HCN2 + TRIP8b. **B)** Graph of the optical density of the internalized HCN2

doublet divided by the optical density of the total surface fraction of HCN2, (t-test, **C)** Representative traces of HEK-HCN2 plus TRIP8b, TRIP8b with SUMO + UBC9, and TRIP8b and RAB11aS25N. **D)** Maximal conductance of HEK-HCN2 increases significantly when TRIP8b is transiently transfected (10.89 ± 1.449 v. 23.40 ± 0.9090), but there is no significant difference between HCN2 + TRIP8b and HCN2 + TRIP8b + SUMO + UBC9 (21.04 ± 1.504), ANOVA with Tukey's multiple comparisons, $F(3, 30) = 14.34$. HCN2 + TRIP8b + Rab11S25N is not significantly different from HCN2 + Rab11S25N, but it is significantly reduced from HCN2 + TRIP8b. Data presented as mean ± SEM, * represents $p<0.05$.

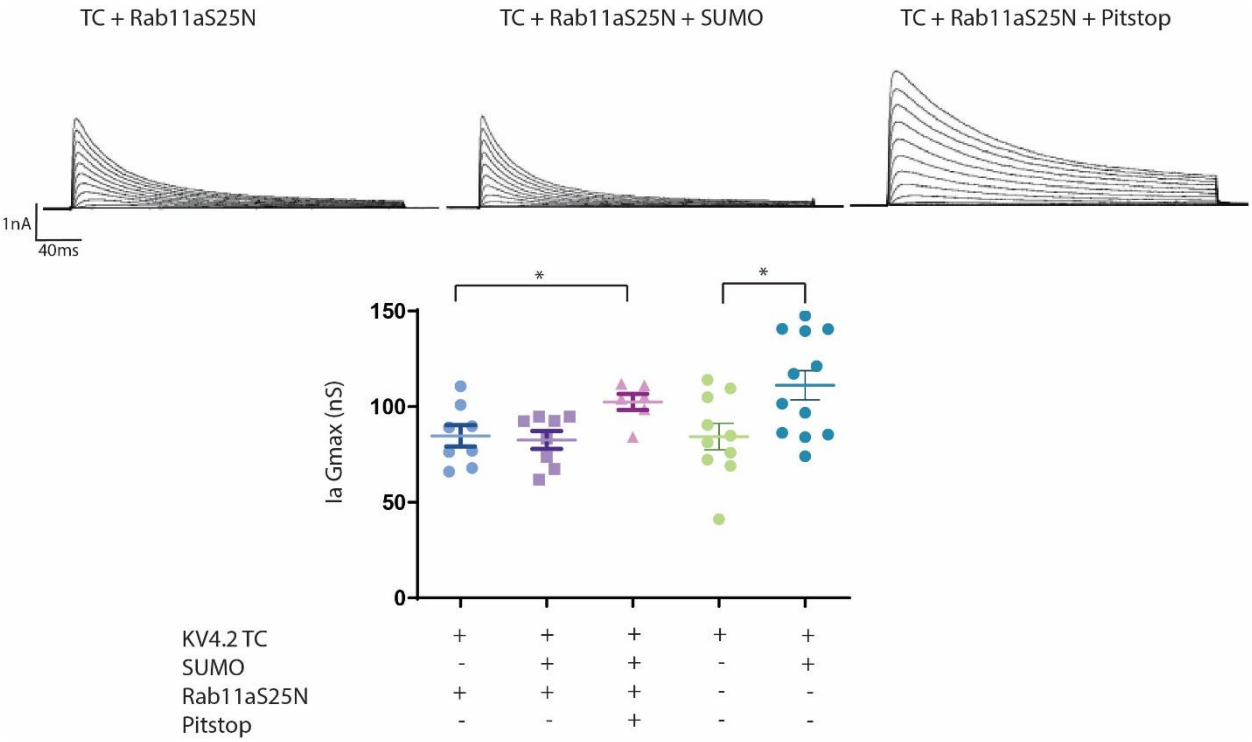

Figure 4-7 SUMOylation regulates rab11a dependent recycling of Kv4.2

A) Representative traces of Kv4.2 ternary complex (Kv4.2g + DPP10c + KChIP2a). Scale bars, 500pA by 40ms. **B)** Graph showing maximal conductance of IA ternary complex. IA significantly increases after SUMO is added in patch pipette, data adapted from (Welch et al., 2021). **C)** Graph showing maximal conductance of IA when Rab11aS25N is transiently transfected, there is no significant difference between Gmax of the Kv4.2 ternary complex and Kv4.2 ternary complex with SUMO in the patch pipette, but Gmax still increases with the endocytosis inhibitor Pitstop2 (ANOVA with Dunnett's multiple comparisons test, $F(2, 19) = 4.238$, $p=0.0301$, 84.73 ± 5.582 v. 82.59 ± 4.699 v. 102.5 ± 4.179). Data presented as mean ± SEM, * represents $p<0.05$.

5 CONCLUSION

In this dissertation work we show that HCN2 is SUMOylated in the rat DRG by both SUMO1 and SUMO2/3. HCN2 SUMOylation in the DRG increases after CFA induced inflammation. The increase in SUMOylation occurs unilaterally, with the changes in SUMOylation occurring in the ipsilateral DRG when compared to the contralateral DRG. However, the changes in HCN2 expression occur bilaterally following inflammation. These results suggest that SUMOylation of the HCN2 channel may be, in part, mediating the changes in unilateral behavior following inflammation rather than just increases in protein expression. The mechanism of regulating HCN2 channels following SUMOylation was then explored further. Here we show that HCN2 SUMOylation increases the maximal conductance of the channel, and that increases in SUMOylation are associated with an increase in colocalization of the channel with the endocytic recycling compartment. Using a dominant negative form of rab11a the effects of SUMOylation were blocked, suggesting that rab11a slow recycling is mediating the increase in maximal conductance by SUMOylation of HCN2. The effect of SUMOylation was not dependent on increasing the association of the channel with alpha-adaptin, a subunit of AP-2 adaptor protein for clathrin mediated endocytosis. Together these data suggest that SUMOylation is increasing recycling of the channel, and that clathrin mediated endocytosis of the channel is not altered by SUMOylation. Additionally, we observed an increase in expression of the HCN2 protein following SUMOylation. However, this was also present in the K669R mutant. These data suggest that SUMOylation of K669 is not increasing stability of the channel. When qPCR was performed, we observed a non-significant but comparable increase in mRNA when compared to the increase in protein. These data suggest that

transiently transfecting SUMO and UBC9 increases transcription of the channel which is what is mediating the increase in protein expression. We next examined the effect of SUMOylation of the Kv4.2 channel in recycling. SUMOylation of Kv4.2 ternary complex increases Ia Gmax. When dominant negative rab11a was transiently transfected we no longer observe an increase in IA gmax following addition of SUMO in the patch pipette. These findings raise some questions. One, is c-terminal SUMOylation a common mechanism to regulate ion channel recycling? And, if it is, how is SUMOylation acting? Two, is ion channel SUMOylation increasing the excitability of DRG neurons during pain?

5.1 C-terminal SUMOylation regulates slow recycling of ion channels

In primary cells, ventricular cardiomyocytes and hippocampal neurons, perinuclear staining of HCN4 is observed. This staining pattern matched the perinuclear distribution of HCN1, 2 and 4 observed in opossum kidney cells with the ion channel transiently transfected. This suggests that the channel may be stored in intracellular compartments. These authors next investigated recycling of HCN channels through the endocytic recycling compartment. Here they showed that the recycling endosome compartment regulates the surface expression of HCN2 and HCN4 in opossum kidney cells. Co-transfection of dominant negative Rab11a reduced the surface expression of these channels (Hardel et al., 2008). This suggested to us, in combination with alpha adaptin interaction not changing following SUMOylation of HCN2, that SUMOylation of the HCN2 channel may be altering recycling of the channel via the slow recycling pathway through rab11a. While in our study dominant negative rab11a did not reduce the maximal conductance compared to HCN2 without dominant negative rab11, we were using different cell types (HEK293 vs OK), and stable transfections vs transient transfections, dominant negative rab11a did prevent the increase in maximal conductance by addition of

SUMO in the patch pipette, suggesting that SUMOylation of the channel mediates the increase in recycling to the cell surface. In addition, Kv4.2 ternary complex uses rab11a to increase recycling of the channel and increases Ia Gmax when SUMO is added to the patch pipette.

Could SUMOylation of the c-terminus be a common mechanism to regulate surface expression? In order for a protein to be sorted for recycling, it must first avoid being sorted into intraluminal vesicles fated for the lysosome during cargo retrieval. Cargo retrieved for recycling will be sorted into tubular like micro-domains that are then sorted to the endocytic recycling compartment for slow recycling, or bud off into vesicles that are sent directly back to the plasma membrane during fast recycling (Cullen & Steinberg, 2018). A marker of the endocytic recycling compartment is Rab11a, where we used a dominant negative form in order to prevent recycling of the channel in chapter 4. Deciding the fate of cargo is mediated in part by the endosomal sorting complexes required for transport (ESCRT) system. In the early endosome, ESCRT-0, and binds to ubiquitinated proteins and forms clusters of ubiquitinated cargo. ESCRT-I/II also bind to ubiquitinated proteins and aid to further enrich these regions with ubiquitinated cargo. ESCRT-III does not contain ubiquitin binding domains, but instead is thought to be targeted to these microdomains of ubiquitinated cargo through the density of ESCRT-II. It brings with it deubiquitinating enzymes so that the ubiquitinated moieties may be reused (Cullen & Steinberg, 2018).

Ubiquitination serves as both a signal for internalization as well as a sorting signal into the lysosome. While mono-ubiquitination is generally thought of for internalization and degradation by the lysosome, endocytic proteins with ubiquitin binding domains can recognize other forms of ubiquitin modifications such as K63 or K48 linked poly-ubiquitination (Piper, Dikic, & Lukacs, 2014). Additionally, during internalization there is often multiple mono-

ubiquitinations or K63-linked polyubiquitination (Boname & Lehner, 2011). During internalization ubiquitination is a sorting signal recognized by the ESCRT system to route the channel to either be degraded or recycled. The HCN2 channel has 7 putative ubiquitination sites in it's c-terminus (K534, K553, K567, K570, K573, K638 and K639) (X. Li, 2009). SUMOylation may be increasing or decreasing the association of the ion channel with a deubiquitinase or ubiquitin ligase, respectively. When mass spectrometry was performed on Kv4.2 interacting proteins multiple ubiquitin ligases/deubiquitinases were identified (Hu et al., 2020). It is possible that one of these ligases/deubiquitinases may be influencing Kv4.2s trafficking following SUMOylation. Indeed, when investigating how SUMO regulates trafficking of other ion channels, ubiquitination changes were observed. The dopamine transporter (DAT) is SUMOylated and following SUMOylation there is a decrease in ubiquitination of DAT, and an increase in plasma membrane levels (Cartier et al., 2019). SUMOylation of CRMP2 regulates surface expression of the NaV1.7 channel. When CRMP2 is decorated with SUMO there is a reduction of interaction with Nedd4-2 ubiquitin ligase. Nedd4-2 mono ubiquitinates NaV1.7 and this is associated with internalization of the channel (Laedermann et al., 2013). Additionally, following CRMP2 SUMOylation there is a reduction in NaV1.7 association with Eps17, which is required for generating the membrane curvature needed to internalize the channel (Dustrude et al., 2016). When Smoothened (smo) is SUMOylated there is an increase in accumulation of the receptor at the plasma membrane. This is mediated in part by SUMOylation decreasing the amount of ubquitinated smo through recruitment of a SIM domain containing UBPY deubiquitinase (S. Li et al., 2012; Ma et al., 2016). The deubiquitinase USP5 interacts with the CaV3.2 channel and decreases channel ubiquitination and leads to an increase in the Ca2+ current. SUMOylation of USP5 prevents interaction of USP5 and CaV3.2,

leading to an increase in CaV3.2 ubiquitination and a decrease in the T-Type Ca2+ current (Garcia-Caballero et al., 2014; Garcia-Caballero et al., 2019). The two pore domain potassium channel, TWIK, is SUMOylated and SUMOylation may play a role in function expression of the channel in the plasma membrane. Additionally, it associates with EFA6, which is involved in clathrin-independent endocytosis. Following internalization these channels are found in the endocytic recycling compartment (Mathie, Rees, El Hachmane, & Veale, 2010). It is possible that SUMOylation may be acting in a similar mechanism in this case to enhance recycling and expression in the plasma membrane as we observed for HCN2 and Kv4.2 in chapter 4. There we observe an enhancement of SUMOylated HCN2 channels in the endocytic recycling compartment as seen by the increase in colocalization of HCN2 and Rab11a following expression of SUMO and UBC9. Performing stable isotope labelling using amino acids in cell culture (SILAC) we could examine if there are differences in ubiquitin ligases/deubiquitinases that are associated with the HCN2 channel following over expression of SUMO and UBC9 plasmids when compared to when they are not expressed. This would allow us to predict ubiquitin associated proteins are differentially interacting with the channel and could then have follow up experiments to test if they are altering trafficking of the HCN2 channel through whole cell patch clamp.

5.2 Ion channel SUMOylation increases hyperexcitability of DRG neurons

As described in chapters 2 and 3, HCN2 channels are SUMOylated following inflammatory pain. Ih is increased following inflammation, and spontaneous activity of c-fibers are increased following inflammation. The spontaneous activity is blocked following inhibition of HCN channels. As HCN2 channels protein expression is increased bilaterally following inflammation, and SUMOylation is changing unilaterally, SUMOylation of the channel may be

what is mediating the pain behavior following inflammation rather than just a change in protein expression. Other ion channels are SUMOylated in pain. Preventing their SUMOylation prevents pain behavior. For example the Nav1.8 channel is associated with the CRMP2 auxiliary subunit. CRMP2 SUMOylation is increased in the ipsilateral dorsal horn of the spinal cord relative to the contralateral side following spared nerve injury. By expressing a SUMOylation deficient mutant of CRMP2 the paw withdrawal threshold to mechanical force was increased for 2 days (Moutal, Dustrude, et al., 2017). CRMP4 is also SUMOylated. When SUMOylated it shows a reduced affinity for the Cav1.2 channel. The TRPV1 channel is also SUMOylated during pain. When SUMOylated at K822 mice were able to develop thermal hyperalgesia. When the SUMOylation deficient K822R TRPV1 was expressed in TRPV1 knockout mice, the animals failed to develop thermal hyperalgesia but upon expression of wildtype TRPV1, the development of thermal hyperalgesia was rescued. This suggests that SUMOylation of the channel is required for development of inflammatory hyperalgesia (Y. Wang et al., 2018b). Following the spared nerve injury model of neuropathic pain, the deubiquitinase USP5 shows a reduction in SUMOylation by SUMO2/3 in the DRG which is associated with a decrease in association with the Cav3.2 channel (Garcia-Caballero et al., 2019). The Kir7.1 channel shows an increase in SUMO1 decoration and a reduction in membrane expression in the spinal dorsal horn following neuropathic pain. This was associated with an increase in mechanical hypersensitivity, suggesting that SUMOylation of Kir7.1 contributes to the development of mechanical hyperalgesia by reducing Kir7.1 surface expression (Lv et al., 2022). An exception to the increase in hyperexcitability would be CRMP4. CRMP4 is SUMOylated. When SUMOylated it shows a reduced affinity for the Cav1.2 channel. Association of CRMP4 with Cav1.2 is associated with an increase in the calcium current and increased thermal pain sensitivity in rats.

Therefore, an increase in SUMOylation would be associated with a decrease in pain sensitivity, however the authors did not investigate if SUMOylation of CRMP4 was altered following pain (Lai et al., 2021).

5.3 Limitations of animal models and heterologous expression systems

In this work both a rodent model and HEK cells were used to examine HCN2 SUMOylation. While using model systems, such as the CFA model of inflammation, can be advantageous to study ion channels in a biologically relevant system, it can also provide numerous challenges that can limit the scope of the work. For example, the CFA model of inflammation is often described as a model of arthritis, as used by other researchers who previously examined the role of HCN2 in inflammatory pain. However, these authors used a model where both the hindpaw and the knee joint was injected with CFA. This causes extreme swelling of the hindlimb. These experiments are hard to gather approval by IACUC as it causes significant distress to the animal without much increase in answerable research questions than using the CFA model we used where only the hindpaw was injected. By only injecting the hindpaw this is really not a model of arthritis, as the inflammation is not in the knees and hindlimb as experienced in osteoarthritis in humans. However, we did observe results that were comparable in effect on HCN2 channel expression with a single injection as the previous studies observed with two. Additionally, by using the animal model we experienced limitations due to the heterogeneity of DRG neurons. We used crude grouping measures, by using the diameter of the DRG neurons, to classify neurons as putative c-, Aδ- or Aβ- nociceptors. Using breeding strategies to directly label neurons by class type would improve this work and allow identification of the population of neurons that mediate inflammatory nociception and rely upon expression of HCN2. Additionally, measures such as AAV mediated expression of mutant HCN2

channels to study the SUMOylation site involved have significant limitations such as performing partial laminectomies in order to directly inject AAVs into the lumbar DRGs. This would cause inflammation from the surgery, as well as the difficulty of removing part of the vertebrae without causing damage to the spinal cord and ganglia beneath. As such, using heterologous expression systems to study site specific SUMOylation of HCN2 and the molecular mechanisms underpinning the changes in surface expression by SUMOylation of HCN2 made the task of examining SUMOylation much easier as HEK cells do not endogenously express HCN2 or Kv4.2. However, this is limited by not knowing if K669 is indeed the site that is SUMOylated following inflammation. Additionally, using stable lines expressing the protein of interest also can have downsides. For example, the data collected from stably expressing GFP-HCN2 can not be directly compared to stably expressing GFP-HCN2-K669R due to the copy number of the plasmid that becomes stably integrated in the HEK cell genome. This could be mitigated by transiently transfecting HEK cells with the ion channel rather than using stable cell lines. Additionally in this work to manipulate SUMOylation, we transiently transfected SUMO and UBC9 plasmids. Because SUMOylation impacts numerous proteins, and a large number of proteins in the nucleus, the effect of globally increasing SUMOylation this way over several days can yield results that are non-specific rather than just increasing SUMOylation of the HCN2 channel. An example of this is that we observe a non-significant, but comparable increase in HCN2 mRNA and the significant increase in HCN2 protein following transient transfection with SUMO and UBC9. While using K669R mutants did not prevent this increase in protein expression, it suggests that this effect is due to a non-specific effect of SUMO and UBC9 on transcription of the channel that is not responsible for the increase in maximal conductance. One way to get around this was by using SUMO peptide in the patch pipette. This increased SUMO

for long enough to record a current and lessen the non-specific effects of globally increasing SUMO over time. Additionally, it allowed us to observe time effects, as we could increase SUMOylation after the addition of another drug, Pitstop2, to be able to observe if Pitstop2 blocked or occluded the effects of SUMOylation.

In conclusion this work shows that the HCN2 ion channel is differentially SUMOylated in the dorsal root ganglia following inflammatory pain. How HCN2 channels are regulated by SUMOylation was then further examined. Here this work shows that SUMOylation of HCN2 alters HCN2 maximal conductance through increased recycling to the plasma membrane by rab11a mediated slow recycling. Additionally, SUMOylation may have a newly identified role in regulating ion channels, where c-terminal SUMOylation is acting as a sorting signal to route channels through the endocytic pathway. Together, this work suggests that SUMOylation may have impacts on regulating hyperexcitability of ion channels by aiding in regulation of surface expression and channel density in membranes of excitable cells.

REFERENCES

Acosta, C., McMullan, S., Djouhri, L., Gao, L., Watkins, R., Berry, C., . . . Lawson, S. N. (2012). HCN1 and HCN2 in Rat DRG neurons: levels in nociceptors and non-nociceptors, NT3-dependence and influence of CFA-induced skin inflammation on HCN2 and NT3 expression. *PLoS One, 7*(12), e50442. doi:10.1371/journal.pone.0050442

Baruscotti, M., Bucchi, A., & Difrancesco, D. (2005). Physiology and pharmacology of the cardiac pacemaker ("funny") current. *Pharmacol Ther, 107*(1), 59-79. doi:10.1016/j.pharmthera.2005.01.005

Basbaum, A. I., Bautista, D. M., Scherrer, G., & Julius, D. (2009). Cellular and molecular mechanisms of pain. *Cell, 139*(2), 267-284. doi:10.1016/j.cell.2009.09.028

Belkouch, M., Dansereau, M. A., Tetreault, P., Biet, M., Beaudet, N., Dumaine, R., . . . Sarret, P. (2014). Functional up-regulation of Nav1.8 sodium channel in Abeta afferent fibers subjected to chronic peripheral inflammation. *J Neuroinflammation, 11*, 45. doi:10.1186/1742-2094-11-45

Benson, M. D., Li, Q. J., Kieckhafer, K., Dudek, D., Whorton, M. R., Sunahara, R. K., . . . Martens, J. R. (2007). SUMO modification regulates inactivation of the voltage-gated potassium channel Kv1.5. *Proc Natl Acad Sci U S A, 104*(6), 1805-1810. doi:10.1073/pnas.0606702104

Berta, T., Qadri, Y., Tan, P. H., & Ji, R. R. (2017). Targeting dorsal root ganglia and primary sensory neurons for the treatment of chronic pain. *Expert Opin Ther Targets, 21*(7), 695-703. doi:10.1080/14728222.2017.1328057

Blackwell, D. L., Lucas, J. W., & Clarke, T. C. (2014). Summary health statistics for U.S. adults: national health interview survey, 2012. *Vital Health Stat 10*(260), 1-161.

Boadas-Vaello, P., Homs, J., Reina, F., Carrera, A., & Verdu, E. (2017). Neuroplasticity of Supraspinal Structures Associated with Pathological Pain. *Anat Rec (Hoboken), 300*(8), 1481-1501. doi:10.1002/ar.23587

Boname, J. M., & Lehner, P. J. (2011). What has the study of the K3 and K5 viral ubiquitin E3 ligases taught us about ubiquitin-mediated receptor regulation? *Viruses, 3*(2), 118-131. doi:10.3390/v3020118

Brandt, M. C., Endres-Becker, J., Zagidullin, N., Motloch, L. J., Er, F., Rottlaender, D., . . . Hoppe, U. C. (2009). Effects of KCNE2 on HCN isoforms: distinct modulation of membrane expression and single channel properties. *Am J Physiol Heart Circ Physiol, 297*(1), H355-363. doi:10.1152/ajpheart.00154.2009

Braz, J., Solorzano, C., Wang, X., & Basbaum, A. I. (2014). Transmitting pain and itch messages: a contemporary view of the spinal cord circuits that generate gate control. *Neuron, 82*(3), 522-536. doi:10.1016/j.neuron.2014.01.018

Calcutt, N. A. (2020). Diabetic neuropathy and neuropathic pain: a (con)fusion of pathogenic mechanisms? *Pain, 161*(Suppl 1), S65-S86. doi:10.1097/j.pain.0000000000001922

Cartier, E., Garcia-Olivares, J., Janezic, E., Viana, J., Moore, M., Lin, M. L., . . . Kim, Y. H. (2019). The SUMO-Conjugase Ubc9 Prevents the Degradation of the Dopamine Transporter, Enhancing Its Cell Surface Level and Dopamine Uptake. *Front Cell Neurosci, 13*, 35. doi:10.3389/fncel.2019.00035

Chaplan, S. R., Guo, H. Q., Lee, D. H., Luo, L., Liu, C., Kuei, C., . . . Dubin, A. E. (2003). Neuronal hyperpolarization-activated pacemaker channels drive neuropathic pain. *J Neurosci, 23*(4), 1169-1178.

Chapman, C. R., & Vierck, C. J. (2017). The Transition of Acute Postoperative Pain to Chronic Pain: An Integrative Overview of Research on Mechanisms. *J Pain, 18*(4), 359 e351-359 e338. doi:10.1016/j.jpain.2016.11.004

Chen, X., Zhang, Y., Ren, X., Su, Q., Liu, Y., Dang, X., . . . Qi, Y. (2021). The SUMO-specific protease SENP2 plays an essential role in the regulation of Kv7.2 and Kv7.3 potassium channels. *J Biol Chem, 297*(4), 101183. doi:10.1016/j.jbc.2021.101183

Cheng, J. K., & Ji, R. R. (2008). Intracellular signaling in primary sensory neurons and persistent pain. *Neurochem Res, 33*(10), 1970-1978. doi:10.1007/s11064-008-9711-z

Cho, H. J., Staikopoulos, V., Furness, J. B., & Jennings, E. A. (2009). Inflammation-induced increase in hyperpolarization-activated, cyclic nucleotide-gated channel protein in trigeminal ganglion neurons and the effect of buprenorphine. *Neuroscience, 162*(2), 453-461. doi:10.1016/j.neuroscience.2009.04.063

Cullen, P. J., & Steinberg, F. (2018). To degrade or not to degrade: mechanisms and significance of endocytic recycling. *Nat Rev Mol Cell Biol, 19*(11), 679-696. doi:10.1038/s41580-018-0053-7

Cuomo, O., Casamassa, A., Brancaccio, P., Laudati, G., Valsecchi, V., Anzilotti, S., . . . Annunziato, L. (2020). Sumoylation of sodium/calcium exchanger in brain ischemia and ischemic preconditioning. *Cell Calcium, 87*, 102195. doi:10.1016/j.ceca.2020.102195

Dai, X. Q., Kolic, J., Marchi, P., Sipione, S., & Macdonald, P. E. (2009). SUMOylation regulates Kv2.1 and modulates pancreatic beta-cell excitability. *J Cell Sci, 122*(Pt 6), 775-779. doi:10.1242/jcs.036632

Dalle, C., & Eisenach, J. C. (2005). Peripheral block of the hyperpolarization-activated cation current (Ih) reduces mechanical allodynia in animal models of postoperative and neuropathic pain. *Reg Anesth Pain Med, 30*(3), 243-248. doi:10.1016/j.rapm.2005.01.010

Devor, M. (1999). Unexplained peculiarities of the dorsal root ganglion. *Pain, Suppl 6*, S27-35.

DiFrancesco, J. C., & DiFrancesco, D. (2015). Dysfunctional HCN ion channels in neurological diseases. *Front Cell Neurosci, 6*, 174. doi:10.3389/fncel.2015.00071

Dini, L., Del Lungo, M., Resta, F., Melchiorre, M., Spinelli, V., Di Cesare Mannelli, L., . . . Romanelli, M. N. (2018). Selective Blockade of HCN1/HCN2 Channels as a Potential Pharmacological Strategy Against Pain. *Front Pharmacol, 9*, 1252. doi:10.3389/fphar.2018.01252

Djouhri, L., Al Otaibi, M., Kahlat, K., Smith, T., Sathish, J., & Weng, X. (2015). Persistent hindlimb inflammation induces changes in activation properties of hyperpolarization-activated current (Ih) in rat C-fiber nociceptors in vivo. *Neuroscience, 301*, 121-133. doi:10.1016/j.neuroscience.2015.05.074

Djouhri, L., Dawbarn, D., Robertson, A., Newton, R., & Lawson, S. N. (2001). Time course and nerve growth factor dependence of inflammation-induced alterations in electrophysiological membrane properties in nociceptive primary afferent neurons. *J Neurosci, 21*(22), 8722-8733.

Djouhri, L., & Lawson, S. N. (2004). Abeta-fiber nociceptive primary afferent neurons: a review of incidence and properties in relation to other afferent A-fiber neurons in mammals. *Brain Res Brain Res Rev, 46*(2), 131-145. doi:10.1016/j.brainresrev.2004.07.015

Du, L., Wang, S. J., Cui, J., He, W. J., & Ruan, H. Z. (2013a). Inhibition of HCN channels within the periaqueductal gray attenuates neuropathic pain in rats. *Behav Neurosci, 127*(2), 325-329. doi:10.1037/a0031893

Du, L., Wang, S. J., Cui, J., He, W. J., & Ruan, H. Z. (2013b). The role of HCN channels within the periaqueductal gray in neuropathic pain. *Brain Res, 1500*, 36-44. doi:10.1016/j.brainres.2013.01.035

Dubin, A. E., & Patapoutian, A. (2010). Nociceptors: the sensors of the pain pathway. *J Clin Invest, 120*(11), 3760-3772. doi:10.1172/JCI42843

Dustrude, E. T., Moutal, A., Yang, X., Wang, Y., Khanna, M., & Khanna, R. (2016). Hierarchical CRMP2 posttranslational modifications control NaV1.7 function. *Proc Natl Acad Sci U S A, 113*(52), E8443-E8452. doi:10.1073/pnas.1610531113

Dustrude, E. T., Wilson, S. M., Ju, W., Xiao, Y., & Khanna, R. (2013). CRMP2 protein SUMOylation modulates NaV1.7 channel trafficking. *J Biol Chem, 288*(34), 24316-24331. doi:10.1074/jbc.M113.474924

Emery, E. C., Young, G. T., Berrocoso, E. M., Chen, L., & McNaughton, P. A. (2011). HCN2 ion channels play a central role in inflammatory and neuropathic pain. *Science, 333*(6048), 1462-1466. doi:10.1126/science.1206243

Emery, E. C., Young, G. T., & McNaughton, P. A. (2012). HCN2 ion channels: an emerging role as the pacemakers of pain. *Trends Pharmacol Sci, 33*(8), 456-463. doi:10.1016/j.tips.2012.04.004

Flotho, A., & Melchior, F. (2013). Sumoylation: a regulatory protein modification in health and disease. *Annu Rev Biochem, 82*, 357-385. doi:10.1146/annurev-biochem-061909-093311

Forster, L. A., Jansen, L. R., Rubaharan, M., Murphy, A. Z., & Baro, D. J. (2020a). Alterations in SUMOylation of the hyperpolarization-activated cyclic nucleotide-gated ion channel 2 during persistent inflammation. *Eur J Pain*. doi:10.1002/ejp.1606

Forster, L. A., Jansen, L. R., Rubaharan, M., Murphy, A. Z., & Baro, D. J. (2020b). Alterations in SUMOylation of the hyperpolarization-activated cyclic nucleotide gated ion channel 2 during persistent inflammation. *Eur J Pain*. doi:10.1002/ejp.1606

Francois-Moutal, L., Dustrude, E. T., Wang, Y., Brustovetsky, T., Dorame, A., Ju, W., . . . Khanna, R. (2018). Inhibition of the Ubc9 E2 SUMO-conjugating enzyme-CRMP2 interaction decreases NaV1.7 currents and reverses experimental neuropathic pain. *Pain, 159*(10), 2115-2127. doi:10.1097/j.pain.0000000000001294

Francois-Moutal, L., Scott, D. D., Perez-Miller, S., Gokhale, V., Khanna, M., & Khanna, R. (2018). Chemical shift perturbation mapping of the Ubc9-CRMP2 interface identifies a pocket in CRMP2 amenable for allosteric modulation of Nav1.7 channels. *Channels (Austin), 12*(1), 219-227. doi:10.1080/19336950.2018.1491244

Frykman, S., Inoue, M., Ikeda, A., Teranishi, Y., Kihara, T., Lundgren, J. L., . . . Tjernberg, L. O. (2017). Maturation and processing of the amyloid precursor protein is regulated by the potassium/sodium hyperpolarization-activated cyclic nucleotide-gated ion channel 2 (HCN2). *Biochem Biophys Res Commun, 483*(1), 352-358. doi:10.1016/j.bbrc.2016.12.140

Fujimuro, M., Sawada, H., & Yokosawa, H. (1994). Production and characterization of monoclonal antibodies specific to multi-ubiquitin chains of polyubiquitinated proteins. *FEBS Lett, 349*(2), 173-180. doi:10.1016/0014-5793(94)00647-4

Gao, L. L., McMullan, S., Djouhri, L., Acosta, C., Harper, A. A., & Lawson, S. N. (2012). Expression and properties of hyperpolarization-activated current in rat dorsal root ganglion neurons with known sensory function. *J Physiol, 590*(19), 4691-4705. doi:10.1113/jphysiol.2012.238485

Garcia-Caballero, A., Gadotti, V. M., Stemkowski, P., Weiss, N., Souza, I. A., Hodgkinson, V., . . . Zamponi, G. W. (2014). The deubiquitinating enzyme USP5 modulates neuropathic and inflammatory pain by enhancing Cav3.2 channel activity. *Neuron, 83*(5), 1144-1158. doi:10.1016/j.neuron.2014.07.036

Garcia-Caballero, A., Zhang, F. X., Chen, L., M'Dahoma, S., Huang, J., & Zamponi, G. W. (2019). SUMOylation regulates USP5-Cav3.2 calcium channel interactions. *Mol Brain, 12*(1), 73. doi:10.1186/s13041-019-0493-9

Gold, M. S., & Gebhart, G. F. (2010). Nociceptor sensitization in pain pathogenesis. *Nat Med, 16*(11), 1248-1257. doi:10.1038/nm.2235

Guo, D., & Hu, J. (2014). Spinal presynaptic inhibition in pain control. *Neuroscience, 283*, 95-106. doi:10.1016/j.neuroscience.2014.09.032

Hardel, N., Harmel, N., Zolles, G., Fakler, B., & Klocker, N. (2008). Recycling endosomes supply cardiac pacemaker channels for regulated surface expression. *Cardiovasc Res, 79*(1), 52-60. doi:10.1093/cvr/cvn062

Hendriks, I. A., D'Souza, R. C., Chang, J. G., Mann, M., & Vertegaal, A. C. (2015). System-wide identification of wild-type SUMO-2 conjugation sites. *Nat Commun, 6*, 7289. doi:10.1038/ncomms8289

Henley, J. M., Craig, T. J., & Wilkinson, K. A. (2014). Neuronal SUMOylation: mechanisms, physiology, and roles in neuronal dysfunction. *Physiol Rev, 94*(4), 1249-1285. doi:10.1152/physrev.00008.2014

Herrity, A. N., Rau, K. K., Petruska, J. C., Stirling, D. P., & Hubscher, C. H. (2014). Identification of bladder and colon afferents in the nodose ganglia of male rats. *J Comp Neurol, 522*(16), 3667-3682. doi:10.1002/cne.23629

Herrmann, S., Rajab, H., Christ, I., Schirdewahn, C., Hofler, D., Fischer, M. J. M., . . . Ludwig, A. (2017). Protein kinase A regulates inflammatory pain sensitization by modulating HCN2 channel activity in nociceptive sensory neurons. *Pain, 158*(10), 2012-2024. doi:10.1097/j.pain.0000000000001005

Hu, J. H., Malloy, C., Tabor, G. T., Gutzmann, J. J., Liu, Y., Abebe, D., . . . Hoffman, D. A. (2020). Activity-dependent isomerization of Kv4.2 by Pin1 regulates cognitive flexibility. *Nat Commun, 11*(1), 1567. doi:10.1038/s41467-020-15390-x

Huang, H., Zhang, Z., & Huang, D. (2019). Decreased HCN2 channel expression attenuates neuropathic pain by inhibiting pro-inflammatory reactions and NF-kappaB activation in mice. *Int J Clin Exp Pathol, 12*(1), 154-163.

Hucho, T., & Levine, J. D. (2007). Signaling pathways in sensitization: toward a nociceptor cell biology. *Neuron, 55*(3), 365-376. doi:10.1016/j.neuron.2007.07.008

Hutcheon, B., & Yarom, Y. (2000). Resonance, oscillation and the intrinsic frequency preferences of neurons. *Trends Neurosci, 23*(5), 216-222. doi:10.1016/s0166-2236(00)01547-2

Jansen, L. R., Forster, L. A., Smith, X. L., Rubaharan, M., Murphy, A. Z., & Baro, D. J. (2021). Changes in peripheral HCN2 channels during persistent inflammation. *Channels (Austin), 15*(1), 165-179. doi:10.1080/19336950.2020.1870086

Jentsch, S., & Psakhye, I. (2013). Control of nuclear activities by substrate-selective and protein-group SUMOylation. *Annu Rev Genet, 47*, 167-186. doi:10.1146/annurev-genet-111212-133453

Jiang, Y. Q., Xing, G. G., Wang, S. L., Tu, H. Y., Chi, Y. N., Li, J., . . . Wan, Y. (2008). Axonal accumulation of hyperpolarization-activated cyclic nucleotide-gated cation channels

contributes to mechanical allodynia after peripheral nerve injury in rat. *Pain, 137*(3), 495-506. doi:10.1016/j.pain.2007.10.011

Johnson, E. S. (2004). Protein modification by SUMO. *Annu Rev Biochem, 73*, 355-382. doi:10.1146/annurev.biochem.73.011303.074118

Kase, D., & Imoto, K. (2012). The Role of HCN Channels on Membrane Excitability in the Nervous System. *J Signal Transduct, 2012*, 619747. doi:10.1155/2012/619747

Keiten-Schmitz, J., Wagner, K., Piller, T., Kaulich, M., Alberti, S., & Muller, S. (2020). The Nuclear SUMO-Targeted Ubiquitin Quality Control Network Regulates the Dynamics of Cytoplasmic Stress Granules. *Mol Cell, 79*(1), 54-67 e57. doi:10.1016/j.molcel.2020.05.017

Kimura, K., Kitano, J., Nakajima, Y., & Nakanishi, S. (2004). Hyperpolarization-activated, cyclic nucleotide-gated HCN2 cation channel forms a protein assembly with multiple neuronal scaffold proteins in distinct modes of protein-protein interaction. *Genes Cells, 9*(7), 631-640. doi:10.1111/j.1356-9597.2004.00752.x

Kjenseth, A., Fykerud, T. A., Sirnes, S., Bruun, J., Yohannes, Z., Kolberg, M., . . . Leithe, E. (2012). The gap junction channel protein connexin 43 is covalently modified and regulated by SUMOylation. *J Biol Chem, 287*(19), 15851-15861. doi:10.1074/jbc.M111.281832

Koltzenburg, M., Wall, P. D., & McMahon, S. B. (1999). Does the right side know what the left is doing? *Trends Neurosci, 22*(3), 122-127. doi:10.1016/s0166-2236(98)01302-2

Kouranova, E. V., Strassle, B. W., Ring, R. H., Bowlby, M. R., & Vasilyev, D. V. (2008). Hyperpolarization-activated cyclic nucleotide-gated channel mRNA and protein expression in large versus small diameter dorsal root ganglion neurons: correlation with hyperpolarization-activated current gating. *Neuroscience, 153*(4), 1008-1019. doi:10.1016/j.neuroscience.2008.03.032

Kruse, M., Schulze-Bahr, E., Corfield, V., Beckmann, A., Stallmeyer, B., Kurtbay, G., . . . Pongs, O. (2009). Impaired endocytosis of the ion channel TRPM4 is associated with human progressive familial heart block type I. *J Clin Invest, 119*(9), 2737-2744. doi:10.1172/JCI38292

Kumar, R., Gonzalez-Prieto, R., Xiao, Z., Verlaan-de Vries, M., & Vertegaal, A. C. O. (2017). The STUbL RNF4 regulates protein group SUMOylation by targeting the SUMO conjugation machinery. *Nat Commun, 8*(1), 1809. doi:10.1038/s41467-017-01900-x

Kuner, R., & Flor, H. (2016). Structural plasticity and reorganisation in chronic pain. *Nat Rev Neurosci, 18*(1), 20-30. doi:10.1038/nrn.2016.162

Laedermann, C. J., Cachemaille, M., Kirschmann, G., Pertin, M., Gosselin, R. D., Chang, I., . . . Decosterd, I. (2013). Dysregulation of voltage-gated sodium channels by ubiquitin ligase NEDD4-2 in neuropathic pain. *J Clin Invest, 123*(7), 3002-3013. doi:10.1172/JCI68996

Lai, S., Pan, M., Liao, H., Chen, J., Jiang, Y., & Li, Y. (2021). The impact of CRMP4 SUMOylation on the Cav1.2 interaction, neurite outgrowth and thermal pain sensitivity. *J Integr Neurosci, 20*(3), 595-603. doi:10.31083/j.jin2003063

Lainez, S., Tsantoulas, C., Biel, M., & McNaughton, P. A. (2019). HCN3 ion channels: roles in sensory neuronal excitability and pain. *J Physiol, 597*(17), 4661-4675. doi:10.1113/JP278211

Lee, D. H., Chang, L., Sorkin, L. S., & Chaplan, S. R. (2005). Hyperpolarization-activated, cation-nonselective, cyclic nucleotide-modulated channel blockade alleviates mechanical

allodynia and suppresses ectopic discharge in spinal nerve ligated rats. *Journal of Pain, 6*(7), 417-424. doi:10.1016/j.jpain.2005.02.002

Lewis, A. S., Schwartz, E., Chan, C. S., Noam, Y., Shin, M., Wadman, W. J., . . . Chetkovich, D. M. (2009). Alternatively spliced isoforms of TRIP8b differentially control h channel trafficking and function. *J Neurosci, 29*(19), 6250-6265. doi:10.1523/JNEUROSCI.0856-09.2009

Li, C. L., Li, K. C., Wu, D., Chen, Y., Luo, H., Zhao, J. R., . . . Zhang, X. (2016). Somatosensory neuron types identified by high-coverage single-cell RNA-sequencing and functional heterogeneity. *Cell Res, 26*(1), 83-102. doi:10.1038/cr.2015.149

Li, S., Chen, Y., Shi, Q., Yue, T., Wang, B., & Jiang, J. (2012). Hedgehog-regulated ubiquitination controls smoothened trafficking and cell surface expression in Drosophila. *PLoS Biol, 10*(1), e1001239. doi:10.1371/journal.pbio.1001239

Li, W. M., Cui, K. M., Li, N., Gu, Q. B., Schwarz, W., Ding, G. H., & Wu, G. C. (2005). Analgesic effect of electroacupuncture on complete Freund's adjuvant-induced inflammatory pain in mice: a model of antipain treatment by acupuncture in mice. *Jpn J Physiol, 55*(6), 339-344. doi:10.2170/jjphysiol.RP001505

Liu, Y., Feng, Y., & Zhang, T. (2015). Pulsed Radiofrequency Treatment Enhances Dorsal Root Ganglion Expression of Hyperpolarization-Activated Cyclic Nucleotide-Gated Channels in a Rat Model of Neuropathic Pain. *J Mol Neurosci, 57*(1), 97-105. doi:10.1007/s12031-015-0582-x

Luo, L., Chang, L., Brown, S. M., Ao, H., Lee, D. H., Higuera, E. S., . . . Chaplan, S. R. (2007). Role of peripheral hyperpolarization-activated cyclic nucleotide-modulated channel pacemaker channels in acute and chronic pain models in the rat. *Neuroscience, 144*(4), 1477-1485. doi:10.1016/j.neuroscience.2006.10.048

Lv, Y. Y., Wang, H., Fan, H. T., Xu, T., Xin, W. J., & Guo, R. X. (2022). SUMOylation of Kir7.1 participates in neuropathic pain through regulating its membrane expression in spinal cord neurons. *CNS Neurosci Ther, 28*(8), 1259-1267. doi:10.1111/cns.13871

Ma, G., Li, S., Han, Y., Li, S., Yue, T., Wang, B., & Jiang, J. (2016). Regulation of Smoothened Trafficking and Hedgehog Signaling by the SUMO Pathway. *Dev Cell, 39*(4), 438-451. doi:10.1016/j.devcel.2016.09.014

MacDonald, E., Savage, B., & Zech, T. (2020). Connecting the dots: combined control of endocytic recycling and degradation. *Biochem Soc Trans, 48*(6), 2377-2386. doi:10.1042/BST20180255

Malmberg, A. B., Brandon, E. P., Idzerda, R. L., Liu, H., McKnight, G. S., & Basbaum, A. I. (1997). Diminished inflammation and nociceptive pain with preservation of neuropathic pain in mice with a targeted mutation of the type I regulatory subunit of cAMP-dependent protein kinase. *J Neurosci, 17*(19), 7462-7470.

Mathie, A., Rees, K. A., El Hachmane, M. F., & Veale, E. L. (2010). Trafficking of neuronal two pore domain potassium channels. *Curr Neuropharmacol, 8*(3), 276-286. doi:10.2174/157015910792246146

Mendell, L. M. (2014). Constructing and deconstructing the gate theory of pain. *Pain, 155*(2), 210-216. doi:10.1016/j.pain.2013.12.010

Michels, G., Er, F., Khan, I. F., Endres-Becker, J., Brandt, M. C., Gassanov, N., . . . Hoppe, U. C. (2008). K+ channel regulator KCR1 suppresses heart rhythm by modulating the pacemaker current If. *PLoS One, 3*(1), e1511. doi:10.1371/journal.pone.0001511

Millan, M. J., Czlonkowski, A., Morris, B., Stein, C., Arendt, R., Huber, A., . . . Herz, A. (1988). Inflammation of the hind limb as a model of unilateral, localized pain: influence on multiple opioid systems in the spinal cord of the rat. *Pain, 35*(3), 299-312.

Momin, A., Cadiou, H., Mason, A., & McNaughton, P. A. (2008). Role of the hyperpolarization-activated current Ih in somatosensory neurons. *J Physiol, 586*(24), 5911-5929. doi:10.1113/jphysiol.2008.163154

Moutal, A., Dustrude, E. T., Largent-Milnes, T. M., Vanderah, T. W., Khanna, M., & Khanna, R. (2017). Blocking CRMP2 SUMOylation reverses neuropathic pain. *Mol Psychiatry*. doi:10.1038/mp.2017.117

Moutal, A., Yang, X., Li, W., Gilbraith, K. B., Luo, S., Cai, S., . . . Khanna, R. (2017). CRISPR/Cas9 editing of Nf1 gene identifies CRMP2 as a therapeutic target in neurofibromatosis type 1-related pain that is reversed by (S)-Lacosamide. *Pain, 158*(12), 2301-2319. doi:10.1097/j.pain.0000000000001002

Muley, M. M., Krustev, E., & McDougall, J. J. (2016). Preclinical Assessment of Inflammatory Pain. *CNS Neurosci Ther, 22*(2), 88-101. doi:10.1111/cns.12486

Nagi, S. S., Marshall, A. G., Makdani, A., Jarocka, E., Liljencrantz, J., Ridderstrom, M., . . . Olausson, H. (2019). An ultrafast system for signaling mechanical pain in human skin. *Sci Adv, 5*(7), eaaw1297. doi:10.1126/sciadv.aaw1297

Nakajima, T., Ohtori, S., Inoue, G., Koshi, T., Yamamoto, S., Nakamura, J., . . . Harada, Y. (2008). The characteristics of dorsal-root ganglia and sensory innervation of the hip in rats. *J Bone Joint Surg Br, 90*(2), 254-257. doi:10.1302/0301-620X.90B2.19808

Nawathe, P. A., Kryukova, Y., Oren, R. V., Milanesi, R., Clancy, C. E., Lu, J. T., . . . Robinson, R. B. (2013). An LQTS6 MiRP1 mutation suppresses pacemaker current and is associated with sinus bradycardia. *J Cardiovasc Electrophysiol, 24*(9), 1021-1027. doi:10.1111/jce.12163

Pace, M. C., Passavanti, M. B., De Nardis, L., Bosco, F., Sansone, P., Pota, V., . . . Aurilio, C. (2018). Nociceptor plasticity: A closer look. *J Cell Physiol, 233*(4), 2824-2838. doi:10.1002/jcp.25993

Papp, I., Hollo, K., & Antal, M. (2010). Plasticity of hyperpolarization-activated and cyclic nucleotid-gated cation channel subunit 2 expression in the spinal dorsal horn in inflammatory pain. *Eur J Neurosci, 32*(7), 1193-1201. doi:10.1111/j.1460-9568.2010.07370.x

Parker, A. R., Forster, L. A., & Baro, D. J. (2019). Modulator-Gated, SUMOylation-Mediated, Activity-Dependent Regulation of Ionic Current Densities Contributes to Short-Term Activity Homeostasis. *J Neurosci, 39*(4), 596-611. doi:10.1523/JNEUROSCI.1379-18.2018

Parker, A. R., Welch, M. A., Forster, L. A., Tasneem, S. M., Dubhashi, J. A., & Baro, D. J. (2016). SUMOylation of the Hyperpolarization-Activated Cyclic Nucleotide-Gated Channel 2 Increases Surface Expression and the Maximal Conductance of the Hyperpolarization-Activated Current. *Front Mol Neurosci, 9*, 168. doi:10.3389/fnmol.2016.00168

Parker, A. R., Welch, M. A., Forster, L. A., Tasneem, S. M., Dubhashi, J. A., & Baro, D. J. (2017). SUMOylation of the Hyperpolarization-Activated Cyclic Nucleotide-Gated Channel 2 Increases Surface Expression and the Maximal Conductance of the Hyperpolarization-Activated Current. *Front Mol Neurosci, 9*, 168. doi:10.3389/fnmol.2016.00168

Pinho-Ribeiro, F. A., Verri, W. A., Jr., & Chiu, I. M. (2017). Nociceptor Sensory Neuron-Immune Interactions in Pain and Inflammation. *Trends Immunol, 38*(1), 5-19. doi:10.1016/j.it.2016.10.001

Piper, R. C., Dikic, I., & Lukacs, G. L. (2014). Ubiquitin-dependent sorting in endocytosis. *Cold Spring Harb Perspect Biol, 6*(1). doi:10.1101/cshperspect.a016808

Plant, L. D., Dementieva, I. S., Kollewe, A., Olikara, S., Marks, J. D., & Goldstein, S. A. (2010). One SUMO is sufficient to silence the dimeric potassium channel K2P1. *Proc Natl Acad Sci U S A, 107*(23), 10743-10748. doi:10.1073/pnas.1004712107

Plant, L. D., Dowdell, E. J., Dementieva, I. S., Marks, J. D., & Goldstein, S. A. (2011). SUMO modification of cell surface Kv2.1 potassium channels regulates the activity of rat hippocampal neurons. *J Gen Physiol, 137*(5), 441-454. doi:10.1085/jgp.201110604

Plant, L. D., Marks, J. D., & Goldstein, S. A. (2016). SUMOylation of NaV1.2 channels mediates the early response to acute hypoxia in central neurons. *Elife, 5*. doi:10.7554/eLife.20054

Plant, L. D., Xiong, D., Romero, J., Dai, H., & Goldstein, S. A. N. (2020). Hypoxia Produces Pro-arrhythmic Late Sodium Current in Cardiac Myocytes by SUMOylation of NaV1.5 Channels. *Cell Rep, 30*(7), 2225-2236 e2224. doi:10.1016/j.celrep.2020.01.025

Poolos, N. P. (2012). Hyperpolarization-Activated Cyclic Nucleotide-Gated (HCN) Ion Channelopathy in Epilepsy. In th, J. L. Noebels, M. Avoli, M. A. Rogawski, R. W. Olsen, & A. V. Delgado-Escueta (Eds.), *Jasper's Basic Mechanisms of the Epilepsies*. Bethesda (MD).

Psakhye, I., & Jentsch, S. (2016). Identification of Substrates of Protein-Group SUMOylation. *Methods Mol Biol, 1475*, 219-231. doi:10.1007/978-1-4939-6358-4_16

Qi, Y., Wang, J., Bomben, V. C., Li, D. P., Chen, S. R., Sun, H., . . . Yeh, E. T. (2014). Hyper-SUMOylation of the Kv7 potassium channel diminishes the M-current leading to seizures and sudden death. *Neuron, 83*(5), 1159-1171. doi:10.1016/j.neuron.2014.07.042

Qu, J., Kryukova, Y., Potapova, I. A., Doronin, S. V., Larsen, M., Krishnamurthy, G., . . . Robinson, R. B. (2004). MiRP1 modulates HCN2 channel expression and gating in cardiac myocytes. *J Biol Chem, 279*(42), 43497-43502. doi:10.1074/jbc.M405018200

Rajan, S., Plant, L. D., Rabin, M. L., Butler, M. H., & Goldstein, S. A. (2005). Sumoylation silences the plasma membrane leak K+ channel K2P1. *Cell, 121*(1), 37-47. doi:10.1016/j.cell.2005.01.019

Reichling, D. B., & Levine, J. D. (2009). Critical role of nociceptor plasticity in chronic pain. *Trends Neurosci, 32*(12), 611-618. doi:10.1016/j.tins.2009.07.007

Resta, F., Masi, A., Sili, M., Laurino, A., Moroni, F., & Mannaioni, G. (2016). Kynurenic acid and zaprinast induce analgesia by modulating HCN channels through GPR35 activation. *Neuropharmacology, 108*, 136-143. doi:10.1016/j.neuropharm.2016.04.038

Resta, F., Micheli, L., Laurino, A., Spinelli, V., Mello, T., Sartiani, L., . . . Masi, A. (2018). Selective HCN1 block as a strategy to control oxaliplatin-induced neuropathy. *Neuropharmacology, 131*, 403-413. doi:10.1016/j.neuropharm.2018.01.014

Richards, N., & Dilley, A. (2015). Contribution of hyperpolarization-activated channels to heat hypersensitivity and ongoing activity in the neuritis model. *Neuroscience, 284*, 87-98. doi:10.1016/j.neuroscience.2014.08.058

Rigaud, M., Gemes, G., Barabas, M. E., Chernoff, D. I., Abram, S. E., Stucky, C. L., & Hogan, Q. H. (2008). Species and strain differences in rodent sciatic nerve anatomy: implications for studies of neuropathic pain. *Pain, 136*(1-2), 188-201. doi:10.1016/j.pain.2008.01.016

Ronai, Z. A. (2016). Monoubiquitination in proteasomal degradation. *Proc Natl Acad Sci U S A, 113*(32), 8894-8896. doi:10.1073/pnas.1610186113

Rott, R., Szargel, R., Shani, V., Hamza, H., Savyon, M., Abd Elghani, F., . . . Engelender, S. (2017). SUMOylation and ubiquitination reciprocally regulate alpha-synuclein degradation and pathological aggregation. *Proc Natl Acad Sci U S A, 114*(50), 13176-13181. doi:10.1073/pnas.1704351114

Salas-Lloret, D., & Gonzalez-Prieto, R. (2022). Insights in Post-Translational Modifications: Ubiquitin and SUMO. *Int J Mol Sci, 23*(6). doi:10.3390/ijms23063281

Salo, P. T., & Theriault, E. (1997). Number, distribution and neuropeptide content of rat knee joint afferents. *J Anat, 190 (Pt 4)*, 515-522. doi:10.1046/j.1469-7580.1997.19040515.x

Santoro, B., Piskorowski, R. A., Pian, P., Hu, L., Liu, H., & Siegelbaum, S. A. (2009). TRIP8b splice variants form a family of auxiliary subunits that regulate gating and trafficking of HCN channels in the brain. *Neuron, 62*(6), 802-813. doi:10.1016/j.neuron.2009.05.009

Santoro, B., Wainger, B. J., & Siegelbaum, S. A. (2004). Regulation of HCN channel surface expression by a novel C-terminal protein-protein interaction. *J Neurosci, 24*(47), 10750-10762. doi:10.1523/JNEUROSCI.3300-04.2004

Sartiani, L., Mannaioni, G., Masi, A., Novella Romanelli, M., & Cerbai, E. (2017). The Hyperpolarization-Activated Cyclic Nucleotide-Gated Channels: from Biophysics to Pharmacology of a Unique Family of Ion Channels. *Pharmacol Rev, 69*(4), 354-395. doi:10.1124/pr.117.014035

Schnorr, S., Eberhardt, M., Kistner, K., Rajab, H., Kasser, J., Hess, A., . . . Herrmann, S. (2014). HCN2 channels account for mechanical (but not heat) hyperalgesia during long-standing inflammation. *Pain, 155*(6), 1079-1090. doi:10.1016/j.pain.2014.02.006

Seifert, A., Schofield, P., Barton, G. J., & Hay, R. T. (2015). Proteotoxic stress reprograms the chromatin landscape of SUMO modification. *Sci Signal, 8*(384), rs7. doi:10.1126/scisignal.aaa2213

Shah, M. M. (2014). Cortical HCN channels: function, trafficking and plasticity. *J Physiol, 592*(13), 2711-2719. doi:10.1113/jphysiol.2013.270058

Silveirinha, V. C., Lin, H., Tanifuji, S., Mochida, S., Cottrell, G. S., Cimarosti, H., & Stephens, G. J. (2021). CaV2.2 (N-type) voltage-gated calcium channels are activated by SUMOylation pathways. *Cell Calcium, 93*, 102326. doi:10.1016/j.ceca.2020.102326

Smith, T., Al Otaibi, M., Sathish, J., & Djouhri, L. (2015). Increased expression of HCN2 channel protein in L4 dorsal root ganglion neurons following axotomy of L5- and inflammation of L4-spinal nerves in rats. *Neuroscience, 295*, 90-102. doi:10.1016/j.neuroscience.2015.03.041

Steffensen, A. B., Andersen, M. N., Mutsaers, N., Mujezinovic, A., & Schmitt, N. (2018). SUMO co-expression modifies KV 11.1 channel activity. *Acta Physiol (Oxf), 222*(3). doi:10.1111/apha.12974

Stein, C., Millan, M. J., & Herz, A. (1988). Unilateral inflammation of the hindpaw in rats as a model of prolonged noxious stimulation: alterations in behavior and nociceptive thresholds. *Pharmacol Biochem Behav, 31*(2), 445-451.

Streich, F. C., Jr., & Lima, C. D. (2016). Capturing a substrate in an activated RING E3/E2-SUMO complex. *Nature, 536*(7616), 304-308. doi:10.1038/nature19071

Sun, Q., Xing, G. G., Tu, H. Y., Han, J. S., & Wan, Y. (2005). Inhibition of hyperpolarization-activated current by ZD7288 suppresses ectopic discharges of injured dorsal root

ganglion neurons in a rat model of neuropathic pain. *Brain Res, 1032*(1-2), 63-69. doi:10.1016/j.brainres.2004.10.033

Swett, J. E., Torigoe, Y., Elie, V. R., Bourassa, C. M., & Miller, P. G. (1991). Sensory neurons of the rat sciatic nerve. *Exp Neurol, 114*(1), 82-103. doi:10.1016/0014-4886(91)90087-s

Taiwo, Y. O., & Levine, J. D. (1991). Further confirmation of the role of adenyl cyclase and of cAMP-dependent protein kinase in primary afferent hyperalgesia. *Neuroscience, 44*(1), 131-135. doi:10.1016/0306-4522(91)90255-m

Takasu, K., Ono, H., & Tanabe, M. (2010). Spinal hyperpolarization-activated cyclic nucleotide-gated cation channels at primary afferent terminals contribute to chronic pain. *Pain, 151*(1), 87-96. doi:10.1016/j.pain.2010.06.020

Tibbs, G. R., Posson, D. J., & Goldstein, P. A. (2016). Voltage-Gated Ion Channels in the PNS: Novel Therapies for Neuropathic Pain? *Trends Pharmacol Sci, 37*(7), 522-542. doi:10.1016/j.tips.2016.05.002

Tossidou, I., Himmelseher, E., Teng, B., Haller, H., & Schiffer, M. (2014). SUMOylation determines turnover and localization of nephrin at the plasma membrane. *Kidney Int, 86*(6), 1161-1173. doi:10.1038/ki.2014.198

Tsantoulas, C., Lainez, S., Wong, S., Mehta, I., Vilar, B., & McNaughton, P. A. (2017). Hyperpolarization-activated cyclic nucleotide-gated 2 (HCN2) ion channels drive pain in mouse models of diabetic neuropathy. *Sci Transl Med, 9*(409), eaam6072. doi:10.1126/scitranslmed.aam6072

Tsantoulas, C., Mooney, E. R., & McNaughton, P. A. (2016). HCN2 ion channels: basic science opens up possibilities for therapeutic intervention in neuropathic pain. *Biochem J, 473*(18), 2717-2736. doi:10.1042/BCJ20160287

Ulman, A., Levin, T., Dassa, B., Javitt, A., Kacen, A., Shmueli, M. D., . . . Merbl, Y. (2021). Altered Protein Abundance and Localization Inferred from Sites of Alternative Modification by Ubiquitin and SUMO. *J Mol Biol, 433*(21), 167219. doi:10.1016/j.jmb.2021.167219

Usoskin, D., Furlan, A., Islam, S., Abdo, H., Lonnerberg, P., Lou, D., . . . Ernfors, P. (2015). Unbiased classification of sensory neuron types by large-scale single-cell RNA sequencing. *Nat Neurosci, 18*(1), 145-153. doi:10.1038/nn.3881

Vertegaal, A. C. O. (2022). Signalling mechanisms and cellular functions of SUMO. *Nat Rev Mol Cell Biol*. doi:10.1038/s41580-022-00500-y

Wahl-Schott, C., & Biel, M. (2009). HCN channels: structure, cellular regulation and physiological function. *Cell Mol Life Sci, 66*(3), 470-494. doi:10.1007/s00018-008-8525-0

Wang, X., Wang, S., Wang, W., Duan, J., Zhang, M., Lv, X., . . . Xing, J. (2016). A novel intrinsic analgesic mechanism: the enhancement of the conduction failure along polymodal nociceptive C-fibers. *Pain, 157*(10), 2235-2247. doi:10.1097/j.pain.0000000000000632

Wang, Y., Gao, Y., Tian, Q., Deng, Q., Wang, Y., Zhou, T., . . . Li, Y. (2018a). Author Correction: TRPV1 SUMOylation regulates nociceptive signaling in models of inflammatory pain. *Nat Commun, 9*(1), 2593. doi:10.1038/s41467-018-05022-w

Wang, Y., Gao, Y., Tian, Q., Deng, Q., Wang, Y., Zhou, T., . . . Li, Y. (2018b). TRPV1 SUMOylation regulates nociceptive signaling in models of inflammatory pain. *Nat Commun, 9*(1), 1529. doi:10.1038/s41467-018-03974-7

Weeratunga, S., Paul, B., & Collins, B. M. (2020). Recognising the signals for endosomal trafficking. *Curr Opin Cell Biol, 65*, 17-27. doi:10.1016/j.ceb.2020.02.005

Welch, M. A., Forster, L. A., Atlas, S. I., & Baro, D. J. (2019). SUMOylating Two Distinct Sites on the A-type Potassium Channel, Kv4.2, Increases Surface Expression and Decreases Current Amplitude. *Frontiers in Molecular Neuroscience, 12*(144). doi:10.3389/fnmol.2019.00144

Welch, M. A., Forster, L. A., Atlas, S. I., & Baro, D. J. (2019). SUMOylating Two Distinct Sites on the A-type Potassium Channel, Kv4.2, Increases Surface Expression and Decreases Current Amplitude. *Front Mol Neurosci, 12*, 144. doi:10.3389/fnmol.2019.00144

Welch, M. A., Jansen, L. R., & Baro, D. J. (2021). SUMOylation of the Kv4.2 Ternary Complex Increases Surface Expression and Current Amplitude by Reducing Internalization in HEK 293 Cells. *Front Mol Neurosci, 14*, 757278. doi:10.3389/fnmol.2021.757278

Weng, X., Smith, T., Sathish, J., & Djouhri, L. (2012). Chronic inflammatory pain is associated with increased excitability and hyperpolarization-activated current (Ih) in C- but not Adelta-nociceptors. *Pain, 153*(4), 900-914. doi:10.1016/j.pain.2012.01.019

X. Li, X. G., J Ren, C Jin, Y Xue (2009). BDM-PUB: Computational prediction of protein ubiquitination sites with a bayesian discriminant method.

Xiong, D., Li, T., Dai, H., Arena, A. F., Plant, L. D., & Goldstein, S. A. N. (2017). SUMOylation determines the voltage required to activate cardiac IKs channels. *Proc Natl Acad Sci U S A, 114*(32), E6686-E6694. doi:10.1073/pnas.1706267114

Xu, Q., & Yaksh, T. L. (2011). A brief comparison of the pathophysiology of inflammatory versus neuropathic pain. *Curr Opin Anaesthesiol, 24*(4), 400-407. doi:10.1097/ACO.0b013e32834871df

Yagi, J., & Sumino, R. (1998). Inhibition of a hyperpolarization-activated current by clonidine in rat dorsal root ganglion neurons. *J Neurophysiol, 80*(3), 1094-1104. doi:10.1152/jn.1998.80.3.1094

Yao, H., Donnelly, D. F., Ma, C., & LaMotte, R. H. (2003). Upregulation of the hyperpolarization-activated cation current after chronic compression of the dorsal root ganglion. *J Neurosci, 23*(6), 2069-2074.

Zajacova, A., Grol-Prokopczyk, H., & Zimmer, Z. (2021). Pain Trends Among American Adults, 2002-2018: Patterns, Disparities, and Correlates. *Demography, 58*(2), 711-738. doi:10.1215/00703370-8977691

Zemel, B. M., Ritter, D. M., Covarrubias, M., & Muqeem, T. (2018). A-Type KV Channels in Dorsal Root Ganglion Neurons: Diversity, Function, and Dysfunction. *Front Mol Neurosci, 11*, 253. doi:10.3389/fnmol.2018.00253

Zhong, P., Vickstrom, C. R., Liu, X., Hu, Y., Yu, L., Yu, H. G., & Liu, Q. S. (2018). HCN2 channels in the ventral tegmental area regulate behavioral responses to chronic stress. *Elife, 7*. doi:10.7554/eLife.32420